1-1-2014

Mutual Reinforcement Between Telomere Capping and Canonical Wnt Pathway Activity in the Intestinal Stem Cell Niche

Ting-Lin Yang
University of Pennsylvania, tingy@mail.med.upenn.edu

Mutual Reinforcement Between Telomere Capping and Canonical Wnt Pathway Activity in the Intestinal Stem Cell Niche

Abstract
Mice lacking telomerase (e.g. mTR-/-) for several generations develop dysfunctional telomeres and severe gastrointestinal pathology. Intestinal stem cell (ISC) abnormalities in late-generation mTR mice have been described, and we set out to characterize it in more detail. Expression profiling of mTR-/- crypts and an unbiased gene set enrichment analysis revealed broadly decreased expression of Wnt pathway genes in crypt epithelia and underlying stroma. We describe abnormalities in the Wnt-dependent intestinal stem cell (ISC) niche in these mice, including decreased expression of ISC marker genes Ascl2, Lgr5, and Sox9. The importance of these changes was revealed by rescue of crypt apoptosis along with Ascl2 and Sox9 expression upon treatment of mice with Wnt pathway agonists, as well as enhanced survival and Lgr5 expression in cultured mTR-/- intestinal crypts. Rescue was associated with reduced telomere-dysfunction induced foci (TIFs) and anaphase bridges, indicating improved telomere capping, which correlates with upregulation of Trf2 and Pot1a, encoding capping proteins in the shelterin complex. Similar gene expression changes, and rescue by Wnt pathway activation, were observed in human cells suffering from telomere dysfunction, including those derived from dyskeratosis congenita and Werner syndrome patients. These findings are independent of previously suggested connections between Wnt and the catalytic component of telomerase, TERT, and demonstrate a mutually reinforcing relationship between telomere capping and Wnt signaling, which may provide new approaches to diseases characterized by telomere dysfunction.

Degree Type
Dissertation

Degree Name
Doctor of Philosophy (PhD)

Graduate Group
Cell & Molecular Biology

First Advisor
Frederick B. Johnson

Keywords
intestinal stem cell, microRNA, telomeres, Wnt signaling

Subject Categories
Biology | Cell Biology | Genetics

MUTUAL REINFORCEMENT BETWEEN TELOMERE CAPPING AND CANONICAL WNT PATHWAY ACTIVITY IN THE INTESTINAL STEM CELL NICHE

Ting-Lin Yang

A DISSERTATION

in

Cell and Molecular Biology

Presented to the Faculties of the University of Pennsylvania

in

Partial Fulfillment of the Requirements for the

Degree of Doctor of Philosophy

2014

Supervisor of Dissertation:

_____

F. Bradley Johnson, M.D., Ph.D.

Associate Professor of Pathology and Laboratory Medicine

Graduate Group Chairperson:

_____

Daniel Kessler, Ph.D.

Associate Professor of Cell and Developmental Biology

Dissertation Committee:

Chair: Aimee S. Payne, M.D., Ph.D., Assistant Professor of Dermatology

Peter S. Klein, M.D., Ph.D., Associate Professor of Medicine

Christopher J. Lengner, Ph.D., Assistant Professor of School of Veterinary Medicine

Paul M. Lieberman, Ph.D., Professor of Gene Expression and Regulation Program

John P. Lynch, M.D., Ph.D., Associate Professor of Medicine

ACKNOWLEDGMENTS

Thanks to everyone past and present at Brad's lab for their support. Many thanks are also due to Brad, who is an inspiring mentor and scientist. His enthusiasm and love of science is infectious. The MSTP family has also been incredibly supportive in the past 6 years I've been at Penn. And special thanks are due to my committee members, who have been incredibly supportive in my goals thus far. A huge acknowledgment is due to Arturo Londoño and his lab members at the Institut Curie, for welcoming me into their lab for 10 months and making me feel at home in a foreign country. And I am also feel very lucky and thankful for my family and friends, a mixture of quirky, intelligent, fun, and supportive people. Specific mentions of people are in the Preface section to acknowledge those who have assisted in particular aspects of the thesis work.

ABSTRACT

MUTUAL REINFORCEMENT BETWEEN TELOMERE CAPPING AND CANONICAL WNT PATHWAY ACTIVITY IN THE INTESTINAL STEM CELL NICHE
Ting-Lin Yang
F. Bradley Johnson

Mice lacking telomerase (e.g. *mTR*$^{-/-}$) for several generations develop dysfunctional telomeres and severe gastrointestinal pathology. Intestinal stem cell (ISC) abnormalities in late-generation mTR mice have been described, and we set out to characterize it in more detail. Expression profiling of *mTR*$^{-/-}$ crypts and an unbiased gene set enrichment analysis revealed broadly decreased expression of Wnt pathway genes in crypt epithelia and underlying stroma. We describe abnormalities in the Wnt-dependent intestinal stem cell (ISC) niche in these mice, including decreased expression of ISC marker genes *Ascl2*, *Lgr5*, and *Sox9*. The importance of these changes was revealed by rescue of crypt apoptosis along with *Ascl2* and *Sox9* expression upon treatment of mice with Wnt pathway agonists, as well as enhanced survival and *Lgr5* expression in cultured *mTR*$^{-/-}$ intestinal crypts. Rescue was associated with reduced telomere-dysfunction induced foci (TIFs) and anaphase bridges, indicating improved telomere capping, which correlates with upregulation of *Trf2* and *Pot1a*, encoding capping proteins in the shelterin complex. Similar gene expression changes, and rescue by Wnt pathway activation, were observed in human cells suffering from telomere dysfunction, including those derived from dyskeratosis congenita and Werner syndrome patients. These findings are independent of previously suggested connections between Wnt and the catalytic component of telomerase, TERT, and demonstrate a mutually reinforcing relationship between telomere capping and Wnt signaling, which may provide new approaches to diseases characterized by telomere dysfunction.

TABLE OF CONTENTS

LIST OF TABLES

LIST OF FIGURES

PREFACE

Parts of “Chapter 1: The Introduction” are adapted from the draft of the book chapter, “Contributions of Telomere Biology to Human Age-Related Disease” written by Ting-Lin B. Yang, Sophie Song, and F. Bradley Johnson for The Handbook of the Biology of Aging, Eighth Edition. Many people have helped contribute to the making of this thesis, and it would take up another chapter to mention a fraction of the people who have made these experiments possible.

Special thanks are due to Qijun Chen, who was the main driver of this project for many years before I joined the lab. She performed much of the histological staining and analyses in Chapter 3-5, along with much of the animal husbandry and experiments. John Lynch provided us with a lot of guidance, helpful suggestions, and valuable reagents for experiments, and John Tobias helped us analyze mRNA and miRNA data shown in Chapters 3 and 4. Chris Lengner was instrumental in providing ideas for experimental designs and reagents, such as the *Axin2-TdTomato* reporter mouse (from John Epstein’s lab), and Msi1 antibody. Many thanks are due to David Schultz and Lakshmi at the Wistar Institute, for providing us with R-spondin1 and making our lentiviruses. Also at the Wistar, Zhong Deng from Paul Lieberman’s lab, who guided us to James Hayden and Fred Keeney, who were instrumental in helping us with Q-FISH analyses. Lastly, the entirety of Chapter 6 could not have been possible without the generous help and support of Arturo Londoño’s lab at the Institut Curie, and Win-Yan Bordes, who helped me with all of the colonoscopies and organ harvests. Also from the Institut Curie are Sophie Richon and Youmna Attie from Danijela Matic-Vignjevic’s lab, who taught Win-Yan and me how to use the endoscope machine.

CHAPTER 1: INTRODUCTION

The idea that a limited ability of cells to divide might contribute to the pathogenesis of age-related diseases was first raised by Hayflick and Moorehead a half century ago. It was based on their observation that human fibroblasts have a finite replicative capacity when cultured in the laboratory, a process termed cell senescence (1, 2). It is now known that a major factor limiting cellular replicative lifespan is the shortening and consequent dysfunction of telomeres, structures that normally cap and protect the ends of chromosomes. And because telomeres shorten with cell division and age in most human tissues, it has been hypothesized that such shortening might lead to loss of telomere function and thus be a fundamental driver of aging. Although an attractive and seemingly simple concept, it has taken decades to begin to assess potential roles for telomere dysfunction in human aging. Recently, substantial evidence has emerged supporting such roles, but the details are proving more complex than perhaps envisioned originally. Furthermore, many questions remain concerning the degree to which telomere biology contributes to human age-related pathologies, and concerning underlying mechanisms. We will begin with brief descriptions of telomere structure and function, and findings from cultured human cells and from mice.

TELOMERES AND TELOMERASE

Telomere Structure and Function

Telomeres are the structures at chromosome ends and are composed of tandem-repeats of DNA sequences $((5'\text{-TTAGGG-}3')_n$ in all vertebrates including

humans) and associated factors such as the shelterin proteins. When fully intact, telomeres perform several functions collectively known as “capping” (3). First, capped telomeres protect chromosome ends from degradation by exonucleases. Second, they prevent chromosome ends from being recognized as generic double strand breaks and thus eliciting cell cycle checkpoint responses leading to either stable cessation of cell division (cell senescence) or programmed cell death (apoptosis). Third, capped telomeres inhibit DNA repair reactions that could otherwise lead to deleterious products, e.g. end-to-end chromosome fusions. In addition to these well-established functions, recent evidence indicates that telomere status also impacts gene expression on a broad scale. Capped telomeres are thus critical for genome stability, for the progression of cell division and survival, and for normal cell physiology.

An important contributor to capping is the length of the telomere repeat DNA, and critical shortening leads to uncapping. Adult human telomeres are approximately 5 – 15 kb in length, and end with 3’ single-stranded overhang extending roughly between 50 and 300 nucleotides. For several reasons, telomere length can shorten through rounds of cell division. Shortening is most commonly attributed to the so-called “end replication problem”, which is the inability of the standard replication machinery to generate a DNA copy extending all the way to the 3’ terminus of the chromosome (4, 5). This is because the telomere strand that ends in the 3’ direction (the so-called G-strand) must be copied by lagging strand synthesis, and each Okazaki fragment begins with a 12-14 nt long RNA primer that is ultimately removed. For the final Okazaki

fragment, this leaves a terminal gap that cannot be filled by additional DNA synthesis. However, actual measured rates of telomere shortening, e.g. 50 – 100 bp per cell division in cultured human fibroblasts, exceed those predicted by the simplest version of the end replication problem, in which the RNA primer is laid down at the very end of the telomere. Recent measurements indicate that final RNA primer is actually located ~70-100 nt internal to the very end, helping to explain the faster rate of telomere shortening (6). Furthermore, exonucleolytic processing events lead to shortening of the other telomere strand, i.e. the C-strand, following its replication. The C-strand is copied by leading strand synthesis, which can yield a full copy, but subsequent 5'-to-3' exonucleolytic end-resection occurs to generate a single-stranded 3' overhang, thus shortening the telomere (7). This makes sense, because the 3' overhang is essential for telomere capping. Thus cells intentionally use mechanisms to replicate and process telomere ends that promote capping of longer telomeres, even though they can ultimately contribute to uncapping *via* shortening.

Additional, less telomere-intrinsic, mechanisms also contribute to telomere shortening. First, oxidative damage can accelerate telomere shortening, apparently by increasing the level of single-stranded breaks in telomeres, which are converted into double-stranded breaks during replication (8-10). Similarly, high levels of UV light can cause telomere shortening apparently by inducing DNA oxidative damage (11). However, even though telomeres are particularly susceptible to UV-specific damage, primarily the formation of cyclobutane pyrimidine dimers (CPD), elevated telomere CPD may not lead to enhanced

shortening (12). Second, telomeres are intrinsically difficult to replicate, similar to so-called fragile sites and perhaps due to formation of DNA secondary structures that impede replication. Thus conditions that lead to replication stress, e.g. activation of oncogenes, RNA bound to DNA ahead of the fork, and limiting levels of dNTPs, can lead to sudden and dramatic telomere shortening caused by broken replication forks (13-16). To what extent the telomere-extrinsic and telomere–intrinsic mechanisms of shortening described here and above are modulated by the environment and with age to contribute to telomere losses in aging tissues is currently not well understood, but they have the potential to have significant impacts.

In some tissues telomere shortening is countered by the enzyme telomerase. Telomerase is a reverse transcriptase that carries its own RNA template, which it uses to encode repeat DNA added to the 3' end of telomeres, and which is followed by lagging-strand synthesis to generate the complementary strand of the telomere duplex (17). However, in most human tissues telomerase activity is present at levels insufficient to prevent age-related telomere losses.

Also critical for capping are several factors that associate with telomere DNA. In humans, central players are the six shelterin complex proteins, TRF1, TRF2, RAP1, TIN2, TPP1 and POT1 (18), and the three components of the CST complex, CTC1, STN1 and TEN1. TRF1 and TRF2 each bind as homodimers to duplex telomere repeats in a sequence-specific fashion. POT1 binds the 3' single-stranded overhang, also in a sequence-specific fashion, and the bridging of TRF1/TRF2 to POT1 by the TIN2 and TPP1 proteins yields a protein complex

that targets the telomere DNA with high affinity and specificity. All six shelterin proteins exist in mice, with the exception of Pot1 having two forms in mice, Pot1a and Pot1b, which have different functions: Pot1a appears to play a more important role in telomere capping and suppresses the DNA damage response while Pot1b regulates length of the 3' telomeric overhang (19). Shelterin uses its components in different ways to suppress ATM and ATR-dependent DNA damage responses and to inhibit DNA break repair pathways (20, 21). One particularly remarkable way is the TRF2-dependent assembly of the telomere end into a t-loop, formed by the invasion of the 3' ss-overhang into the base of the telomere repeats to form a D-loop (or possibly a Holliday junction), thus obscuring the end (22, 23). Shelterin also helps recruit and regulate the activity of many additional proteins that maintain telomere structure and function. Remarkably, among these are proteins involved in recognizing and repairing DNA breaks, but under the influence of shelterin at capped telomeres these functions are tamed and redirected toward telomere maintenance. The CST complex plays a general role in DNA replication, facilitating restart of damaged replication forks (24). This is particularly important at telomeres, because they are generally each replicated by only a single fork, in contrast to other genomic regions, which, if their replication by one fork fails, can often be replicated by a convergent fork from a neighboring origin of replication. Furthermore, the CST complex also facilitates fill-in of the C-strand after elongation of the G-strand by telomerase (25). Both the shelterin and the CST complexes also play roles in regulating telomerase action at telomere ends (26).

Although it is clear that inherited mutations in telomerase, shelterins, and other telomere maintenance factors can cause premature telomere dysfunction and thus diseases (some of which resemble natural age-related pathology; see below), there is little evidence that age-related changes in the activity of these factors underlie normal diseases. Whereas such changes are possible, and are worthy of investigation, current understanding suggests that damage to the telomeric DNA itself (e.g. critical shortening) with age is a more likely primary driver of age-related telomere defects.

Measurement of Telomere Lengths

Different techniques are used to measure telomere lengths. Because of their relative ease and ability to measure small amounts of material, real-time PCR-based approaches that measure telomere repeat content in comparison to a single copy gene (T/S ratio) are most common (27, 28). However, this provides only a mean telomere length measurement, and because there is strong evidence that the shortest telomere or telomeres are more important in driving cell senescence than mean telomere length, this is a potential drawback (29-32). This also holds true for “flow-FISH”, which measures the mean telomere length per cell (33). Other approaches used less widely primarily due to their labor-intensiveness, are classical Southern analysis of chromosome terminal restriction fragments, and Q-FISH, which uses quantitative fluorescence microscopy to measure individual telomere intensities in metaphase chromosome spreads (34, 35). These can reveal information about length distributions, though Southern analysis is not sensitive for detecting extremely short telomeres and is also

affected by inter-individual and inter-telomere variability in subtelomeric sequences. The Southern approach can be more precise than real-time PCR, but in typical use they yield similar findings for mean length (36, 37). A new automated method, HT Q-FISH, provides benefits of Q-FISH in a high-throughput format, although it required dissociated cells and also cannot detect chromosome ends lacking all (or almost all) telomere repeats (38-40).

Telomerase Structure and Function

Telomerase is a ribonucleoprotein complex composed of the enzymatic reverse transcriptase protein TERT and the RNA template TR (also known as TERC), which encodes the telomere repeat. Multiple accessory proteins have been implicated in telomerase assembly, function, and localization, but *in vitro* analyses have determined that TR RNA and TERT together are sufficient for synthesizing telomeric DNA repeats (41, 42). The first step of telomeric DNA synthesis requires base pair formation between TR and the 3' telomeric G-rich overhang within the active site of TERT. The second step involves the addition of nucleotides onto the 3' telomeric end to elongate telomeres. Telomerase then translocates to the new 3' overhang to restart the telomeric synthesis process again (reviewed in (17, 43)). Over 30 proteins have been proposed to associate with telomerase, but the heart of the catalytic core of human telomerase is composed of two copies each of TERT, TR, and dyskerin (44). Telomerase likely exists in different conformations (reviewed in (45)), and the secondary structure of hTR seems to be important for TERT tethering and telomerase interaction with accessory proteins, including dyskerin, hGAR1, NHP2, NOP10, and TCAB1 (46).

Telomerase activity may be regulated by several different mechanisms, and levels of telomerase expression do not always correlate with its activity. Both hTR and hTERT are required to be expressed in the cell. In fact, hTR is generally ubiquitously expressed, even in cells without telomerase activity (47). hTERT expression exhibits more tissue specificity and seems to be the rate-limiting factor for telomerase activity. Indeed, telomerase activity can be induced when hTERT is overexpressed in mortal cells without telomerase activity (41, 48).

Telomerase activity can be measured by the TRAP assay, a PCR-based method compatible with crude cell or tissue extracts (49). Telomerase present in the extract extends a synthetic substrate primer, and the extended products are then amplified by PCR. On an electrophoretic gel, reaction products of the TRAP assay have a distinctive banding pattern, which corresponds to the discrete 6 bp additions of telomeric repeats by telomerase, and can thus give some information for both overall activity and approximate levels of processivity of the telomerase activity. A real time PCR-based assay also exists, which is convenient to run on large numbers of samples but gives information related only to overall activity (50). Based on early TRAP assays, telomerase activity was detected in almost all cancer cells and in developing human embryonic tissues and germ cells but not in quiescent or terminally differentiated somatic cells (49, 51, 52). During embryonic development, telomerase activity disappears in brain and bone extracts after 16 weeks of gestation and progressively shuts off in other tissues (adrenal gland, muscle, lung, skin, and liver) during fetal development. Later studies showed that many tissues that naturally undergo regeneration express

telomerase activity, including the esophageal epithelium (53), intestinal epithelium (54), basal keratinocytes (55), cycling endometrium (56, 57), and hematopoietic stem cells (58). It is now apparent that many adult human stem and progenitor cells exhibit telomerase activity. Telomerase activity is present in the proliferative and regenerative zones of the human skin and hair follicles (59, 60). Similarly, in the intestine, where a crypt-villus axis exists to reflect stem to progenitor to differentiated cell states, telomerase activity is restricted to the crypt base with no detectable activity in the villi (54). Proliferating spermatozoa have constitutive telomerase activity throughout the entire lifespan. Telomerase activity can also be activated in other physiologic states, such as growth-stimulated lymphocytes and uroepithelial cells (61, 62).

Telomerase activity may also be regulated by *hTERT* mRNA alternate splicing and hTERT localization. In the fetal kidney, full length *hTERT* mRNA is expressed until gestational week 15, when telomerase activity is present. After week 15, when inactive splice variants of *hTERT* are expressed instead of full-length *hTERT* transcripts, telomerase activity is no longer detectable (63). Likewise, lymphocytes can control telomerase activity independent of hTERT protein levels. Telomerase activity-positive thymocytes and telomerase-activity negative peripheral T cells express hTERT protein levels at a comparable level. Upon CD4 T cell activation, telomerase activity can be induced by the nuclear translocation of hTERT in a phosphorylation-dependent manner (64).

Cellular Consequences of Telomere Dysfunction

The cellular consequences of telomere shortening and uncapping are manifold and can vary according to cell type. Uncapped telomeres lose their ability to be masked as double strand breaks, and so a proximal response is the activation of the ATM and ATR-dependent DNA damage responses (31, 65, 66). Indeed, one way to detect uncapped telomeres in cells and tissues is using the microscopy-based TIF (**t**elomere dysfunction-**i**nduced **f**ocus) assay, which visualizes the colocalization between telomere ends and DNA damage response (DDR) factors (e.g. γH2AX or 53BP1) (66, 67). A remarkable feature of telomeres is their capacity to resist DNA repair, even after levels of uncapping sufficient to activate DNA damage responses (which can occur before all telomere repeat DNA is lost, thus allowing aspects of telomeric character to persist; see below) (68, 69). This suppression of repair leads to persistent DDR signaling that consolidates further cellular responses. One general cellular response is apoptosis, which has relatively simple consequences because the cell in question is eliminated. Apoptosis seems most common in cell types whose corpses are easily disposed of, for example skin and intestinal epithelial cells, which are normally and efficiently shed into the environment, or lymphocytes, which are efficiently cleared by macrophages.

Cell senescence is another general cellular response to uncapped telomeres, wherein the cell survives but undergoes substantial changes in its physiology, including stable arrest of its cell cycle. Senescent cells are thus marked by a number of phenotypic changes - for example expression of lysosomal senescence-associated β-galactoside activity, increased levels of

heterochromatic proteins such as macroH2A, increased levels of cell cycle inhibitors such as p21 and p16 - but no known marker is perfectly sensitive or specific for detecting senescence in all settings (70). Senescence is a programmed response to diverse stresses, including telomere uncapping as well as oncogene activation, oxidative damage, ionizing radiation, and changes in chromatin structure (70). The program is thought to have evolved to prevent the growth of pre-cancerous cells into more advanced tumors, and a large body of evidence strongly supports this view, although it also appears to play important roles during development and in anti-viral responses (71-73). Senescent cells may be cleared by the immune system, but in some cases can persist. For example melanocytes in benign nevi (i.e. skin moles) appear to be in a senescence state for decades (74). Remarkably, there is some evidence that seemingly telomere-independent stresses that induce senescence (e.g. oxidative stress; activated oncogenes) may actually lead to senescence, at least in part, by their effects at telomeres. For example, oncogene-induced replicative stress may be particularly pronounced at telomeres, and any resulting broken replication forks may be least likely to be repaired at telomeres, leading to their premature shortening. Thus a global stress is transformed into a more telomere-focused one (16).

Senescence is thought to contribute to age-related pathology in at least two ways. First, senescence of stem cells may limit their capacity to produce progeny needed to maintain tissue homeostasis. Support for this idea includes mouse experiments in which genetic inactivation of $p16^{INK4a}$, a cyclin kinase

inhibitor that enforces cell senescence by preventing cell cycle progression, was shown to prevent age-related stem cell deficits in the brain, pancreas, and bone marrow (75-77). Second, senescent cells are thought to contribute to aging by having dominant effects on their surrounding cells. Central to this idea is the so-called senescence-associated secretory phenotype (SASP), substances released by senescent cells, including matrix metalloproteinases and inflammatory cytokines that can have profound tissue effects (78-80). Direct support for the contribution of senescent cells to tissue pathology was demonstrated by inducing selective apoptosis of p16-expressing (i.e. senescent) cells in a mutant BubR1 mouse model. The BubR1 mutant accumulates an unusually high level of senescent cells, and elimination of the cells alleviated pathology in several tissues (81). It will be important to determine if these findings translate to telomere-induced senescence and to natural aging.

Shortened and uncapped telomeres have other effects, which may contribute to apoptosis and senescence but are also separate from these processes and might contribute independently to aging. First, they lead to dramatic changes in gene expression that may contribute to cell and tissue dysfunction. The mechanisms underlying these changes are under active investigation, and appear to involve widespread changes in chromatin architecture that suggest important communication between telomere events and the rest of the genome (82-84). Of particular interest, evidence is emerging that even before a telomere has become short enough to be uncapped, its shortening can influence gene expression (85, 86). Therefore changes in telomere lengths

with age may contribute to changes in gene expression prior to the onset of apoptosis or senescence. A second set of important changes include compromised mitochondrial biogenesis and function (87-89). Studies in telomerase-deficient mice with critically shortened telomeres showed these effects are mediated in large part by p53-dependent inhibition of the Pgc1a and Pgc1b transcriptional co-activators, and are accompanied by other broad changes in metabolism also regulated by these co-activators (90). Interestingly, these changes occurred in several tissues, including those with very low cell turnover (e.g. myocardium), suggesting these mechanisms may connect telomere changes to aging of post-mitotic cells. And third, uncapped telomeres can lead to inter-telomere recombination. This can take the form of homologous recombination-dependent telomere lengthening, which occurs at undefined rates in some normal cells and is used as an alternative to telomerase for telomere length maintenance in about 10% of cancers (91, 92). Alternatively, and more ominously, inter-telomere recombination can take the form of non-homologous end joining-mediated fusions between telomere ends. Such fusions can lead to chromosomal aneuploidy, because at mitosis the resulting dicentric chromosomes can break at sites outside the point of fusion or are not disjoined, and thus unequal chromosomes complements are inherited by the daughter cells. This can lead to cell death, senescence, or to cancer (see below). However, even though it is sometimes implied in the scientific literature that such fusions are a frequent outcome of telomere uncapping and are a primary cause of senescence, in normal human cells such fusions occur at a minority of

uncapped telomeres and are not required for senescence (29, 93, 94). Indeed, there appear to be intermediate degrees of telomere uncapping sufficient to activate partial DNA damage responses that drive senescence, but which occur before a telomere has become further uncapped and fusogenic (29, 95). Cells that have lost responses to intermediate levels of uncapping (e.g. p53-deficient cells) can continue to shorten telomeres to the point of full uncapping, leading to fusions and thus genome instability that can drive cancer.

Given that the loss of replicative capacity was the original attribute that led to the identification of cell senescence, it has been natural to assume that the transition from a replicative to a non-replicative state is an essential feature of senescence. This is consistent with the idea that a key purpose of the senescence program is to inhibit the growth of pre-cancerous cells. However, recent evidence suggests that even cells that are already post-mitotic can display other features of senescence. As such, senescence might be viewed as a programmed response of cells to particular stresses. For example, elevated markers of oxidative and DNA damage, and senescence-associated changes in chromatin and gene expression including upregulation of the inflammatory cytokine IL-6 and of the cyclin kinase inhibitors p16 and p21 have been reported in neurons of aged mice (96). It is possible that telomere dysfunction contributes to this type of neuronal senescence, because the markers were more pronounced in telomerase-deficient mice. Furthermore persistent DNA damage foci in the neurons of normal mice exposed to ionizing radiation occur

preferentially at telomeres, indicating telomeres may be key transducers of stresses into senescence responses even in post-mitotic cells (68).

Proof that telomere shortening is an important cause of cultured human cell senescence was demonstrated by the bypass of senescence upon upregulation of telomerase activity *via* artificial overexpression of hTERT (97). hTERT expression was sufficient to provide telomerase activity, and thus telomere lengthening, because other telomerase components (e.g. *hTR*) were already expressed naturally. Although potential extra-telomeric roles for hTERT have been reported, e.g. in mitochondria, DNA repair, stem cell maintenance, and modulation of Wnt signaling (46, 98-100), some of these are controversial (101), and regardless it is the extension of telomere length that most likely underlies the bypass of senescence. Strongly supporting this idea is the demonstration the degree of telomere lengthening following a transient pulse of telomerase activity correlates with subsequent cell replicative lifespan (102). However, we want to emphasize that even though telomere shortening clearly drives the senescence of cultured cells, it is not yet clear to what extent senescence in humans is a telomere-driven process, and more work needs to be done to determine whether senescent cells, particularly those driven into senescence by telomere dysfunction, contribute to age-related pathology in humans.

Telomeres and Aging, and Telomere Syndromes

In the normal human population, telomere lengths range from approximately 5 to 15 kb and change during pre and postnatal development and

aging. There is ample support for the idea that telomeres tend to shorten with age in most human tissues, even including tissues with low levels of cell turnover such as brain (103) (104-106).

Telomere lengths are highly similar among tissues within an individual *in utero* and soon after birth (107, 108). However, they vary among individuals but are not different between male and female newborns, suggesting that increased variability in length between individuals and genders arises from different rates of telomere attrition later in life. After birth, telomerase activity is repressed in most somatic cells, and thus telomeres shorten during growth to adulthood. Importantly, there is some telomerase activity in stem and progenitor cells, which helps counter but not prevent shortening. Telomeres shorten most during the rapid growth to adulthood, around 1kb from birth to 4 years of age and decreasing to less than 100bp per year thereafter in leukocytes (109). They shorten in rough proportion to the proliferative rate of the tissue, e.g. telomeres shorten more rapidly in peripheral blood leukocytes than in skeletal muscle, but shortening rates may also be influenced by differences in levels of telomerase among tissues. Telomere lengths are nonetheless correlated among tissues when making comparisons between people, i.e. a person with longer-than-average telomeres in skeletal muscle will also have longer-than-average telomeres in leukocytes (110, 111).

Within a lineage of cell types, telomere lengths correlate positively with telomerase expression and activity, and in stem cells where telomerase expression is high, telomere lengths are also the longest. Stem cells have longer

telomeres than progenitor cells, which in turn have longer telomeres than differentiated cells. Q-FISH analyses of murine skin, intestine, testes, cornea, and brain found the longest telomeres to be located in stem cell compartments, with progressively shorter telomeres towards the more differentiated cell compartments (112). Stem cells also undergo telomere attrition with age, despite expressing telomerase activity. Telomeres in stem cells from two year old mice are significantly shorter than from two month old mice, which may be explained in part by the concurrent decline in telomerase activity with age (112, 113). Similarly, in humans, despite the presence of telomerase activity in stem cells, telomere attrition still occurs in stem cells with age – hematopoietic stem cells (HSCs) and mesenchymal stem cells (MSCs) have shorter telomeres with age (114, 115). However, the converse seems to be true in male germ cells – telomeres are longer in spermatozoa produced by older men (116).

There is clear evidence that telomeres shorten with age, but is the shortening during the lifetime of an individual enough to contribute to telomere dysfunction in aging mammals? Indeed, there exists direct evidence that links aging and uncapped telomere in primates. There is an exponential increase in the frequency of dysfunctional telomeres in baboon dermal fibroblasts with age, as measured by TIFs. Correspondingly, there is also an exponential increase in cellular senescence and $p16^{INK4a}$ expression in the baboon skin fibroblasts with age, with 80% of the senescent fibroblasts positive for TIFs (117). Several rare genetic diseases displaying premature onset of some features of aging, called progeroid disorders, are associated with defects in telomere maintenance

factors. Understanding the mechanisms underlying these diseases can therefore provide insight into potential contributions of telomere dysfunction to age-related pathologies.

The first progeroid disease to be connected clearly to telomeres is dyskeratosis congenita (DC) (118). DC was originally defined by a classical triad of clinical signs including oral leukoplakia, dystrophic nails, and skin hyperpigmentation, but includes several other pathologies including IPF, GI dysfunction, osteoporosis, cirrhosis, bone marrow failure and increased rates of cancer, the last two which are the primary causes of death. Mutations in several different genes cause DC, and most of these lead to decreased levels of telomerase function, including *TERT, TERC, DKC1, NOP10, NHP2, and TCAB1.* Recently, mutations in other telomere maintenance factors *TINF2, CTC1, and RTEL* have been found to cause rare cases of DC, and about a third of cases remain of unknown genetic origin. DC is now recognized as part of a spectrum of diseases, including the more severe Hoyeraal-Hreiderasson, Coats Plus and Revesz syndromes, which are also caused by more severe mutations in some of the same genes. Accordingly, all of these diseases are characterized by prematurely shortened telomeres, which appear to be central to pathogenesis.

There are other progeroid diseases in which telomere maintenance is compromised, including Werner syndrome (WS), Hutchinson-Gilford progeria syndrome (HGPS), ataxia telangiectasia, Fanconi anemia, Bloom syndrome and Rothmund Thompson syndrome. Each of these is caused by mutations in proteins that also have clear effects outside of telomeres, e.g. in each of these

diseases, the genome is destabilized globally, and thus it is unclear to what extent the telomere defects are the primary drivers of pathology. WS is caused by the loss of the WRN DNA helicase, which is important for efficient recombination and DNA replication, including telomere lagging strand synthesis (119, 120). WS is particularly notable for two reasons. First, among all progeroid diseases, its spectrum of pathologies most closely mimics that of natural aging (121). These include atherosclerosis, type II diabetes mellitus, osteoporosis, loss of subcutaneous adipose tissue, hair greying, bilateral cataracts, and elevated rates of cancer, albeit with some notable differences from natural aging, e.g. the osteoporosis affects primarily the limbs rather than axial skeleton, and the cancer spectrum is skewed from carcinomas to sarcomas. Along these lines, it is noteworthy that *WRN* polymorphisms have been associated with longevity (122, 123). Second, there is strong evidence that telomere defects in fact make major contributions to WS. Artificial expression of hTERT in cultured WS fibroblasts rescues their short telomeres and growth defects, and strongly suppresses the elevated rate at which chromosome aberrations are generated, indicating chromosome instability is driven by telomere dysfunction (124). And in mice, the naturally high levels of telomerase appear to mask defects that otherwise emerge when WRN is lost (125, 126). Therefore it may be that telomere-related degenerative defects in WS are skewed toward those occurring in tissues in which telomerase activity is particularly low, e.g. in several mesenchymal tissues, which are generally most affected in WS (this excludes bone marrow, where telomerase activity is relatively high).

The DC spectrum of diseases have come to be known as “the telomere syndromes” or “telomeropathies”, and for good reason, given the clear primary role of telomere defects in these diseases and their overlap with telomere-related pathologies in “normally” aged individuals such as aplastic anemia or idiopathic pulmonary fibrosis. However, as suggested previously (127), it may be that the DC spectrum of diseases reveals primarily how telomere dysfunction affects highly proliferative tissues (e.g. bone marrow, GI epithelium, epidermis, or tissues that are induced to proliferate by injury, e.g. lung epithelium, liver epithelium), whereas WS may provide complementary information on the consequences of telomere defects in less proliferative tissues, and thus the full spectrum of “telomere syndromes” may be broader than those illustrated by the DC-related set of diseases. This idea fits reasonably well with mutations in telomerase components being the chief source of DC spectrum diseases, and with higher levels of telomerase expression in highly proliferative tissues. It is not yet clear if telomere defects play more important roles in natural aging in tissues with low levels of proliferation and telomerase or with high levels of proliferation and telomerase.

MOUSE MODELS OF TELOMERE DYSFUNCTION

Telomeres in Mice

Inbred lab mice are the most widely used mammalian models for the study of telomerase and telomere biology. Compared with humans, these mice have much longer telomeres, higher telomerase activity in somatic tissues, and yet a much shorter lifespan. These facts are sometimes used to argue that telomere

shortening cannot be a cause of human aging, but this assertion is based on the notion that aging mechanisms need to be evolutionarily conserved. In fact, because they are executed primarily after the age of reproduction, pro-aging mechanisms are under relatively little selective pressure, and so are more free to vary among species (128). As argued above, humans appear to have evolved a strategy that uses telomere shortening to combat cancer, whereas mice have not, and so humans may be more subject to the downside of this strategy, i.e. tissue homeostasis limited by telomere dysfunction at later ages (129, 130). Consistent with this view, there is no correlation between telomere length and longevity among mouse strains. Commonly used strains of inbred lab mice (C57BL/6J, FVB/NJ, and 129/SvJ) with long heterogeneous telomere lengths ranging from 30-150 kb do not live significantly longer than other wild-derived inbred lab mice (*Mus spretus* and *Mus musculus castaneus*) with shorter telomere lengths (18-20 kb). Moreover, the non-*Mus* wild-derived *Peromyscus leucopus* mouse has a long relative lifespan of 5-7 years compared to that of the inbred lab mouse (~2 years), yet its average telomere length (~12 kb) is relatively short (131). Also consistent with the view that telomere length is not limiting in inbred lab mice are observations that when a core component of telomerase (*mTR* or *mTert*) is knocked out telomeres shorten, but the first generation (G1) of such mice have little apparent phenotypes or pathologies because telomeres apparently do not shorten to a critical length (132-135).

Nonetheless, there is evidence that telomeres may affect cancer and aging in normal mice to some degree. Telomere attrition does occur with age in

mice, and even though only to mean lengths that are longer than dysfunctional human telomeres, one cannot rule out the possibility that critically shortened telomeres may be present (136). Indeed, TIFs increase in frequency with age in mice - and caloric restriction, which delays aging, delays telomere shortening (69, 137). Furthermore, overexpression of telomerase causes elevated rates of cancer in mice, but in mice protected from cancer by additional copies of p53 and p16/Arf, the extra telomerase extended median (but not maximum) lifespan approximately 15% and delayed age-related pathologies (138). To the extent that telomeres play more limiting roles in humans than in mice, one would expect that strategies to improve telomere maintenance would have much larger effects in humans. These effects might be beneficial, as well as deleterious (e.g. via promoting cancer).

Mouse models of telomere dysfunction

Telomerase deficient mice have helped us understand the consequences of critical telomere shortening (132-135). Since there is no telomerase in the germ line of telomerase knockout mice, they pass on shorter telomeres to their offspring, although it is an open question as to what extent ALT activity during development – particularly prior to the blastocyst stage – might counter critical shortening (139). Regardless, after several generations of breeding, successively shorter telomeres are passed down to the next generation. Eventually, once telomeres have shortened to a critical length, pathologies associated with dysfunctional telomeres become apparent. How many generations must elapse before telomerase deficiency manifests its effects

depends on the starting telomere length. In the CAST/Eij mouse model where the starting telomere length is comparable to humans, telomerase haploinsufficiency (*mTR*$^{+/-}$ or *mTert*$^{+/-}$) is enough to critically shorten telomeres, similar to DC patients who are haploinsufficient for telomerase (140, 141). In C57Bl/6 mice, which have longer telomeres than CAST/Eij mice (142), *mTR*$^{-/-}$ deficiency by later generations (G4-G6) leads to decreased lifespan and signs of premature aging and decreased somatic and germ cell replicative capacities, characterized by apoptosis and growth arrest, particularly in high turnover tissues, similar to pathology in DC. Deletion of shelterin proteins in mice has also informed us of the function of these proteins in mouse telomere biology. *Trf1, Trf2, Tpp1, Pot1a,* and *Tin2* deletion result in embryonic lethality, while *Rap1* and *Pot1b* knockout mice survive to adulthood and have no apparent phenotypes (143-148). Knocking out *Trf1* and *Trf2* in cells rapidly induces end-to-end chromosome fusions and cellular senescence. As mentioned earlier, late-generation *mTR*$^{-/-}$ mice have a phenotype that is characterized by decreased proliferation capacity in organs with high tissue turnover rates. Intestinal atrophy, infertility, poor wound healing, alopecia and greying of the fur, neural tube closure defects, bone marrow aplasia, cardiac dysfunction, and runting are some of the degenerative features of the *mTR*$^{-/-}$ mice (149, 150).

Dysfunctional telomeres are recognized as double stranded DNA breaks and set off DNA damage responses (20). First, the MRN (Mre11-Rad50-Nbs1) complex recognizes double stranded DNA breaks and recruits ATM to the site of damage. Following auto-phosphorylation and thus activation, ATM

phosphorylates key proteins to activate the DNA damage checkpoint, leading to DNA repair, cell cycle arrest, or apoptosis. CHK2, H2AX, and p53 are some of the DNA damage proteins that ATM directly phosphorylates and activates. Uncapped telomeres results in the activation of p53, a tumor suppressor gene that can initiate apoptosis or cell cycle arrest and activate DNA repair proteins. Activated p53 can act as a transcription factor and can activate expression of several genes such as microRNA-34a (miR-34a), CDKN1a (i.e. p21), PUMA, and SIAH1 (151).

p53 conducts many of the downstream effects seen with uncapped telomeres. Deletion of p53 in different contexts of telomere dysfunction (caused by critical telomere shortening or telomere uncapping from shelterin defects) is able to rescue many aspects of the pathology, such as cell cycle arrest, apoptosis, and stem cell function. For example, mice lacking *Trf1* in the stratified epithelium die perinatally but survive to adulthood when p53 is deleted (152). Similarly, p53 deletion rescues many aspects of stem cell dysfunction in late-generation $mTR^{-/-}$ mice (which we will discuss in more detail later) (153-156). However, deletion of p53 leads to unchecked cell cycle progression in these cells, which allows the cells to further accumulate genomic instability, resulting in end-to-end chromosome fusions and breakage-fusion-bridge cycles during mitosis. This sets the stage for the cell to turn into cancer through genomic deletions, duplications, and rearrangements. Indeed, rates of cancer are increased in mice lacking p53 and *mTR* or *Trf1* in stratified epithelium.

Conversely, telomere dysfunction with an intact p53 response exerts a tumor suppressive effect, as *mTR*$^{-/-}$ mice have reduced incidences of cancer, and delays cancer onset in the cancer-prone *Ink4a/Arf*$^{-/-}$ mice (157). Telomere dysfunction can be thought of a driver for genomic instability, and may actually increase cancer *initiation* (e.g. late-generation *mTR*$^{-/-}$*APC*$^{+/min}$ mice increases numbers of early-stage microadenomas), but decrease cancer *progression* – telomere shortening in the absence of telomerase but in the presence of functional p53 can inhibit malignant cell division (e.g. late-generation *mTR*$^{-/-}$ *APC*$^{+/min}$ mice have decreased numbers of late-stage macroadenomas) (158, 159).

Cell senescence or apoptosis caused by telomere uncapping has been thought to be cell autonomous. Thus, genetic inactivation of factors that minimize telomere degradation (Exo1) or responses to uncapped telomeres (p53, p21, or PUMA) has been found to be of benefit in mice lacking telomerase (156, 160-162). But the recent demonstration that cell senescence can be propagated in an intercellular fashion (80) raises the possibility that non-cell autonomous mechanisms might impact pathology caused by telomere uncapping.

WNT SIGNALING, INTESTINAL STEM CELLS, AND TELOMERES

Wnt Pathway

The Wnt pathway was initially discovered in *Drosophila* when the Wingless (*Wg*) gene was mutated to cause wingless fruitflies (163). *Wg* had a high degree of conservation across species, including the *Int-1* (integration) oncogene in mice (now known as Wnt1), discovered as a site of frequent retroviral integration by

the mouse mammary tumor virus (MMTV), which causes mammary tumors in mice (164). The *Wg* gene is important for segment polarity during embryonic development. The Wg/Int pathway was eventually renamed as Wnt, to reflect both origins of discovery.

The Wnt signaling pathways are a group of highly conserved signal transduction pathways that can be classified into two main categories: the canonical Wnt pathway and the noncanonical Wnt pathway. Both the canonical and the noncanonical pathways are activated by extracellular Wnt protein ligands that bind to specific cell surface receptors (Frizzled receptors, Fzd) to activate downstream intracellular signals through the Dishevelled protein. The canonical Wnt pathway leads to an accumulation of β-catenin to regulate gene expression, while the noncanonical pathways operate independently of β-catenin. The noncanonical Wnt pathway has been described to be involved in planar cell polarity (165, 166).

The canonical Wnt pathway is initiated when extracellular Wnt ligand proteins bind to the Fzd, LRP5/6 cell surface protein receptors, which activate the intracellular Dsh protein. Activated Dsh inhibits the GSK3/Axin/APC destruction complex, which sequesters β-catenin in the cytoplasm and targets it for ubiquitination and subsequent degradation. Once the destruction complex is inhibited, levels of β-catenin build up in the cytoplasm and localize to the nucleus. In the nucleus, β-catenin binds to the TCF/LEF transcription factors to initiate gene expression changes. There are other players involved in the Wnt pathway, including other ligands and receptors. R-spondin proteins are a family of proteins

that are secreted and can activate the canonical Wnt pathway via the Lgr family of receptors, Lgr4/5/6 (167, 168). R-spondin proteins may also bind to and inhibit the ZNRF3 and RNF43 transmembrane molecules, which are Wnt target genes but also negatively feedback on Wnt signaling by increasing turnover of the Fzd receptors (169). Similarly, Ror proteins are a family of tyrosine kinase receptors that can modulate Wnt signaling depending on the cell type, and they may sequester Wnt ligands to prevent them from binding to Fzd receptors. Ryk is another family of tyrosine kinase receptors that can activate the canonical Wnt pathway through Dsh. It has long been thought that specific Wnt ligands activate different Wnt pathways (e.g., Wnt 11 activates the noncanonical Wnt pathway), but it is now thought that the signaling outcome is dependent on the combination of receptors activated (170).

There are several inhibitors of the canonical Wnt pathway, including Wnt inhibitory factor-1 (Wif-1), Dickkopf (Dkk), Cerberus, Wise, SOST, Frzb, and the soluble frizzled proteins (Sfrps). There are also cytosolic inhibitors of Wnt signaling, including Axin2 and Nkd, which are both Wnt targets and negatively feedback on the pathway. Wnt ligand diffusion may be inhibited through interactions with Dally and glypican 3. Dkk (forms 1-4) can bind to LRP and Kremen, which may downregulate LRP from the cell surface. Sfrps are secreted proteins that mimic Fzd proteins (without transmembrane domains) and can sequester Wnt ligands. Similarly, Wif1 also binds Wnt ligands to prevent them from binding to Wnt receptors (171).

Wnt Signaling in Intestinal Stem Cell Homeostasis

The canonical Wnt pathway is important for the embryonic development of the gastrointestinal tract and the maintenance of intestinal stem cell (ISC) homeostasis (172). Mutation of genes involved in canonical Wnt signaling can disrupt the development of the GI tract and can also initiate tumors. When Tcf1 (also known as Tcf7) and Tcf4, transcription factors of canonical Wnt signaling, are both knocked out in mice, severe hindgut and gastrointestinal defects are present (173). Inactivating mutations of APC can lead to unchecked Wnt signaling and intestinal adenomas and cancer in mice and humans (158). Wnt signaling is also important for maintaining the ISC niche environment in adult intestinal crypts.

The normal maintenance of mammalian intestinal epithelium involves remarkably high rates of cell turnover. For example, the small intestinal epithelium of mice is replaced every 3-5 days (174, 175). Fundamental to this homeostasis are the activities of intestinal stem cells (ISCs), which reside within the deepest recesses of the intestinal epithelium at the base of each crypt. ISCs include both so-called crypt base columnar cells (CBCs) and label-retaining cells (LRCs). CBCs divide on a daily basis (176) and are located at the base of crypts where they are intercalated between Paneth cells, which along with underlying stromal cells contribute to the CBC niche. Importantly, both Paneth and stromal cells provide intercellular Wnt signals (e.g. Wnt3 from Paneth cells) to support the CBC niche (177). In contrast, LRCs divide infrequently, are located above Paneth cells at approximately the +4 position, and are independent of Wnt signals (178). Both CBCs and LRCs produce progeny that can differentiate into

all intestinal epithelial cell types, and it is thought that CBCs typically serve this function, whereas LRCs divide to replace CBCs on the occasion of their loss.

The crypt niche environment is composed of ISCs and Paneth cells, which produce bactericidal enzymes but also secrete EGF, the Notch ligand Dll4, and multiple Wnt ligands, Wnt11 and Wnt3 (177). Wnt3 is an important Wnt ligand for ISC maintenance, and Paneth cells are the sole source of Wnt3 production in the crypt epithelium. The underlying stroma is also an important source of Wnts and can compensate for loss of Wnts from Paneth cells (179). Wnt3 is not essential for ISC maintenance *in vivo* because stromal sources of Wnt (e.g. Wnt2B) can compensate, but *ex vivo* cultures of intestinal organoids, without the presence of stromal cells, Wnt3 and Paneth cells are essential for organoid and ISC survival (179). Wnt3 can substitute for R-spondin1 or other Wnt-activating agents, such as CHIR99021 (an inhibitor of GSK3) in *ex vivo* intestinal organoid cultures. The standard recommended *ex vivo/in vitro* organoid culture system is supplemented with the growth factors EGF, Noggin, and R-spondin1 (180).

Wnt and Aging

Wnt signaling is important in development and cancers, and recent reports suggest Wnt signaling is also important in replicative senescence and aging, although many studies report contradictory roles for Wnt signaling. The discrepancies between the studies have yet to be resolved, since it is context-dependent and also depends on the models/tissues/cells used. WI-38 cells undergoing replicative senescence or oncogenic-activated senescence have decreased Wnt2 ligand expression, and knockdown of Wnt2 was sufficient to

induce premature senescence (181). Exogenous Wnt3a delayed oncogene-induced senescence in one setting, but in another study, increased Wnt signaling activity in the Klotho mouse model accelerated cell senescence and aging (182). The Klotho protein has many functions, one of which is to sequester Wnt3 and inhibit it from activating the Wnt pathway. Impairment in *Klotho* gene expression increases Wnt pathway activity, and also decreases stem cells in the skin and intestine (182). However, Klotho also inhibits the insulin/IGF pathway, which has also been implicated in aging and stem cell biology, and can affect additional pathways and so the role of Wnt signaling in these experiments is unclear. Another study saw an increase Wnt pathway activity in mesenchymal stem cells incubated with aged rat serum and inhibition of Wnt signaling promoted proliferation (183). Skeletal muscles have also been observed to convert from a myogenic to a fibrogenic lineage and found to have increased Wnt signaling when incubated with aged serum, and muscle regeneration in aged mice was enhanced by the inhibition of Wnt signaling (184). However, Wnt signaling is typically mediated in a short-range paracrine fashion, and pro-Wnt factors in the serum may be different from short-acting Wnt ligands. Differences in the above conflicting reports may also be explained in part by the pleotropic and tissue-specific effects of Wnt signaling. As mentioned earlier, the combination of Wnt receptors that are activated on the cell surface can result in very different downstream consequences, and the timing and duration of the signals can have opposite effects. For example, even though Wnt signaling promotes

hematopoietic stem cell proliferation, constitutive Wnt activation can drive hematopoietic stem cell exhaustion (185-188).

Wnt and Telomeres

Telomerase and Wnt signaling play important roles in the regulation of cancer, aging, and stem cell biology, and many studies explore their relationship with each other. TERT has been shown in several systems to be a target gene of the canonical Wnt pathway, and other studies have also proposed that TERT acts as a transcription factor within the canonical Wnt pathway, although discrepancies exist which question the validity and the physiologic relevance of the latter model. We will go into a brief overview of the studies that describe these connections, the discrepancies, and their relevance to this thesis.

TERT is a direct and canonical Wnt target gene in normal and cancer cells of humans and mice through the binding of β-catenin directly to the *TERT* promoter. Activation of Wnt signaling by LiCl (which inhibits GSK3, among other activities), Wnt3a-conditioned medium, or overexpression of constitutively active β-catenin induced *hTERT* expression and telomerase activity in multiple human cell lines, through TCF4-mediated transcription. Inhibition of β-catenin expression reduced *hTERT* expression, telomerase activity, and increased rates of telomere shortening (189). Similar results were found in a separate study looking at mouse embryonic stem cells, mouse intestinal cancers caused by overactive Wnt signaling and human cancer cell lines, mediated by β-catenin and KLF4 binding at the *Tert* promoter (190). These observations are in addition to what is already

known about the regulation of *TERT* transcription through the c-Myc transcription factor, which itself can be regulated by β-catenin/Wnt signaling.

Many investigators have studied the overexpression of TERT in human and mouse systems, and many have observed non-telomere lengthening effects of telomerase, including the inhibition of apoptosis and promotion of cell division. TERT overexpression in mouse skin induced robust follicular bulge stem cell proliferation that resulted in robust hair growth, which was still the case even when telomerase-lengthening effects were abolished (i.e. in mice lacking *mTR* or when a catalytically-inactive form of TERT was overexpressed)(191, 192). The authors identified changes in gene expression regulated by the Myc and Wnt pathways when TERT expression was switched off (192). Follow-up studies by the group identified direct association of endogenously FLAG-tagged mTERT with β-catenin and BRG1, a chromatin remodeling factor shown to promote β-catenin target gene expression (99). The authors also describe mild homeotic transformations in first-generation *mTERT*$^{-/-}$ mice (before telomeres are critically short), characterized by loss of the 13th rib on one or both sides in 6 out of 13 mice. Multiple groups have attempted to replicate these results, but to date, there have been no success yet. Moreover, it would be expected that extra-telomeric functions of TERT would manifest in phenotypes of *mTERT*$^{-/-}$ mice that are different from *mTR*$^{-/-}$ mice. This was investigated through comparisons of several models – livers from *mTERT*$^{-/-}$ and *mTR*$^{-/-}$ mice, mouse embryonic fibroblasts (MEFs) from *mTERT*$^{-/-}$ and wild-type littermates produced from heterozygous *mTERT*$^{+/-}$ parents, and comparisons between *mTERT*$^{-/-}$ and *mTR*$^{-/-}$ mice on a

different strain background – but there was lack of evidence for any gene expression or phenotypic differences between *mTERT*$^{-/-}$ and *mTR*$^{-/-}$ (140, 193).

Many have also raised the question of physiologic relevance in an overexpression system, where TERT could have gain-of-function phenotypes. TERT overexpression in several human cell lines was also contributed to the increase in Wnt reporter activation (99, 194). However, in hepatocellular carcinomas with mutations in the promoter-region of *hTERT* (which increases *TERT* expression), there was no activation of the Wnt pathway (195). Futhermore, hTERT overexpression failed to activate Wnt signaling in various cancer cells, including some of the same cells from previous studies (101). The authors postulate that the discrepancies are due to differences in cell types and the numbers of TCF/LEF sites in the reporters used. Surprisingly, they also failed to detect interaction between FLAG-hTERT and endogenous BRG1 or between BRG1 and β-catenin. However, they detected interaction between non-affinity-purified anti-FLAG M2 antibody and β-catenin antibody, which raises the possibility that previous reports were detecting artifact from antibody cross-reactivity.

Another connection exists between Wnt and telomeres through the regulation of *TRF2* expression by the Wnt pathway. TRF2 expression was described to be highly upregulated in human hepatocellular carcinomas with activating mutations in β-catenin and similarly in mouse intestines with increased Wnt signaling activity from mutations in *APC* (196). The *TRF2* gene was discovered to contain TCF-LEF transcription binding sites, where β-catenin was

also found to bind. Furthermore, when β-catenin was knocked down by siRNA approach, there was a marked decrease in TRF2 and telomere dysfunction, which was rescued by TRF2 overexpression. Depletion of TRF2 or disruption of TRF2 function in mice and in human cells (through knock-out models or overexpression of a dominant negative form of TRF2, respectively) has been shown to be deleterious, causing rapid telomere uncapping, loss of 3' G-rich overhangs, resulting in non-homologous end joining of chromosome ends (143, 197). In this thesis, I describe functional connections between telomeres and the Wnt pathway that align most closely with this last set of observations, i.e. a role for Wnt signaling in promoting expression of TRF2 and thus telomere capping. And furthermore, I present novel evidence that the regulation runs in the reverse direction as well, with telomere capping helping to support active Wnt signaling, thus describing a positive feedback loop between telomere capping and Wnt pathway activity.

MICRORNAS

Introduction to microRNAs

Less than 2% of the transcribed human genome codes for proteins. Non-coding RNAs (ncRNAs) are divided into two simple classes based on nucleotide length: long ncRNAs (lncRNAs) of transcripts longer than 200 nucleotides, and small ncRNAs less than 200 nucleotides in length. Among the small ncRNAs are microRNAs, Piwi-interacting RNAs, small nucleolar RNAs, tRNAs, short

interfering RNAs, and other RNAs. Of particular interest to this thesis is microRNAs, which are highly conserved across species and are important for the regulation of gene expression (198, 199).

Functional mature microRNAs are 18-25 nucleotide small RNAs that target specific and unique mRNAs for degradation or to inhibit mRNA translation. microRNAs are encoded by their own genes or from introns or exons (200). They are transcribed in the nucleus by RNA polymerase II or III into primary-microRNAs (pri-miRNAs), which are capped at the 5' end, and polyadenylated and spliced. Drosha (a ribonuclease) and DGCR8 (an RNA-binding protein) cleave the pri-miRNAs into the hairpin precursor miRNAs (pre-miRNAs), which are shuttled out of the nucleus by Exportin-5. In the cytoplasm, the RNAse Dicer, along with TRBP (a double-stranded RNA-binding protein), cleaves the loop from pre-miRNAs into a resulting 3' and 5' arm duplex, yielding the mature microRNA duplex (201, 202). The miRNA duplex contains a guide strand, which is ultimately loaded onto the RNA-induced silencing complex (RISC) with Argonaute (Ago2) proteins to direct the functional output of the miRNA, along with an imperfectly-complementary passenger strand (miRNA*), which is typically targeted for degradation (203, 204). When one arm of the duplex is found in much higher amounts and is the predominant guide strand, the asterisk indicates the mature miRNA on the other, less functional, arm (198). However, since in some cases, either the 5' or the 3' arm of the miRNA duplex (termed miRNA-5p or miRNA-3p, respectively) can act as a guide strand, depending on the cell type and the

condition, the -5p or -3p designation is becoming the preferred suffix over the asterisk.

An introduction of miRNAs is not complete without an overview of microRNA nomenclature. MIR refers to the gene encoding the microRNA (e.g. MIR-145) and uncapitalized “mir-“ refers to the pri-miRNA and pre-miRNA (e.g. mir-145), while the capitalized “miR-“ refers to the mature miRNA (miR-145). miRNAs with 1 or 2 nucleotide differences are annotated with a lower case letter (e.g. the sequence of miR-34a is similar to miR-34b and miR-34c, and they are all encoded by different genes). When different genes, pri-miRNAs or pre-miRNAs encode for identical mature miRNA sequences, they are annotated with a dash-number suffix (e.g. pre-miRNAs hsa-mir-194-1 and hsa-mir-194-2 both encode for hsa-miR-194). The species of origin is designated by a 3-letter prefix (e.g. mmu-miR-34a is from *Mus musculus* and hsa-miR-34a is from *Homo sapiens*) (205).

Only one strand of the miRNA duplex is generally loaded onto RISC, and selection of the guide strand is based on the thermodynamic stability of the 5’ ends. Generally, the strand with the less stable 5’ pairing to its complement is incorporated into RISC as the guide (206, 207). Argonaute proteins are important for the function of RISC. They directly bind to the mature miRNA with two RNA-binding domains: the PAZ domain that binds the 3’ end and the PIWI domain that binds the 5’ end of the mature miRNA (208). Argonaute proteins may directly cleave target mRNA transcripts with its endonuclease activity or recruit proteins that will inhibit mRNA translation. In humans, there are two families of Argonaute

proteins, the Ago subfamily (ubiquitously expressed in all mammalian cells) and the Piwi subfamily (expressed in germ cells and hematopoietic stem cells). Ago proteins associate with miRNAs and siRNAs while Piwi proteins associate with piRNAs. Perfect complementarity of miRNAs and target mRNA promotes Ago-mediated degradation of the mRNA, whereas partial complementarity promotes inhibition of mRNA translation or deadenylation (209).

Only ~seven nucleotides of the mature miRNA are required to have complementarity in order to recognize its target, and this is known as the seed region (210). The seed region is at nucleotide positions 2-7 of the mature miRNA, and mutations in the sequence has been attributed to several genetic disorders . Several other features also promote specificity of miRNA recognition to target mRNA (211). A single miRNA can have hundreds of target mRNAs. Attempts to identify miRNA targets include computational approaches to predict mRNA targets based on sequence complementarity, which can result in thousands of predicted targets for a single miRNA, and follow-up functional biological experiments to confirm target specificity is required but can be tedious. HITS-CLIP (high-throughput sequencing of RNA isolated by crosslinking immunoprecipitation) of Argonaute proteins have been able to identify mRNA targets of miRNAs (212).

microRNAs in Aging and Disease

Even though the field of non-coding RNAs is relatively new – with the initial discovery of the miRNA, *lin-4*, in *C. elegans* in 1993 (213), followed by the discovery of *let-7* in 2000 (214) – it is now widely recognized that miRNAs play

important roles in development, aging, and disease. miRNAs fine tunes and does not completely turn off gene expression, and they have been shown to affect gene expression by only 1.2 to 4-fold (215). New miRNAs are still being discovered (approximately 500-1000 have been found by RNA-seq), and we have only begun to scratch the surface in revealing what regulates them and what their functions are. There is a huge need but a lack of a high-throughput approach to evaluate the functional role of miRNAs. Currently, the most common approaches to evaluate miRNA changes is with miRNA microarrays, and *in silico* analyses are used to predict mRNAs targeted by miRNAs, confirmed by functional studies overexpressing, knocking-out, or knocking-down specific miRNAs knocking-down miRNAs.

The profile of miRNAs during aging and senescence is still relatively obscure but of great interest, and several investigators have begun to characterize them. There are common miRNAs that are upregulated and downregulated in different tissues and conditions of aging. In a number of *in vitro* and *in vivo* studies across species and tissues, the most commonly and consistently upregulated miRNA with age is miR-34a (216-220). Overexpression of miR-34a has contributed to accelerated senescence and cell cycle arrest in multiple cell lines (221-226). Furthermore, miR-34a has been found to play a significant role in aging and the lifespan of *C. elegans*, and loss of function of miR-34a delays age-related pathology, reduces oxidative stress and extends lifespan (227). Other notable miRNAs that are upregulated with aging are miR-181, miR146a, miR-195, the miR-200 family members, among others (228, 229).

There are also miRNAs that are consistently downregulated with aging from *C. elegans* to multiple human cell types, such as the miR-17-92 cluster, which encode for six mature miRNAs, one of which (miR-19) targets PTEN and activates the AKT/mTOR pathway, a key pathway involved in lifespan regulation. The paralogous clusters of miR-17-92, which are miR-106a-366 and miR-106b-25, are also downregulated in replicatively senescent cells and aged human tissues (230, 231). Many of the miRNAs upregulated in aging are also involved in inflammatory processes and cancers, such as miR-146a and miR-181 family members (215). It is interesting to note that the same miRNA can be upregulated in some cancers and downregulated in other cancers (e.g. miR-181 family members are upregulated in breast and colorectal cancer but downregulated in glioblastomas and prostate cancer) (232-235).

In summary, telomeres are important for genome stability, cancer and aging, and we do not yet fully comprehend their roles nor the underlying mechanisms. We have found evidence for a positive feedback loop between telomere capping and Wnt pathway activity in the small intestinal stem cell niche, which can also be described as a circuit in which telomere uncapping drives downregulation of the Wnt pathway. Consistent with this idea, and the established role for p53 in mediating DDRs in response to uncapped telomeres, we have found some evidence that the p53-regulated microRNA miR-34a plays roles in downregulating the Wnt pathway in this setting.

CHAPTER 2: GENERAL METHODS

Study Design

Histologic comparisons of WT, G2, and G4 *mTR*$^{-/-}$ mice were made between groups each having similar average age, and all mice were younger than 12 months. RNA samples for microarray analysis and qRT-PCR validation were obtained from WT and G4 *mTR*$^{-/-}$ mice aged 7-8 months. For each of the lithium and Rspo1 treatment experiments, littermates were divided equally into the control and treatment groups. Comparisons were made between littermates to minimize differences in inherited telomere lengths. For cultured crypts experiments, G4 *mTR*$^{-/-}$ mice aged 3 months or younger were used because survival of crypts dropped precipitously beyond this age.

Mice

All mice were on the C57BL/6J background, and *mTR*$^{+/-}$ mice were crossed to generate G1 *mTR*$^{-/-}$ mice, which were crossed to generate G2 mice, and so forth (135). A male *miR-34a*$^{-/-}$ breeder was initially obtained from Jackson Laboratories and crossed with *mTR*$^{-/-}$ mice. All studies were approved by the University of Pennsylvania Institutional Animal Care and Use Committee (IACUC). The mice were housed in a standard animal care room with 12:12-h light-dark cycle with free access to food and water. For lithium treatment, mice were given an *ad libitum* lithium-chow diet of 0.212% lithium chloride-supplemented chow (Harlan Teklad, Madison, WI) for 3 days, followed by 0.4%

lithium chloride-supplemented chow for 7 days. Lithium chow-fed mice were given a supplemental source of drinking water containing 1.5% (w/v) sodium chloride to counteract potential toxicities of lithium. For Rspo1 experiments, mice are injected at 4 µg Rspo1 (in PBS, or PBS alone for controls) per gram body weight subcutaneously daily for 8 days. RSpo1 was expressed and purified as described (236).

Cell lines

Primary human fibroblasts were obtained from the Coriell Institute. The two dyskeratosis congenita (DC) lines were: GM01774 (population doubling level (PD) 25; from 7 year-old male), and AG04646 (PD 21; from 11 year-old male). The three healthy control (WT) lines were: GM01786 (PD 25; 30-year old mother of GM01774), GM00409 (PD ~16; from 7 year-old male), and GM00323 (PD 23.6; from 11 year-old male). The Werner syndrome line was AG05229B (PD ~30; from 25 year-old male), which was retrovirally transduced with pBABE-puro-hTERT, or with the empty pBABE-puro vector as a control. Fibroblasts were cultured in DMEM with 15% FBS, with 1X penicillin/streptomycin/amphotericin-B at 37^{o}C in a 6% $C0_2$ and 3% O_2 atmosphere.

Tissue histology

Standard five-micron sections were cut from formalin-fixed and paraffin-embedded samples. *In situ* hybridization for *Ascl2* was as described (237), and immunostaining for Sox9 and for Ki67 used Millipore AB5535 and Abcam Ab16667 antibodies, respectively. TUNEL assays were performed using the

ApopTag Peroxidase In Situ apoptosis Detection Kit (Chemicon). Images within each set of staining were taken with identical settings on a Nikon Eclipse E600 microscope. Brightness and contrast were adjusted post-capture in a linear and equal fashion for all samples. 120 crypts per mouse from hematoxylin and eosin (H&E) stained sections were surveyed for the presence of anaphase bridges.

Isolation of intestinal crypt and stromal cells for microarrays

8 cm of ileum was longitudinally cut and rinsed in cold PBS, followed by firm scraping of intestinal villi with hemacytometer coverslip, incubation in 10 ml 30 mM EDTA and 1.5 mM DTT in PBS on ice for 20 minutes. The intestine was transferred to 10 ml 30 mM EDTA in PBS at 37°C for 8 minutes, followed by 3 rounds of shaking per second for 30-40 seconds. The supernatant was centrifuged at 200 g for 1 minute at 4°C, followed by passage through a 70 μm cell strainer. The strained supernatant was spun down again at 130 g for 1 minute at 4°C to deplete single cells, and the crypt pellet was collected for RNA extraction. The remaining intestinal tissue is scraped with a coverslip to remove residual epithelial cells and is mechanically homogenized with a TissueRuptor (Qiagen) before RNA extraction.

Crypt culture

Intestinal crypts used for culturing were isolated from the proximal half of the small intestine as described (180), except that the intestinal fragments were incubated with 30 mL of 30 mM EDTA in PBS for 15 minutes on ice, with occasional inversion. Isolated crypts were cultured in Matrigel (BD Biosciences)

with advanced DMEM/F12 medium containing final and basal concentrations of 100 ng/mL noggin, 50 ng/mL mEGF, and 1 µg/mL RSpo1 (higher levels of RSpo1 were used for some experiments as indicated). Approximately 500 crypts/50 µL of Matrigel were plated per well in a pre-warmed 24-well plate and cultured at 37^{o}C in a 6% CO_2 incubator with ambient O_2. CHIR99021 (Tocris Biosciences) was prepared as a 2 mM stock solution in DMSO.

RNA extraction

All RNA extractions were performed with the miRNeasy Kit (Qiagen). RNA quantity and quality were confirmed with Nanodrop spectrophotometry or Agilent Bioanalyzer 2100 with either the Agilent RNA 6000 Nano or Pico kits.

Quantitative RT–PCR

Reverse transcription was performed with miScript II RT Kit (Qiagen) according to the manufacturer, using miScript HiFlex buffer. This allows for the qRT-PCR analysis of both microRNAs and mRNAs. The ability of the miScript II RT Kit to detect mRNAs was confirmed by simultaneous reverse transcription reactions with MultiScribe Reverse Transcriptase (Life Technologies). Real-time PCR was performed on a Roche LightCycler 480 using SYBR Green JumpStart Taq ReadyMix (Sigma). Reactions (10 mL) were performed in triplicate, as follows: 10 minutes at 95^{0}C, 45 cycles of 15s at C95^{o}C, 30s at 59^{o}C, 30s at 72^{o}C. Melt curve and gel electrophoretic analyses were performed to verify specific target amplification. Amplification from experimental samples was normalized to standard curves that were made from dilutions of pooled samples. Cp values

from each amplification curve were computed by the second-derivative method, the mRNA expression levels were normalized to that of β-actin, and the mature miRNA expression levels were normalized to that of RNU6. Primer sequences are provided in the Tables section. Student's t-tests were used for comparisons, except that a 2-way ANOVA (multiple comparisons) was used for statistical analyses of human fibroblasts, comparing the gene expression at each dose of CHIR99021 to no drug within each genotype.

Statistics

p-values were calculated with Prism. Unpaired t-tests assuming equal population SD were performed unless specified.

CHAPTER 3: WNT-SPECIFIC ISC MARKERS ARE DOWNREGULATED IN MICE WITH DYSFUNCTIONAL TELOMERES WITHOUT APPARENT LOSS OF CBCS

INTRODUCTION

Stem cells of the GI tract are located in specific regions: the crypt base of the small intestine, the mid-crypt of the ascending colon, and the crypt base of the descending colon (238). Characterization of intestinal stem cells in *mTR*$^{-/-}$ mice has mostly been described in the small intestine despite pathology existing in the colon as well, most likely because murine models of intestinal cancers have the most pronounced phenotype in the small intestines (in contrast to human intestinal cancers, which are predominantly in the colon) (239). We also focus our studies on the small intestine of *mTR*$^{-/-}$ mice. The small intestine is divided into 3 different parts, the duodenum, jejunum, and ileum, and these distinctive parts are difficult to distinguish grossly in mice, although their location along the small intestine roughly corresponds to thirds by length (i.e. duodenum makes up the first third of the small intestine, and so on). The small intestinal epithelium is composed of villi that project into the lumen and intestinal crypt invaginations. There exists a crypt-villus axis that reflects the differentiation state of the cells. There also exists a gradient of decreasing Wnt signals and increasing BMP signals along the crypt-villus axis, which has been suggested to contribute to the stemness/differentiation state of cells along the axis (172). Each crypt comprises approximately 250 cells, containing ISCs and Paneth cells at or near the crypt base (240). Each crypt of the small intestine has a remarkable

capacity to divide and give rise to cells that differentiate into several lineages that contribute to the epithelium of 2-3 villi. ISCs give rise to rapidly-cycling progenitor cells called transit-amplifying (TA) cells, which differentiate terminally into absorptive enterocytes, goblet cells, Paneth cells, enteroendocrine cells, and other cells. In the mouse small intestine, the movement of cells is from the base of the crypt to the villus tip except for Paneth cells, which are anchored at the base of the crypt . The small intestinal epithelium in mice turns over approximately every 3-5 days, and epithelial cells are shed from villus tips into the lumen (241).

As mentioned briefly in the introduction, two types of ISCs exist, the fast-cycling CBCs at the base of the crypt and the slow-cycling LRCs at the +4 to +7 position from the base of the crypt (they have also been called +4 LRCs). There is an estimated number of 15 CBCs per crypt (242). It has been suggested that LRCs serve as a stem cell reserve pool, and can divide into CBCs to replace damaged/dying CBCs (178, 243). There is also evidence that CBCs have the potential to convert into LRCs (244). Both CBCs and LRCs share some common stem cell markers, but they are also driven by different signals (e.g. CBCs are driven predominantly by Wnt signaling) and have distinct stem cell signatures (241). There is no consensus in regards to what markers define the putative stem cell populations, as there is some controversy in how some have determined the stem cell signature (i.e. based on their position within the crypt, or lineage tracing, etc.) (241). However, there is agreement that *Lgr5* is a specific CBC marker, and that is both a direct Wnt target gene and is itself a Wnt receptor at the cell

membrane (245-247). Gene expression analysis of Lgr5-EGFP crypt cells has determined a signature of CBCs, and identifies *Ascl2* (another Wnt target gene) and *Olfm4*, an indirect Wnt target gene (itself a target gene of *Ascl2*), as robust CBC markers (237, 245). Visualization of single mRNA transcripts by in situ hybridization confirmed that *Lgr5* and *Ascl2* are exclusively expressed in CBCs, while *Olfm4* and *Musashi-1* (*Msi1*) have a broader expression, with *Msi1* extending into the TA cells (248, 249). Many +4 LRC markers have been proposed, with *Bmi1* being the first marker that was described. Bmi1+ cells are distinct from Lgr5 cells, are relatively quiescent, and are independent of Wnt signaling. *HopX*, *mTert*, *Lrig1*, and many other genes have been described to mark +4 LRCs, but there is a lot of evidence that suggest their broad expression in other cell types (241, 249). For example, Lgr5+ cells have the highest levels of endogenous telomerase activity in the crypt (250).

Intestinal stem cell (ISC) exhaustion has been hypothesized to underlie compromised epithelial integrity in late-generation telomerase-deficient mice. We therefore investigated ISC marker gene expression in these mice. Further, as mentioned in the introduction, because the TERT protein has been suggested to have functions beyond telomere maintenance (99), we examined *mTR*-deficient mice (lacking only the telomerase RNA template) to avoid any such non-telomeric effects and instead focus on the consequences of telomere dysfunction.

METHODS

Microarray target preparation, hybridization and analysis

Microarray experiments were conducted by the University of Pennsylvania Molecular Profiling Facility, including quality control tests of the total RNA samples by Agilent Bioanalyzer and Nanodrop spectrophotometry. Crypt and stromal RNA was obtained, respectively, from three or two wild type and three or four G4 *mTR*$^{-/-}$ mice, with samples from each mouse analyzed on an individual array. All protocols were conducted as described in the Ambion WT Expression Manual and the Affymetrix GeneChip Expression Analysis Technical Manual, using 250 ng of total RNA for first-strand cDNA synthesis. cDNA yields ranged from 9.4-10.7 µg, and 5.5 µg of labeled cDNA was hybridized to Mouse Gene 1.0ST GeneChips, stained with streptavidin-phycoerythrin, and visualized with a GeneChip 3000 7G scanner. Affymetrix probe intensity (.cel) files were imported into Partek Genomics Suite (v6.6, Partek Inc., St. Louis, MO) where RMA normalization was applied. The resulting log2-transformed intensities were filtered to exclude the IDs corresponding to technical controls, and analyzed for differential expression using SAM (Significance Analysis of Microarrays, samr v2.0, Stanford University (251)), generating q-values (False Discovery Rate) and fold change for each Transcript ID.

Heat map and gene set enrichment analysis (GSEA):

Heat maps were generated with Multiple Experiment Viewer (MeV) (252) v4.8.1 from the Dana-Farber Cancer Institute. GSEA (253) v2.0.13 from the Broad Institute was used to identify significant enrichments in the microarray data. The C2 collection containing 4850 curated gene sets from the Molecular Signature

Database (MSigDB) v3.1 was used to identify enriched pathways in WT vs. G4 *mTR*$^{-/-}$ crypts. Chip2Chip was used to translate gene identifiers from the C2 collection to the Affymetrix Mouse Gene 1.0ST probeset IDs. GSEA was performed as follows: $\log_2$-transformed RMA values from each individual sample were used for the expression dataset. Parameter details are as follows: Permutations: 1000, 'Collapse dataset' = FALSE, Permutation type = gene_set, Max size = 5000, Min size = 1. GSEA was also performed using user-defined gene sets from the transcriptomic profile of ISCs or downregulated genes in Lgr4/5 KO crypts, described as follows. 361 genes out of 379 genes defined as the transcriptomic profile of Lgr5+ ISCs on the Affymetrix platform (249) matched the Affymetrix Mouse Gene 1.0ST platform that was used for measurements, and these were used to generate the heat map and GSEA enrichment plot. We also used the 125 genes out of 135 genes defined as the ISC transcriptome (237) that matched our microarray platform. For the gene set describing downregulated genes in Lgr4/5 KO crypts (167), 259 of 306 genes from the array platforms matched the Affymetrix platform and were used in GSEA. GSEA was performed for proliferating (PD32) and replicatively senescent (PD88) IMR90 cells using publicly available Gene Expression Omnibus (GEO) dataset GSE36640 (83). Chip2Chip was used to translate gene identifiers from the C2 collection to the Affymetrix Human Genome U133 Plus 2.0 Array. GSEA was performed as follows: raw dataset values from each individual sample were used for the expression dataset. Parameter details are as follows: Permutations: 1000, 'Collapse dataset' = FALSE, Permutation type = gene_set, Max size = 10000,

Min size = 5, and 4721 out of 4722 C2 collection of gene sets from MsigDB v4.0 passed the criteria for analysis.

RESULTS

ISC abnormalities in mice with dysfunctional telomeres are specific to Wnt-responsive stem cell markers

Crypt epithelium and underlying stroma were each isolated from wild type (WT) and G4 *mTR*$^{-/-}$ mice and used for mRNA expression profiling. Gene set enrichment analysis (GSEA) (253) allowed us to take an unbiased approach to determine which gene sets amongst the 4000+ curated gene sets in the Molecular Signature Database are significantly down or upregulated in our G4 *mTR*$^{-/-}$ crypts. One of the sets most significantly downregulated in the mutant crypts is that with genes similarly downregulated in crypts upon deletion of β-catenin, the key mediator of Wnt signaling between the cytoplasm and nucleus (NES -2.27, FDR <0.0001; Table 3.1 and Figure 3.1). Also significantly downregulated were gene sets involved in stem cell maintenance (*TLX*-dependent) and cell cycle progression (*E2F3*-dependent), consistent with stem cell defects.

Table 3.1. Gene set enrichment analysis (GSEA) of G4 *mTerc*$^{-/-}$ versus WT intestinal crypts. Top 5 gene sets downregulated in G4 *mTerc*$^{-/-}$ crypts compared to WT crypts as determined by GSEA, using the C2 (curated) database of gene sets published in the Molecular Signature Database version 3.1.

Gene set name in MSigDB	Enrichment Score	Normalized ES	FDR	Gene set description
ZHANG_TLX_TARGETS_UP	-0.75	-2.41	0.000	Genes upregulated in neural stem cells after cre-lox TLX knockout
FEVR_CTNNB1_TARGETS_DN	**-0.58**	**-2.27**	**0.000**	**Genes downregulated in intestinal crypt cells upon β-catenin deletion**
PUJANA_XPRESS_INT_NETWORK	-0.65	-2.36	0.000	Intersection of genes correlating with BRCA1, BRCA2, ATM, and CHEK2 in normal tissues

REN_BOUND_BY_E2F	-0.69	-2.32	0.000	Genes whose promoters were bound by E2F1 and E2F4 by ChIP in WI-38 fibroblasts
PUJANA_BRCA_CENTERED_NETWORK	-0.66	-2.31	0.000	Genes constituting the BRCA-centered network (genes potentially associated with higher breast cancer risk)

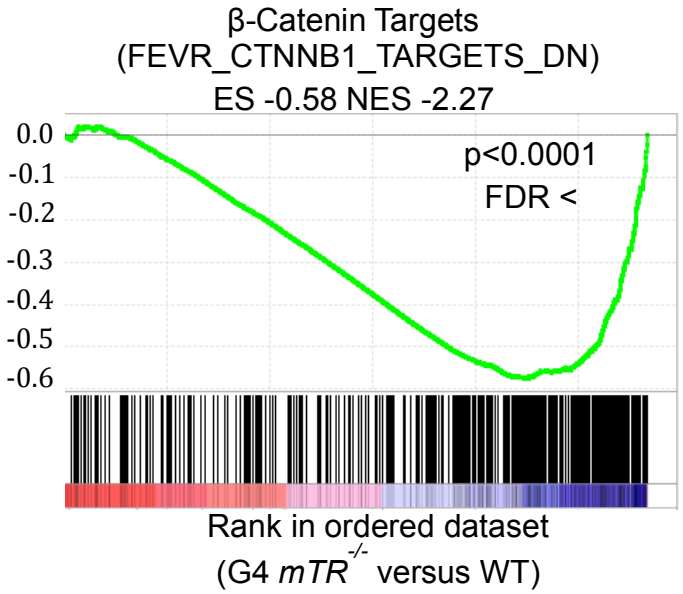

Figure 3.1. Gene set enrichment analysis plots of G4 *mTR*$^{-/-}$ versus WT intestinal crypts. GSEA plot comparing genes with altered expression in the intestinal crypts of G4 *mTR*$^{-/-}$ mice *vs* those downregulated in b-catenin knockout mice (FEVR_CTNNB1_TARGETS_DN)

Examination of Wnt-dependent ISC gene expression, including *in situ* hybridization for *Ascl2* mRNA (CBC-specific) and immunofluorescent staining for Sox9 protein (expressed in CBCs and transit amplifying (TA) cells) revealed dramatically decreased expression in late generation (G4) *mTR*$^{-/-}$ mice (Figure 3.2). There was no difference in the expression of Msi1 protein, an ISC marker that is expressed in a Wnt-independent fashion in +4 LRCs and that persists into CBCs (254, 255) (Figure 3.2). The minimal changes in *Ascl2* and Sox9 expression in G2 mice indicates the defective expression is caused by dysfunctional telomeres rather than telomerase deficiency *per se*.

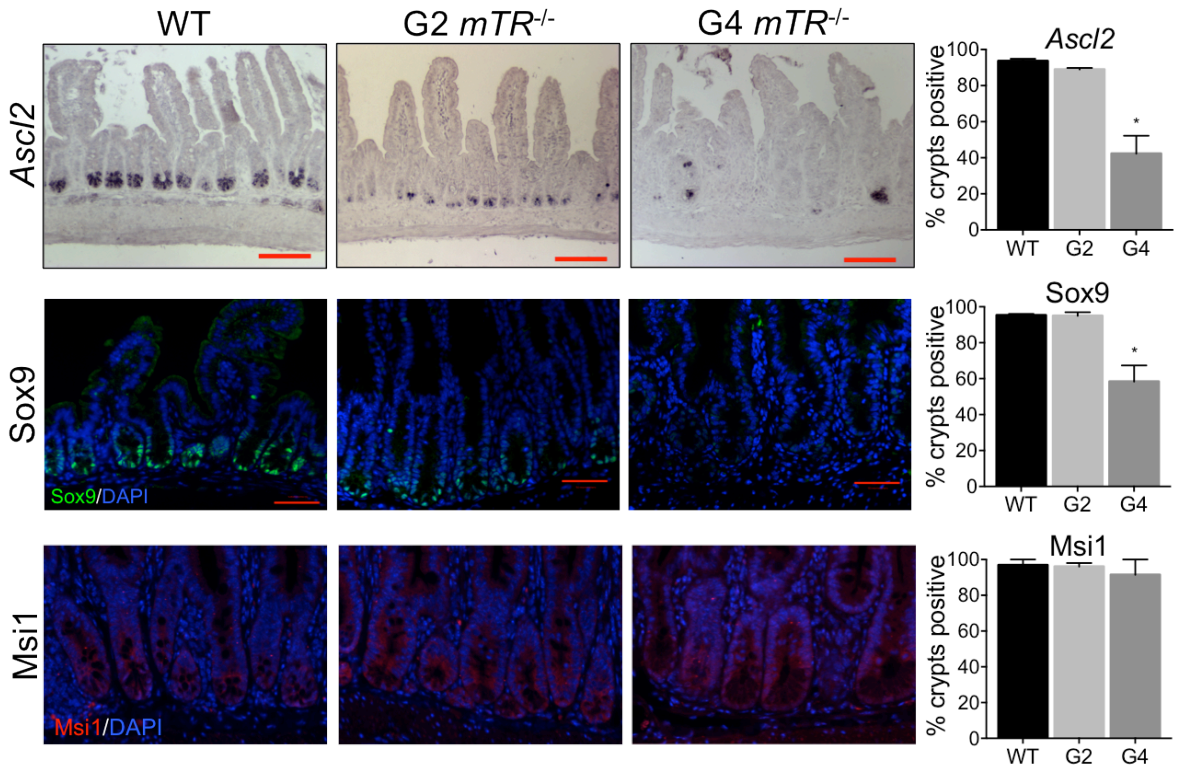

Figure 3.2. Defects in small intestinal Wnt-dependent stem cell markers in late-generation *mTR*$^{-/-}$ mice. *In situ* hybridization for *Ascl2* transcripts (top panel) and immunostaining for Sox9 (middle panel) and Msi1 (bottom panel) in ileum from wild-type and G2 and G4 *mTR*$^{-/-}$mice. N = 3 mice of each genotype for *Ascl2* and Msi1 staining; N = 5 WT mice, 2 G2 mice, and 4 G4 mice for Sox9 staining, * $p<0.05$. Scale bars: 100μm (top) and 50μm (middle and bottom).

Since multiple cell types (Paneth cells, +4LRCs, CBCs, TA cells) reside in crypts, changes in expression profiling could reflect gene expression changes in several cell populations or in a single cell type, or it could reflect a change in the composition of cells that make up the crypt. We wanted to determine whether the alteration in expression profiling reflects a change in a specific pathway (i.e. beta-catenin) or a change in the cellular makeup of the crypt. Staining for lysozyme-positive granules characteristic of Paneth cells revealed neither loss of these cells nor of interposed cells (Figure 3.3), which is where CBCs reside in normal mice. Thus, the diminished expression of CBC marker genes apparently reflects

changes in the state, rather than the presence, of CBCs. This conclusion was also supported by several additional findings, as described below. There were also no significant changes in genes expressed in +4LRCs including *Bmi1, mTert, Hopx,* and *Lrig1* (Figure 3.4). Because +4LRCs are independent of Wnt, this suggests maintenance of some or all Wnt-independent pathways in the mutants. We conclude that expression of at least some CBC-specific genes targeted by the canonical Wnt pathway is compromised in mice with dysfunctional telomeres caused by generations of telomerase deficiency.

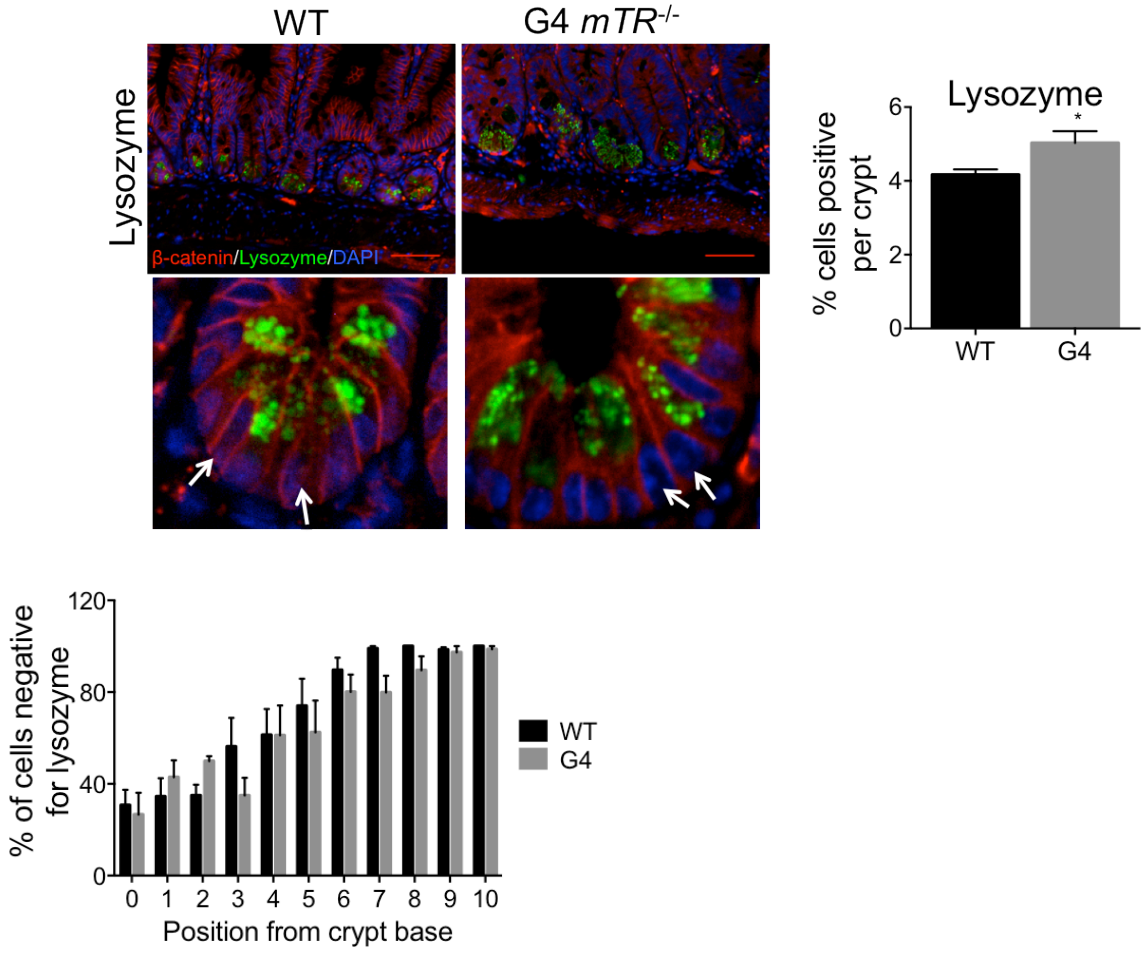

Figure 3.3. CBCs numbers are unchanged in wild-type and G4 *mTR*$^{-/-}$ ileum. Immunostaining for Paneth cell lysozyme in wild-type and G4 *mTerc*$^{-/-}$ ileum and β-catenin staining marks cell peripheries (top panel). (Middle panel) The enlarged

insets show examples of cells at the normal CBC location between lysozyme-positive Paneth cells. Quantitation of Paneth cell counts (top right panel) and intercalated cells (bottom panel) from wild-type and G4 *mTR*$^{-/-}$ crypts. N = 6 of each genotype for lysozyme staining, * p<0.05. Scale bars: 50μm.

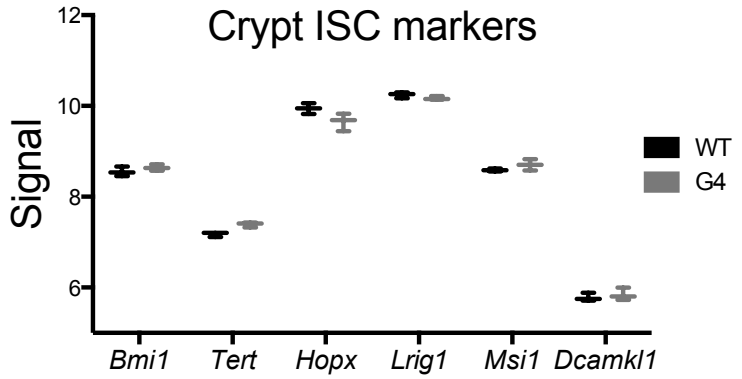

Figure 3.4. Wnt-independent ISC marker gene transcript levels are unchanged in intestinal crypts of *mTR*$^{-/-}$ mice. Microarray signals of Wnt-independent ISC marker genes in WT and G4 *mTR*$^{-/-}$ crypts.

Broadly abnormal expression of Wnt pathway genes in G4 *mTR*$^{-/-}$ crypt epithelium and underlying stroma.

Wnt ligands produced by stromal and Paneth cells provide support essential to CBC function (177). Because *Ascl2 and Sox9* are direct targets of the Wnt signaling pathway, we hypothesized that their diminished expression in G4 *mTR*$^{-/-}$ crypts reflects a defect in the Wnt pathway caused by telomere dysfunction. qRT-PCR was used to verify the altered expression of a number of the Wnt pathway and target genes, including *Wnt3*, *Lrp6, and Lgr5* (Figure 3.5). The decline in *Wnt3* transcripts is particularly revealing, because it occurred even though 1) Paneth cells are the only apparent intestinal source of Wnt3 (177), and 2) there is no loss of Paneth cells in G4 *mTR*$^{-/-}$ crypts (Figure 3.3), thus confirming downregulation of Wnt pathway genes independent of cell losses.

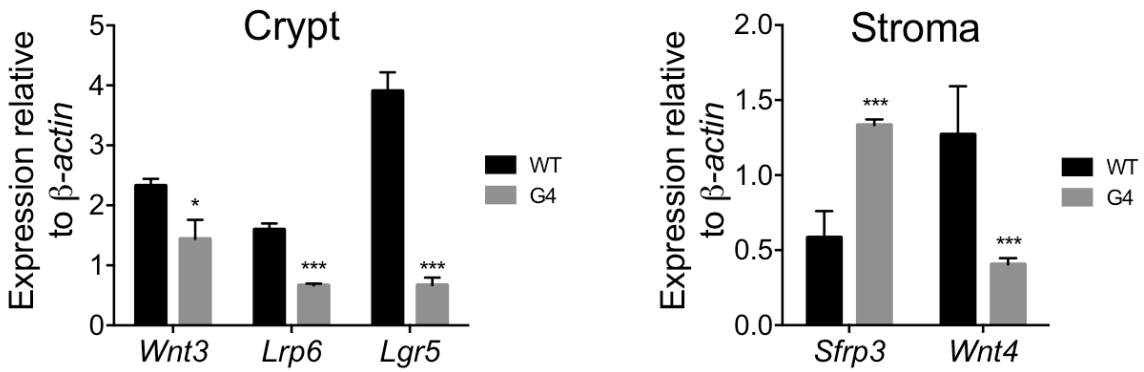

Figure 3.5. G4 *mTR*$^{-/-}$ mice have reduced expression of pro-Wnt pathway genes in ileal crypts and stroma. qRT-PCR analyses of gene expression for the Wnt ligand (*Wnt3*), Wnt co-receptor (*Lrp6*), and Wnt target gene (*Lgr5*) in WT and G4 *mTR*$^{-/-}$ crypts (left). qRT-PCR analyses of gene expression for the Wnt ligand (*Wnt4*) and Wnt receptor inhibitor (*Sfrp3*) in WT and G4 *mTR*$^{-/-}$ stroma (right). N = 4 mice per genotype, * $p<0.05$, *** $p<0.005$.

In the stroma, expression changes were also consistent with decreased Wnt pathway activity, including upregulation of several of the SFRP Wnt antagonists (Figure 3.5 and 3.6). Several Wnts and cell surface receptors (Fzds) were also downregulated in G4 *mTR*$^{-/-}$ crypts (Figure 3.6). qRT-PCR confirmed the altered expression of *Sfrp3* and *Wnt4* (Figure 3.5). Collectively, the data from epithelium and stroma indicate broad suppression of Wnt pathway components in G4 *mTR*$^{-/-}$ intestinal tissues.

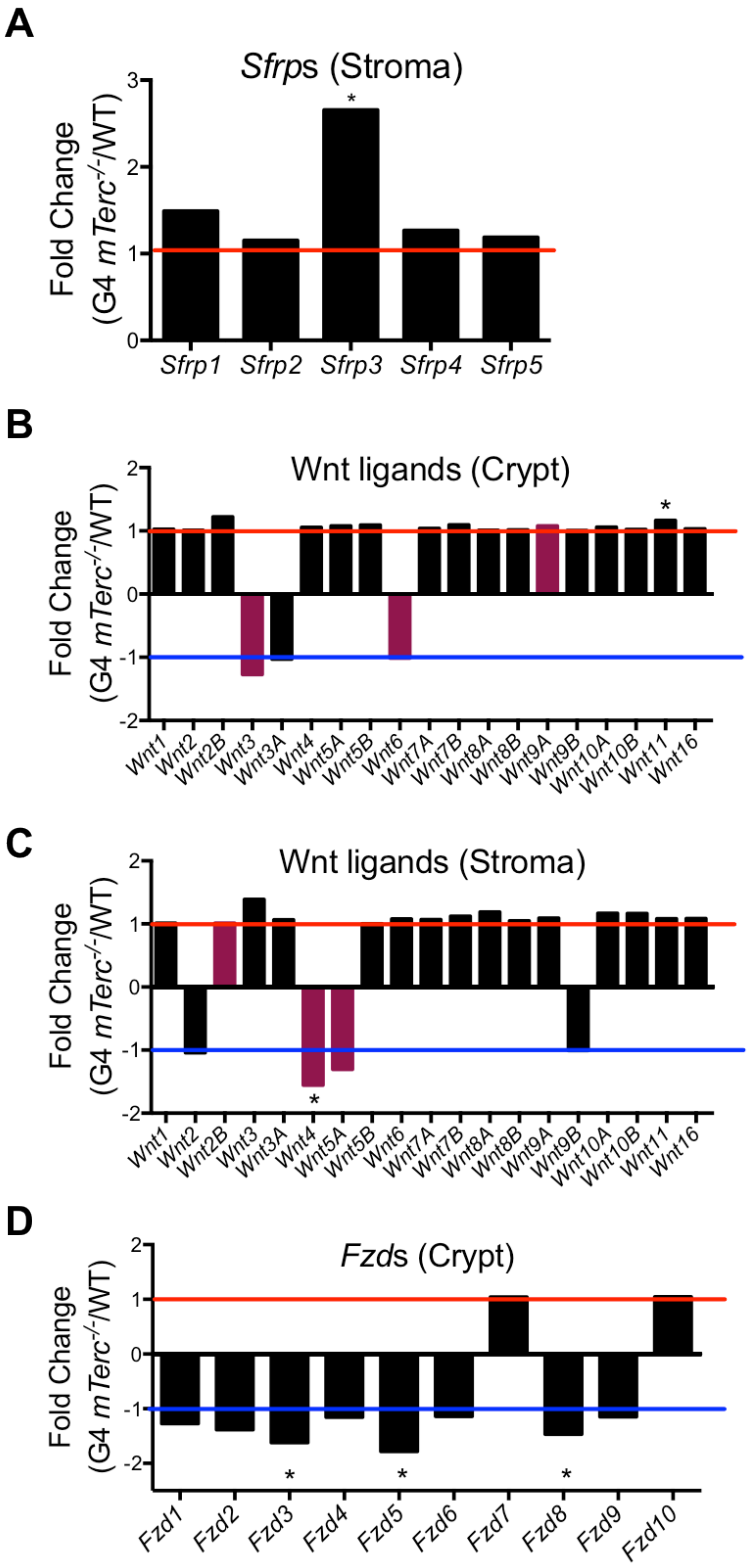

Figure 3.6. Microarray gene profiling of the small intestinal stroma and epithelium of WT and G4 *mTR*$^{-/-}$ crypts. Affymetrix Mouse Gene 1.0ST microarray analyses of mRNA levels were performed on crypts or stroma each isolated from wild-type and G4 *mTR*$^{-/-}$ mice. Examples indicating downregulation of multiple Wnt pathway genes (i.e. Wnt ligands and receptors) and upregulation of Wnt ligand inhibitors (i.e. stromal SFRPs) in G4 *mTR*$^{-/-}$ intestine, which support the GSEA analyses (see Figure S3). (A) Fold changes of SFRPs (Wnt ligand inhibitors) in G4 *mTR*$^{-/-}$ intestinal stroma. (B) Fold changes of Wnt ligands in G4 *mTR*$^{-/-}$ intestinal crypts and (C) stroma; Wnt ligands known to be expressed in robust amounts in each compartment are highlighted in *purple*. (D) Fold changes of *Fzd* genes (Wnt ligand receptors) in G4 *mTR*$^{-/-}$ intestinal crypts. * p<0.05

Based on defects in G1 *mTert*$^{-/-}$ but not G1 *mTR*$^{-/-}$ mice, Park et al. (99) have suggested that Tert but not TR regulates Wnt signaling, and does so independent of its telomere-lengthening function. As discussed in the introduction, this idea has been questioned, and moreover is a story that is quite separate from ours. First, our mice are genetically deficient for *mTR* and not *mTert,* and indeed levels of *mTert* transcripts were not decreased in late-generation *mTR*$^{-/-}$ crypts (Figure 3.4), consistent with published findings (256). Second, the suppression of Wnt pathway gene expression progressed with successive generations of telomerase deficiency (Figure 3.2), confirming that telomere dysfunction, rather than telomerase deficiency *per se* causes the suppression.

We wanted to see if telomere dysfunction induces Wnt signaling suppression in other cell types as well, and we mined the GEO database for expression profiles of cells with telomere dysfunction, and we focused on a dataset that compared early-passage proliferating to replicatively senescent IMR90 fibroblasts (83). GSEA reveals that Wnt pathway gene sets are significantly downregulated within cells that have senesced due to telomere shortening (Table 3.2). Similarly, the expression of Axin2 (the ubiquitous and canonical Wnt target gene in all cells) was significantly decreased in primary human fibroblasts from patients with telomere dysfunction, namely dyskeratosis congenita (Figure 3.7). Furthermore, in primary human fibroblasts with Wrn mutations (which causes telomere dysfunction), Axin2 expression is rescued once telomere capping is restored (with hTERT overexpression) (Figure 3.7).

These data strongly support that telomere dysfunction result in a suppression of Wnt signaling.

Table 3.2. Gene set enrichment analysis (GSEA) of Wnt pathway related gene sets significantly enriched in proliferating versus replicatively senescent IMR90 cells. Wnt pathway related gene sets enriched in proliferating (PD32) as compared to senescent (PD88) IMR90 cells (from GSE36640 dataset of GEO), as determined by GSEA using the C2 (curated) database of 4722 gene sets as published in the Molecular Signature Database version 4.0.

Gene set name in MSigDB	Enrichment Score	Normalized ES	FDR	Gene set description
FEVR_CTNNB1_TARGETS_DN	**0.64**	**2.16**	**0.000**	**Genes downregulated in intestinal crypt cells upon β-catenin deletion**
LABBE_WNT3A_TARGETS_UP	0.55	1.69	0.005	Genes upregulated in NMuMG cells after Wnt3a stimulation
FIRESTEIN_CTNNB1_PATHWAY	0.65	1.67	0.006	Genes required for and β-catenin activation in APC colon cancer cells
FIRESTEIN_CTNNB1_PATHWAY_AND_PROLIFERATION	0.75	1.67	0.006	Genes required for proliferation and β-catenin activation in APC colon cancer cells

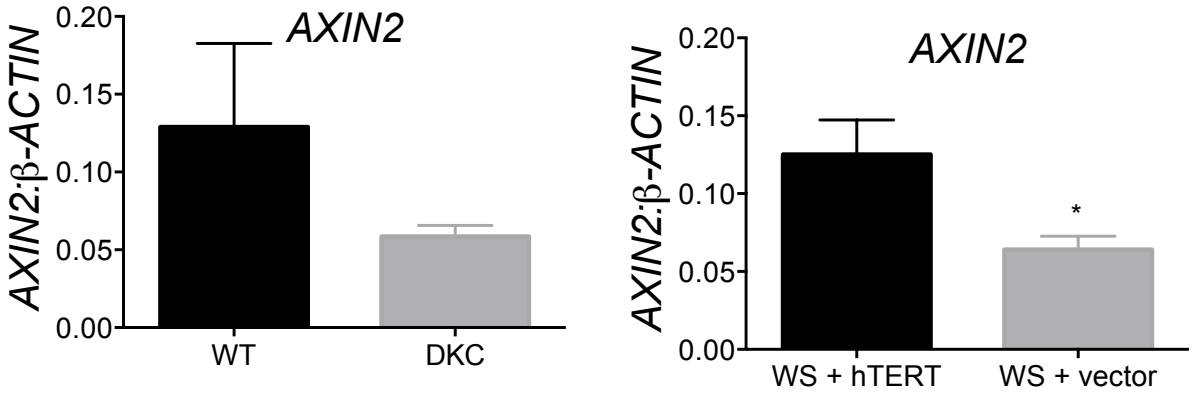

Figure 3.7. qRT-PCR analysis of Axin2 expression in primary human fibroblasts with telomere dysfunction. Expression of *AXIN2* mRNA levels in primary human fibroblasts from (left panel) three healthy people (WT) and two people with dyskeratosis congenita (DC), and (right panel) a person with Werner syndrome (WS) infected with retrovirus expressing hTERT or a vector control. * $p<0.05$

DISCUSSION

Our study reveals that loss of telomere capping can lead to broad suppression of Wnt pathway components and activities in the mouse intestine. Expression of multiple Wnt pathway genes, from those encoding Wnt ligands and receptors, to those that are targets of Wnt-dependent transcription factors, is reduced in the intestinal crypts of late generation *mTR*$^{-/-}$ mice. The changes are most pronounced in crypt epithelium, but also occur in the underlying stroma, including enhanced expression of Wnt pathway inhibitors, which may contribute to inhibition of signaling. The progressive nature of these changes with increasing generation of *mTR*$^{-/-}$ mice, indicates that uncapped telomeres are the basis for Wnt suppression, rather than telomerase deficiency *per se*.

We considered the possibility that the Wnt pathway suppression might be secondary to losses in cells expressing these genes, rather than downregulation in extant cells. Our observations argue against this. First, *Wnt3* transcript levels decline in the intestinal epithelium of G4 *mTR*$^{-/-}$ mice, even though Paneth cells, which are the sole expressors of *Wnt3* in this tissue, are not lost. Second, even though the expression of CBC marker genes (e.g. *Lgr5, Ascl2, Sox9*, all of which are Wnt-dependent) declined, there were no losses of cells intercalated between Paneth cells, which is where CBCs reside, indicating a change in CBC state rather than survival. We emphasize that because the defining gene expression signature of CBCs depends entirely on Wnt pathway genes, it is not possible to use such expression to enumerate CBCs in the G4 mice. Third, we observed a gradual loss in *Ascl2* and Sox9 levels in earlier generations of *mTR*$^{-/-}$ mice (e.g.

intermediate losses in G2 mice; Figure 3.2), indicating declines in expression precede frank losses. Fourth, examination of microarray expression data from proliferative and replicatively senescent IMR90 fibroblasts (83) reveals that Wnt pathway gene sets are significantly downregulated within cells that have senesced due to telomere shortening (Table 3.2), and such downregulation occurs in a setting where changes in gene expression cannot be explained by cell losses.

It would be ideal to explore changes in gene expression specific to a single cell type (i.e. CBCs) with telomere dysfunction, since the crypt contains many populations of cells and the changes we detect may reflect changes in more than one cell type. We considered crossing mice with reporters for ISC-markers (e.g. *Lgr5-EGFP* or *Axin2-TdTomato* mice) onto our *mTR*$^{-/-}$ mice to sort out CBCs and perform expression profiling on an enriched population of CBCs. However, since there are no known Wnt-independent markers specific to CBCs (241), and the phenotype we observe is a suppression in Wnt signaling, we would be sorting and selecting for a population of CBCs that have strong Wnt signaling and not as severe a phenotype as we would otherwise see.

Given these constraints, we have proposed future experiments that may address some of the pitfalls in the design of our original experiments. To address whether acute telomere uncapping results in Wnt pathway suppression, we have recently developed a system of where we can acutely induce telomere dysfunction in organoid cultures established from the *Axin2-TdTomato* reporter mouse. We have cloned and infected a Tet-On lentiviral system to express a

dominant negative form of Trf2, which rapidly uncaps telomeres, in *Axin2-TdTomato* organoids. Axin2 is expressed predominantly in the CBCs (Figure 3.8). If our hypothesis is correct, we expect to see decreased TdTomato intensity (i.e. decreased Wnt target gene expression) upon acute telomere uncapping. We hope to track Axin2-TdTomato intensity before cells die from critical telomere shortening but after telomeres are uncapped, to ensure that any loss of signal intensity is not due from dying cells. We plan to use real-live imaging and flow cytometry to track and measure Axin2-TdTomato intensity upon induced telomere uncapping over time, which will inform us of the Wnt signaling status.

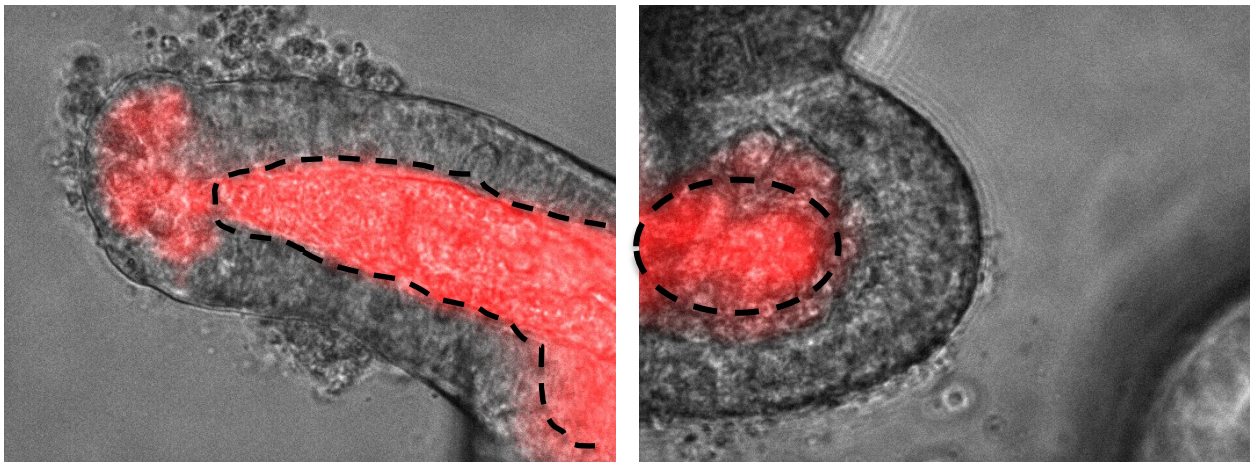

Figure 3.8. Wnt reporter *Axin2-TdTomato* organoid vs WT organoid in culture. (Left panel) *Axin2-TdTomato* organoids grown in culture and (right panel) wild-type organoid grown under the same conditions. Brightfield image superimposed on fluorescent image taken with a Cy3 filter. Autofluorescence in central lumen of organoid (dashed line).

CHAPTER 4: P53 AND MIR-34A IN WNT SUPPRESSION

INTRODUCTION

When expression of many components of the Wnt pathway are downregulated (and not just the targets of Wnt signaling, but components at multiple steps of the pathway), one wonders whether there is a master conductor or several different regulators that can specifically target the pathway. There are a few hypotheses that we generated for the mechanism of Wnt pathway suppression, which we outline below.

Wnt pathway suppression has been attributed to p53 activation, specifically through downstream targets of p53, SIAH1 and miR-34a (223, 226). SIAH1 is an E3 ubiquitin ligase transcriptionally activated by p53, and it targets beta-catenin protein for degradation, and simultaneously targets TRF2 protein for degradation during p53-activated replicative senescence of human cultured cells (151, 257). In our experiments, RNA levels of beta-catenin are unchanged in G4 crypts compared to WT crypts on microarray, and Trf2 RNA levels are decreased (on microarray and confirmed by qRT-PCR). Siah1 is not expected to change RNA levels of beta-catenin or Trf2, and therefore the decreased Trf2 levels that we observe in G4 crypts are presumably due to other factors. Although we have not confirmed Siah1a or Siah1b upregulation in G4 crypts by qRT-PCR or WB, our microarray results suggest that altered Siah1 expression does not explain Wnt pathway downregulation in the intestinal crypt epithelium of mice with uncapped telomeres.

p53 has been conditionally knocked out in the intestine of *mTR*$^{-/-}$ mice (156), and downstream components of p53, p21 and PUMA, have also been knocked out in *mTR*$^{-/-}$ mice (161, 162). G4 *mTR*$^{-/-}$ mice lacking intestinal p53 had rescue in the expression of the CBC marker, *Olfm4*, which is a target of Ascl2, itself a Wnt target gene. These mice had increased crypt proliferation but also increased crypt genomic instability (characterized by increased telomere dysfunction and DNA damage responses) and apoptosis (156). Overall, this strongly suggests that p53 activation mediates the suppression of CBC marker expression in late generation *mTR*$^{-/-}$ crypts. Given that miR-34a is direct transcriptional target of p53 that has been found to suppress expression of multiple genes of the Wnt pathway (258, 259), it is plausible to hypothesize that miR-34a mediates the suppression of Wnt pathway components that we observe.

Several miRNAs have been described to be upregulated in aged tissues and associate with senescence pathways. miRNAs can downregulate a whole class of genes, and miRNAs (specifically miR-34a) are good candidates for the mechanism of suppressed expression of multiple Wnt pathway genes upon telomere uncapping and p53-activation (260, 261). miR-34a is of particular interest, as it is implicated in the DNA damage response pathway and aging, including cardiac aging and aging skeletal muscles (262). miR-34a belongs to a family of miRNAs that include miR34b and miR34c. miR-34a is encoded on chromosome 4 of mice and chromosome 1 of humans, while miR34b and miR34c are both 500bp within each other on the same chromosome 9 in mice and 11 in humans. miR-34a has tumor suppressor activities and is activated by

p53, which is activated upon DNA damage including telomere dysfunction. There are also other important miRNAs that may be important in gene regulation in the G4 crypts.

Deletion of chromosomal region 1p36, where miR-34a is located but no other tumor suppressor genes are, has been described in various cancers, including colon cancer (263, 264). miR-34a-knockout mice on a normal C57BL/6 background, however, have no obvious developmental or pathological abnormalities up to 12 months (265). Apparent phenotypes include increased somatic reprogramming efficiency of *miR-34a*$^{-/-}$ MEFs and increased bone resorption and reduced bone mass (266). However, in aged mice, miR-34a contributes to cardiac aging in mice in part due to its inhibition of PNUTS, which binds to TRF2 to prevent telomere shortening (262). miR-34a is directly downstream of the p53-activation pathway and has also been shown to have a feed-forward effect on p53 activation through inhibition of Mdm4, an inhibitor of p53 (267). Other important targets of miR-34a include SIRT1 (268), and interestingly, multiple genes of the Wnt pathway, namely Wnt1, Wnt3, Lrp6, beta-catenin, and Lef1. We hypothesize that miR-34a mediates part of the pathology we observe in G4 crypts, specifically, the decreased expression of Wnt pathway genes that we have observed.

METHODS

MicroRNA microarray

Microarray experiments were conducted by the University of Pennsylvania Molecular Profiling Facility, including quality control tests of the total RNA

samples by Agilent Bioanalyzer and Nanodrop spectrophotometry. Crypt RNA was obtained from three G4 *mTR*$^{-/-}$ mice, with samples from each mouse analyzed on an individual array. Amplification steps were performed with the Genisphere FlashTag (miRNA) kit and the Affymetrix GeneChip miRNA 3.0 Array chips were used. Affymetrix probe intensity (.cel) files were imported into Partek Genomics Suite (v6.6, Partek Inc., St. Louis, MO) where RMA normalization was applied. The resulting log2-transformed intensities were filtered to exclude the IDs corresponding to technical controls, and analyzed for differential expression using SAM (Significance Analysis of Microarrays, samr v2.0, Stanford University (251)), generating q-values (False Discovery Rate) and fold change for each Transcript ID.

Mice

The breeding scheme for generating *miR-34a*$^{-/-}$ onto the different generations of *mTR*$^{-/-}$ mice is outlined in the following diagram. For simplicity, we will refer to the genotype of *mTR*$^{-/-}$ by generation (e.g. G1 for first generation *mTR*$^{-/-}$ mice) and we will refer to the genotype of miR-34a by allele status (e.g. WT for *miR-34a*$^{+/+}$, HET for *miR-34a*$^{+/-}$, and KO for *miR-34a*$^{-/-}$). For example, a third-generation *mTR*$^{-/-}$ mouse heterozygous for *miR-34a* is referred to G3-het.

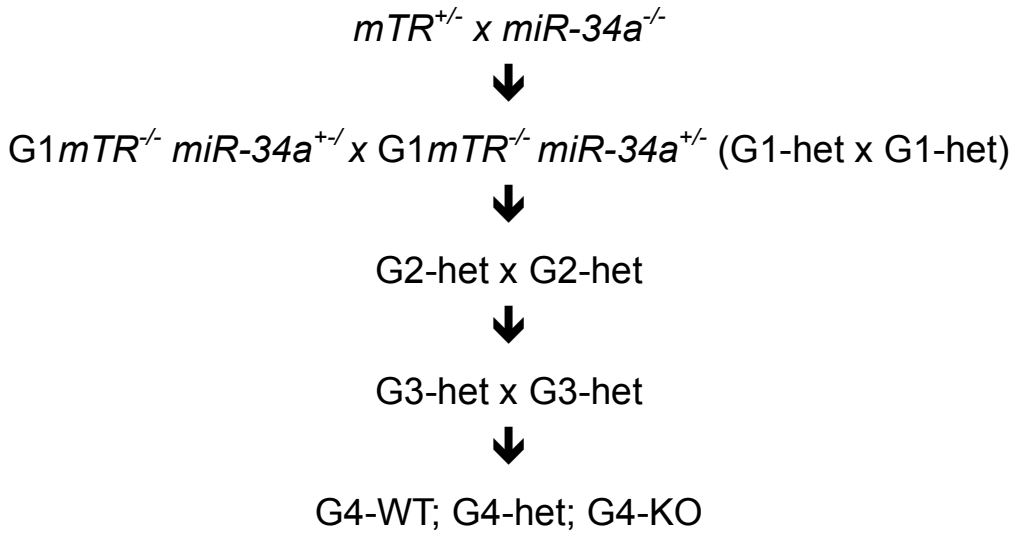

Lentiviral infection of crypt organoid cultures

Lentiviruses were made at the Wistar Vector Core from System Biosciences MirZip vectors coding for with anti-microRNAs: MirZip scramble control vector and MirZip vector targeting miR-34a. Organoids were cultured and established in 5 μM CHIR conditions for several passages before infection. Organoids embedded in Matrigel were counted and washed once with cold PBS, and the organoids and Matrigel were broken up by pipetting. Organoids were spun down at 300g in a cold centrifuge and resuspended in culture media containing 5 μM CHIR. Lentiviruses were added to the organoid suspension at different multiplicities of infection (MOI of 25 or 50) for 4-6 hours in a 37°C incubator. After incubation, organoids were collected and spun down at 300g, resuspended in Matrigel, plated, and grown at 5 μM CHIR for 2-3 days before 2 μg/mL puromycin selection.

RESULTS

We performed a microRNA microarray on WT and G4 crypts (n=3 each) using service from the UPenn Pathology Core (using standard core suggested preparation methods for the Affymetrix GeneChip miRNA 3.0 Array) (data tables in Appendix). Since the chip contains many probes for miRNAs and pre-miRNAs that are not yet experimentally determined and are based on unvalidated *in silico* data (from miRBase version 17), we can rely on the newer version of the online miRBase database (currently at version 21) to investigate individual miRNA hits. miRBase contains information about read counts from available deep sequencing experiments, predicted mRNA targets, experimentally-validated mRNA targets, etc. Out of the top 10 upregulated miRNA in G4 crypts, 8 miRNAs do not have validated mRNA targets or are misannotated. For example, the second most increased miRNA hit, miR-5097, is noted to be a misannotation on miRBase and is actually derived from a fragment of tRNA and it is not processed by Dicer or loaded into RISC. A large proportion of the top 100 upregulated miRNAs belong to the misannotated class or have yet to be experimentally identified. miR-34a is the most upregulated (validated) miRNA in G4 crypts.

There are several other interesting validated miRNAs that have significantly upregulated expression in G4 crypts, including the miR-23a~27a~24-2 cluster . The miR-23a~27a~24-2 cluster is encoded by a single pri-miRNA that generates 3 different mature miRNAs: 23a, 27a, and 24-2. In many pathological conditions the cluster is overexpressed, such as in cancer. *In silico* analysis has shown the cluster to regulate many genes of the Wnt pathway: Wnt3a, Wnt4 are

targeted by miR-27a and -24a, respectively; Lrp5 and Lrp6 by miR-23a and -27a respectively; Fzd4 and Fzd7 by both miR-23a and -27a; Dvl1 by miR-27a; Tcf7 by miR-24. The Wnt target gene Cyclin D is also targeted by miR-23a. Conversely, inhibitors of the Wnt pathway are also targeted – APC by miR-23a and PP2A by miR27a. However, these Wnt pathway gene targets of the miR-23a~27a~24-2 cluster have not been experimentally validated (269). We focus on miR-34a because it has been consistently described and validated to be overexpressed in multiple different tissues across species with aging and DNA damage responses.

How expression of Wnt pathway components is broadly downregulated in the intestines of late-generation *mTR*$^{-/-}$ mice is not yet clear. However, it is well established that dysfunctional telomeres elicit a p53-dependent DNA damage response, and p53-activated upregulation of miR-34a has been implicated recently in the suppression of multiple Wnt pathway genes (258). Indeed, we detected increasing levels of p53 activation (as measured by p21 expression, Figure 4.1) with successive generations of *mTR*$^{-/-}$ crypts along with a corresponding decrease in Wnt target genes, Lgr5 and Trf2 (Figure 4.1), and the suppression in Wnt signaling corresponds to levels of p53 activation. We have validated the increased expression of miR-34a by qRT-PCR in G4 crypts compared to WT. Indeed, there is an incremental increase in miR-34a expression with increasing generations of *mTR*$^{-/-}$ mice (Figure 4.1). The incremental increase in miR-34a also corresponds to the incremental decrease in Wnt target genes, consistent with others' observation of miR-34a activation by p53 to suppress

expression of Wnt pathway genes. One of the targets of miR-34a is PNUTS, which has been described to maintain telomere length through its interaction with TRF2. As expected, PNUTS is downregulated in G4 crypts (Figure 4.2), which may contribute to the further uncapping of telomeres.

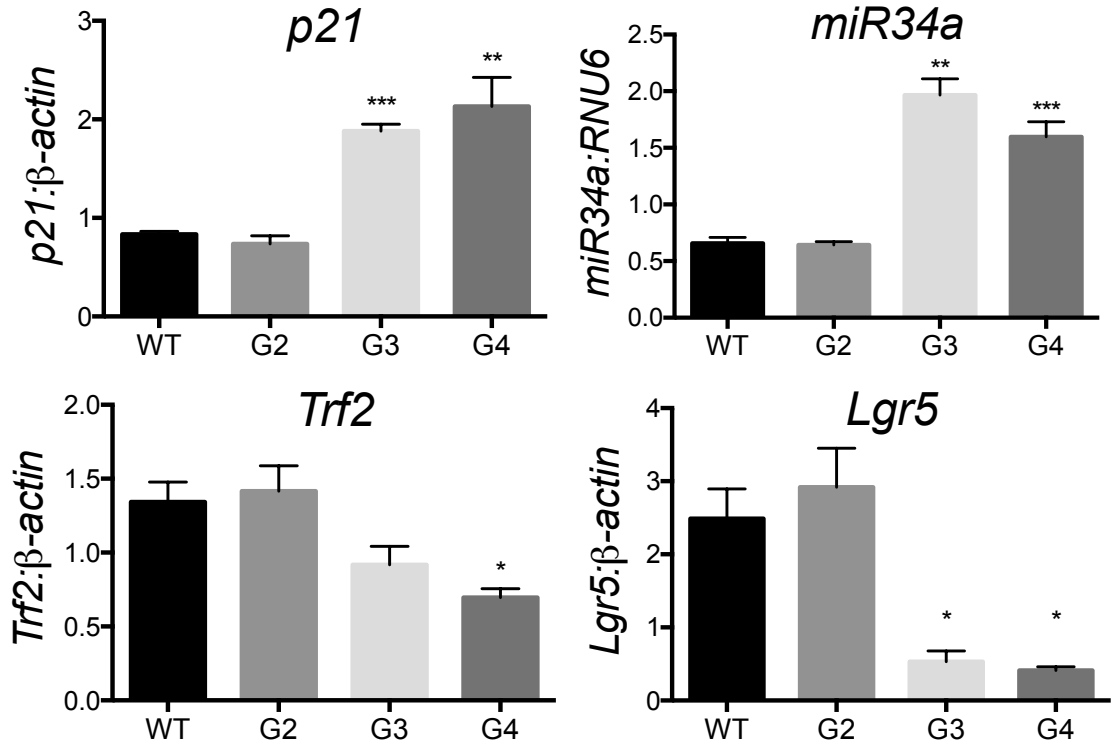

Figure 4.1. Expression of p53-activated genes, Wnt target genes in WT and *mTR*$^{-/-}$ crypts. qRT-PCR of *p21, mir-34a, Lgr5*, and *Trf2* in WT, G2, G3, and G4 *mTR*$^{-/-}$ crypts.

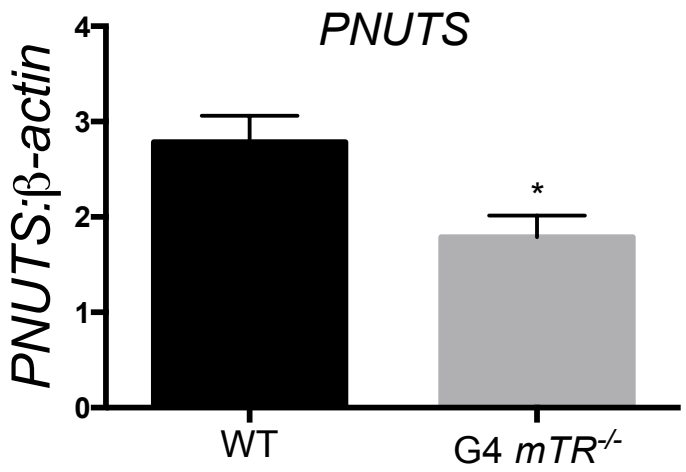

Figure 4.2. Expression of miR-34a target gene PNUTS in WT and G4 *mTR*$^{-/-}$ crypts. qRT-PCR of *PNUTS* in WT and G4 *mTR*$^{-/-}$ crypts.

Given the considerations described above, it is plausible that miR-34a contributes to the suppression of the Wnt pathway in intestinal crypts of late-generation *mTR*$^{-/-}$ mice. To test this hypothesis, we crossed the *miR-34a*$^{-/-}$ mouse onto the *mTR*$^{-/-}$ background. The breeding scheme (described in the Methods section) allows us to obtain *mTR*$^{-/-}$ mice at each generation with the proper littermate controls: *miR-34a*$^{+/+}$, *miR-34a*$^{+/-}$, and *miR-34a*$^{-/-}$. In early generations (G1-3) of *mTR*$^{-/-}$, mice were born with the expected *miR-34a*$^{+/+}$, *miR-34a*$^{+/-}$, and *miR-34a*$^{-/-}$ Mendelian frequencies (Table 4.1). In the 4th generation, the birth frequency is skewed towards more *mTR*$^{-/-}$ mice being born with *miR-34a*$^{-/-}$ (Chi-squared p-value of 0.1170), which suggests that there is an embryonic/neonatal survival advantage of *miR-34a*$^{-/-}$ at later generations of *mTR*$^{-/-}$, when telomeres become critically short and when p53 and miR-34a activation would occur.

Since miR-34a activation occurs after telomeres become dysfunction, we do not see any survival advantage of *miR-34a* deletion until later generations. And since there is a large variation in telomere lengths and consequently varying

degrees of telomere dysfunction within the same generation, and even amongst littermates (270), larger sample sizes are necessary to provide us with more substantial and significant evidence of any survival advantages of *miR-34a* deletion. Indeed, the telomere length variation that exists amongst mice of the same generation might also explain why there seem to be certain G3 breeding pairs that produce G4 pups at the expected miR-34a Mendelian frequency and other breeding pairs that only produce G4 pups with *miR-34a*$^{-/-}$ or *miR-34a*$^{+/-}$ but no *miR-34a*$^{+/+}$ (not shown). We have not yet measured telomere lengths in the different breeding pairs, but we hypothesize that the former pairs would have longer telomeres than the latter pairs.

Table 4.1. Actual vs. expected Mendelian frequencies of *miR-34a*$^{+/+}$, *miR-34a*$^{+/-}$, and *miR-34a*$^{-/-}$ in G2, G3, and G4 *mTR*$^{-/-}$ mice. Chi-squared test two-tailed p-values are 0.3198, 0.9350, and 0.1170, for G2, G3, and G4 *mTR*$^{-/-}$ mice, respectively.

G2 *mTR*$^{-/-}$	Actual genotype	Expected genotype	Total pups
+/+	8	12.5	50
+/-	29	25	
-/-	13	12.5	

G3 *mTR*$^{-/-}$	Actual genotype	Expected genotype	Total pups
+/+	16	16.75	67
+/-	33	33.5	
-/-	18	16.75	

G4 *mTR*$^{-/-}$	Actual genotype	Expected genotype	Total pups
+/+	13	19.75	79
+/-	40	39.5	
-/-	26	19.75	

We have isolated crypts for organoid culturing from two pairs of G4 littermates with *miR-34a*$^{+/+}$ and *miR-34a*$^{-/-}$ statuses. We also obtained crypts from a G4 *miR-34a*$^{+/-}$ littermate for one experiment, from which we also cultured fibroblasts from ears. In addition, we are currently performing miR-34a knockdown experiments with lentiviral vectors expressing anti-miR-34a shRNAs in G4 *miR-34a*$^{+/+}$ organoids and ear fibroblasts. Ear fibroblast and anti-miR-34a shRNA experiments are ongoing, and we will not present those results here. Our preliminary data indicate a survival advantage in G4 organoids lacking miR-34a over those with intact miR-34a (Figure 4.3 and 4.4), with increased expression of the Wnt target gene, *Lgr5* (Figure 4.5). It would be necessary to do parallel control experiments comparing WT vs *miR-34a*$^{-/-}$ mice or early generation G1 *miR-34a*$^{+/+}$ vs G1 *miR-34a*$^{-/-}$ mice, where we would not expect a survival advantage in organoids lacking miR-34a.

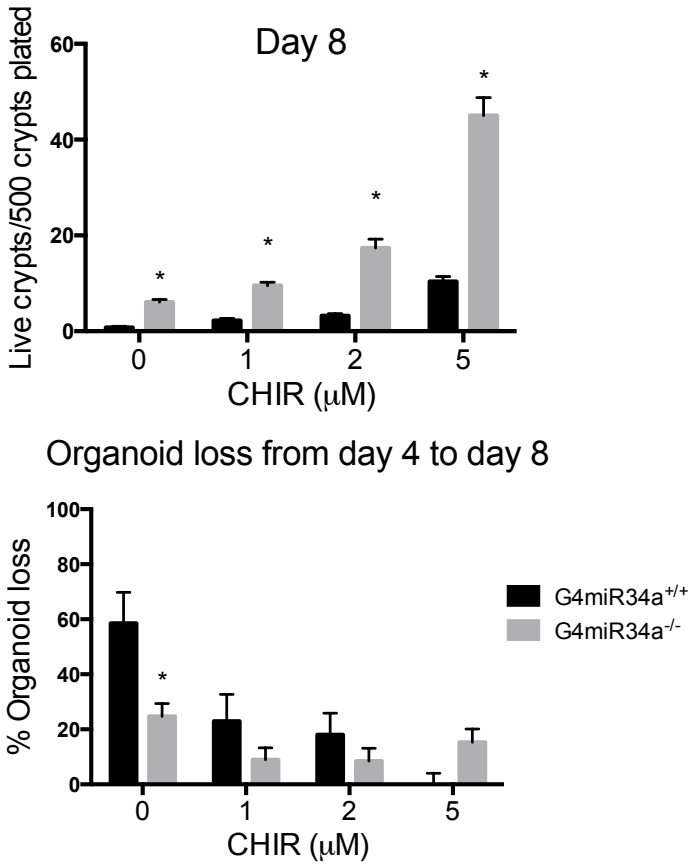

Figure 4.3. G4*miR-34a*$^{+/+}$ and G4*miR-34a*$^{-/-}$ organoid survival 8 days after harvest (left panel) or loss from 4 to 8 days after *ex vivo* harvest (right panel). Intestinal organoids were harvested from one pair of G4*miR-34a*$^{+/+}$ and G4*miR-34a*$^{-/-}$ littermates and cultured under standard conditions (1 μg/ml Rspo1) or augmented with the GSK-3 inhibitor CHIR99021. N=20 wells at 0μM, 8 wells at 1μM, and 5 wells at 2μM and 5μM CHIR; *p<0.0005

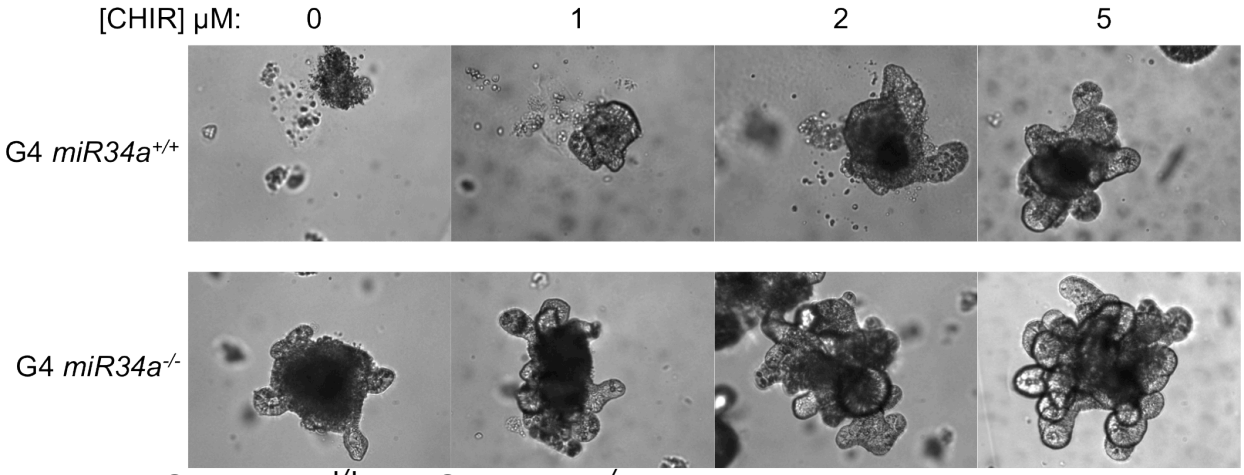

Figure 4.4. G4*miR-34a*$^{+/+}$ and G4*miR-34a*$^{-/-}$ organoids in culture with CHIR99021. Representative brightfield images of intestinal organoids harvested

from one pair of G4*miR-34a*$^{+/+}$ and G4*miR-34a*$^{-/-}$ littermates and cultured under standard conditions (1 μg/ml Rspo1) or augmented with the GSK-3 inhibitor CHIR99021.

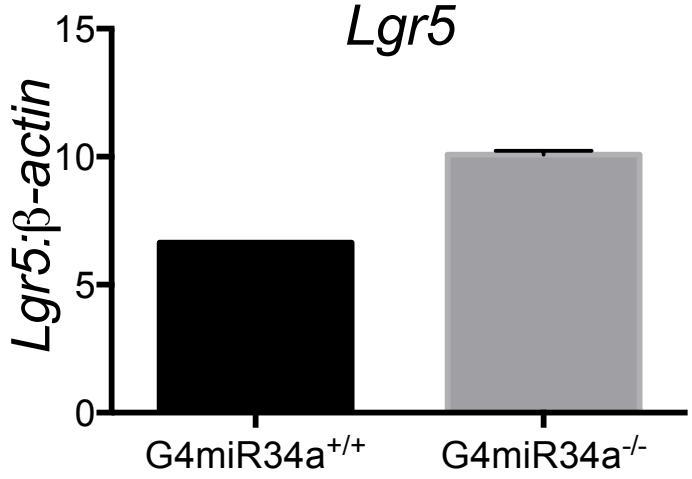

Figure 4.5. qRT-PCR analysis of *Lgr5* expression in G4*miR-34a*$^{+/+}$ and G4*miR-34a*$^{-/-}$ organoids 8 days after *ex vivo* harvest. qRT-PCR measurement of *Lgr5* transcripts in G4*miR-34a*$^{+/+}$ and G4*miR-34a*$^{-/-}$ littermate organoids 8 days after crypt harvest, and treated with 5μM CHIR99021. N=1 for G4*miR-34a*$^{+/+}$ and N=2 for G4*miR-34a*$^{-/-}$ organoids.

DISCUSSION

How uncapped telomeres lead to repressed expression of Wnt pathway factors in the intestine of late generation *mTR*-deficient mice is not yet clear. However, it is well established that uncapped telomeres activate p53-dependent responses, and recently the p53-activated miRNA-34a was found to inhibit expression of Wnt pathway genes (258, 260), including many of those we find downregulated in G4 $mTR^{-/-}$ crypts. We observe increased expression of miR-34a in late generation mutant crypts, where it could contribute to such inhibition. Consistent with this idea, Wnt pathway gene suppression caused by uncapped telomeres likely depends on p53, as deletion of p53 in late-generation $mTR^{-/-}$ mice rescues expression within intestinal CBCs of *Olfm4 (156)*, which is a target of the Wnt-activated transcription factor Ascl2 (237).

The experiments that we have designed and presented above have begun to address the hypothesis that miR-34a contributes to the suppression of Wnt pathway genes we observe in G4 crypts. The fact that we see a trend toward a perinatal survival advantage from miR-34a deletion only in later generations of $mTR^{-/-}$ mice, informs us that miR-34a may have effects beyond the regulation of Wnt suppression in the intestinal crypt. Currently, all of the mice we have not sacrificed for experiments are still alive and since most of these mice are still relatively young, we have not yet had the opportunity to perform a survival curve. We are currently starting to characterize these mice and to perform functional experiments. We would like to assess for telomere capping status through metaphase-TIFs in G4 ear fibroblasts and organoids lacking miR-34a.

We have only concentrated our efforts thus far on miR-34a, which is upregulated in G4 crypts, but of equal interest are miRNAs that are significantly downregulated in G4 crypts. One of the top most downregulated miRNAs belong to that of the miR-181, miR-30, and miR-200 families, and each family play important roles in cancer, inflammation, and development. As mentioned in the introduction, the miR-17-92 family cluster that is consistently downregulated in aging, is also significantly downregulated in G4 crypts. Any of these and other miRNAs that are significantly changed in G4 crypts may play important functional roles in the pathophysiology or downstream effects of telomere dysfunction. A high-throughput approach to assess the functional role of specific miRNAs does not currently exist, but would greatly advance and accelerate the field of miRNA research.

CHAPTER 5: RESCUE OF TELOMERE DYSFUNCTION IN INTESTINAL CRYPTS OF LATE-GENERATION TELOMERASE-KNOCKOUT MICE

INTRODUCTION

Our results indicate that G4 *mTR*$^{-/-}$ ISCs experience a niche poor in the Wnt pathway activities that normally support CBCs. Remarkably, Wnt signaling leads to upregulation of target genes that encode key components of the Wnt pathway itself, e.g. Lgr5. Thus, downregulation of Wnt pathway activity could lead to further downregulation of expression of pathway components *via* this feedback loop. In addition, *Trf2* is a Wnt target gene that encodes a critical telomere capping protein, and thus loss of Wnt pathway activity could lead to enhanced telomere uncapping, in turn leading to additional downregulation of Wnt pathway as described above. We detect incremental decreases in *Trf2* expression that mirrored the decrease in *Axin2* expression from WT to G2 to G4 crypts, and the decrease in *Trf2* could theoretically exacerbate the state of telomere uncapping in G4 crypts. Based on these considerations, it is reasonable to hypothesize that supplementation with exogenous Wnt pathway agonists would ameliorate pathology by restoring the niche environment, perhaps including restoration of *Trf2* expression and rescuing telomere dysfunction.

METHODS

TIF and telomere Q-FISH analyses

Tissue sections were hybridized with a Cy3-labeled PNA telomere repeat probe ($(CCCTAA)_3$)and anti-53BP1 antibodies (Novus, NB100-304) as described (16). Confocal images were obtained with a Nikon Ti-U inverted microscope with CSU-10 spinning disk confocal head (Spectral Boralis) using a Nikon Plan APO60x/1.4 lens and Hamamatsu Orca-ER camera. The Cy3 laser was held at a constant intensity to capture all images. Images from mice treated with lithium and Rspo1 were obtained in 16-bit grey scale and 8-bit RGB24 formats, respectively. To measure telomere lengths, quantitative image analysis was performed on confocal images using Media Cybernetics and ImageProPlus 7.01 software. The DAPI images were used to define the nuclear area in which to measure telomere intensities. Images were first deconvoluted, and nuclear outlines of interest were drawn and applied as a mask onto the Cy3 images. Cy3 images were also deconvoluted, and telomere intensities within each nucleus were obtained (for 16-bit images applied filters were: 1000-65535 pixel intensity threshold and area larger than 11.25sq. microns; for 8-bit images applied filters were: density/intensity ratio threshold of 0-254). Statistical analyses were performed using the Mann-Whitney U-test.

RESULTS

Wnt pathway agonists rescue survival of G4 *mTR*$^{-/-}$ crypt epithelial cells *in vivo* and *in vitro*.

We examined effects of Rspo1 and the selective GSK-3 inhibitor CHIR99021 on epithelial organoids cultured *in vitro*. This provided a test of Wnt pathway agonists under internally controlled conditions (i.e. on tissues from individual mice, rather than between mice). Under standard culture conditions, wild type organoids are long-lived and appear as roughly spherical epithelium surrounding a central cavity representing the lumen, and have crypts radiating outward from their peripheries. G4 *mTR*$^{-/-}$ organoids were prone to degeneration and had fewer crypts, but Rspo1 or CHIR99021 each improved mutant organoid survival and morphology in a dose-dependent manner (Figure 5.1). Although these agents also affected WT organoid survival and morphology, they had more pronounced effects on mutant organoids. G4 *mTR*$^{-/-}$ organoids were larger and grew more buds (each bud is representative of an individual crypt) with higher doses of CHIR99021 (Figure 5.2). At the highest dose (5μM), the organoids lose the budding structures and predominantly obtain the morphology of a large spheroid, which has been observed in organoids cultured from crypts with high Wnt activity. Cultured G4 *mTR*$^{-/-}$ organoids had reduced levels of *Lgr5* transcripts, which were partially rescued by CHIR99021 (Figure 5.3). Furthermore, transcripts encoding the pro-apoptotic protein, Noxa, decreased in proportion to CHIR99021 dose (Figure 5.3). In sum, these *in vitro* data establish roles for Wnt

pathway agonists in rescuing abnormalities in G4 *mTR*$^{-/-}$ crypts related to morphology, apoptosis and CBC-related gene expression.

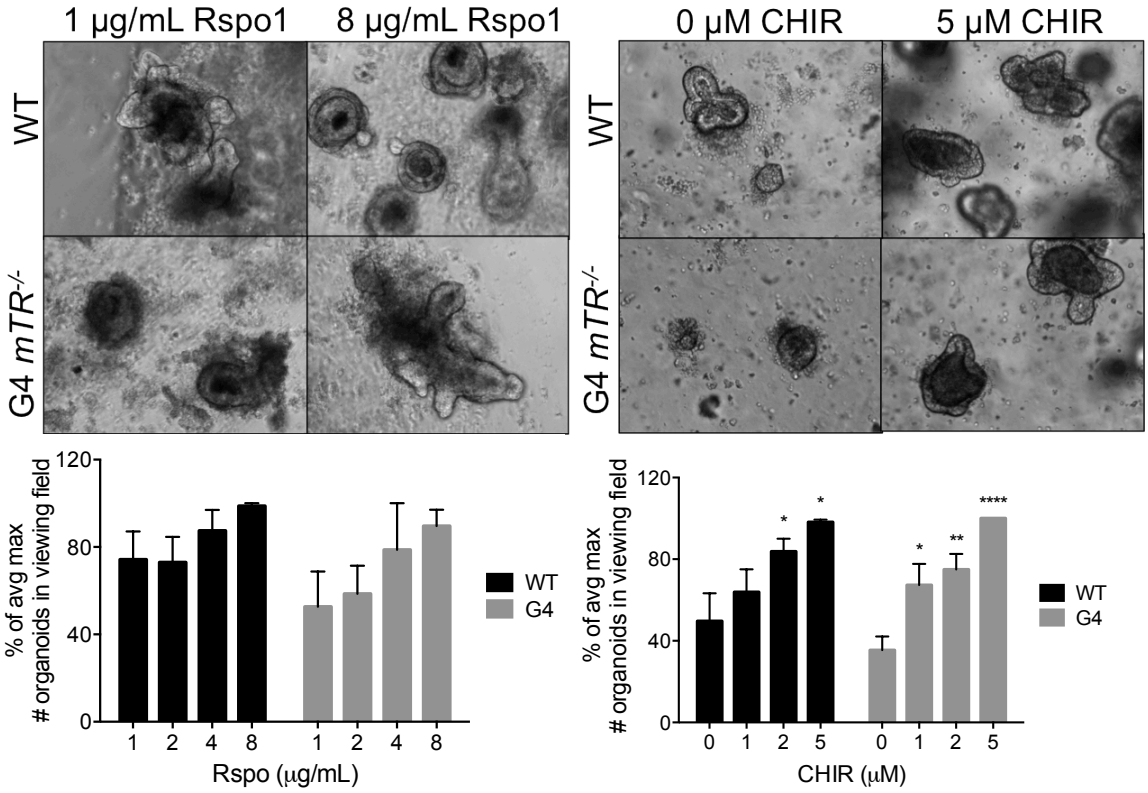

Figure 5.1. Wnt pathway agonists rescue survival and morphology of cultured G4 *mTR*$^{-/-}$ intestinal organoids. (Top panel) Intestinal organoids from WT and G4 *mTR*$^{-/-}$ mice were cultured under standard conditions (1 µg/ml Rspo1) or augmented with elevated levels of Rspo1 or the GSK-3 inhibitor CHIR99021. The survival index is expressed as a percentage of the number of organoids divided by the average maximum number of organoids counted in the viewing field (4 viewing fields per sample were counted with a 4x objective). N = 3 for Rspo1-treated crypts, N = 6 for CHIR-treated crypts. * $p<0.05$, ** $p<0.005$, *** $p<0.0005$, **** $p<0.0001$

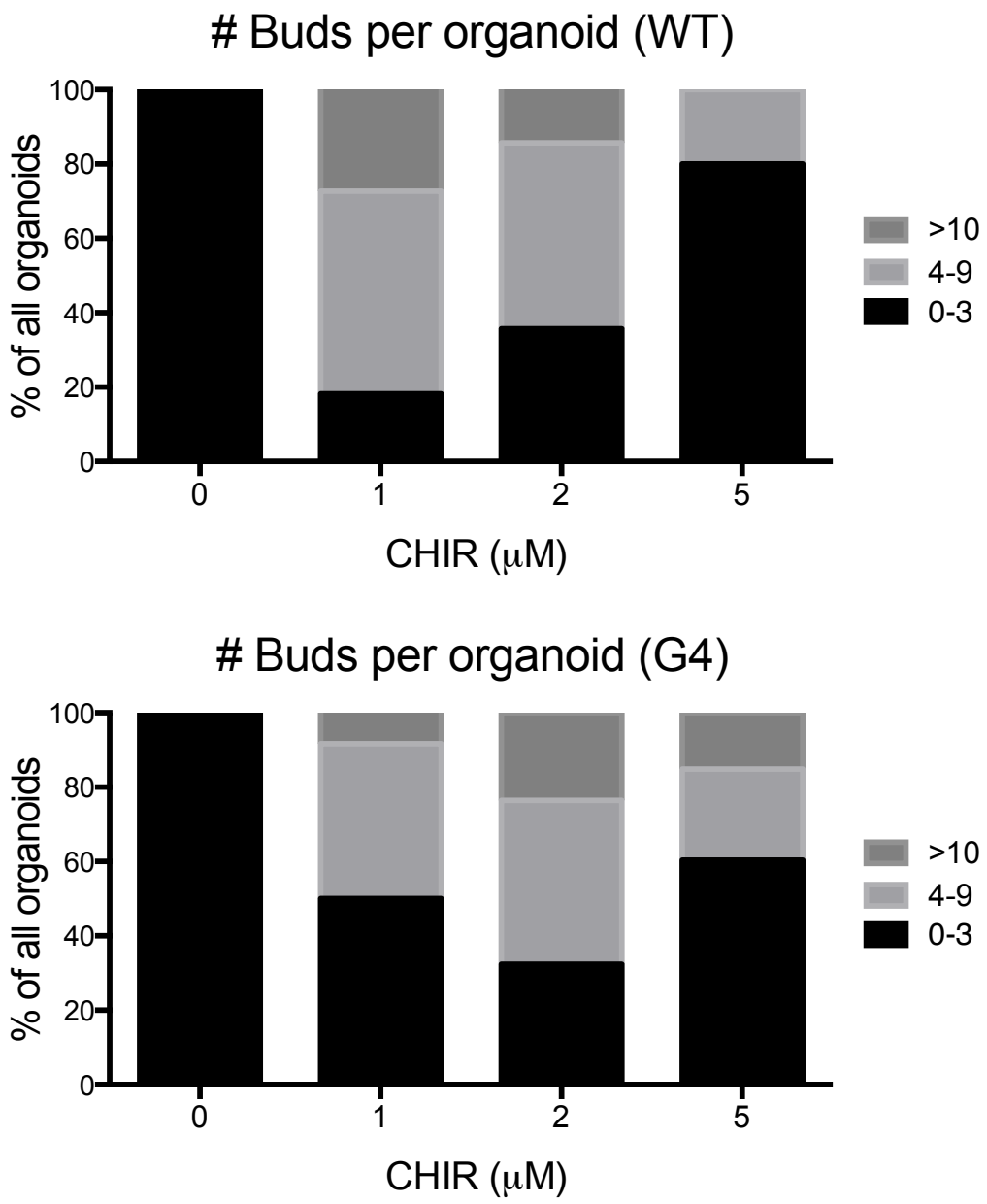

Figure 5.2. Bud count of per WT or G4 *mTR*$^{-/-}$ organoids cultured with CHIR99021. G4 *mTR*$^{-/-}$ organoids were cultured in increasing doses of CHIR99021 and counted for the number of buds on each organoid.

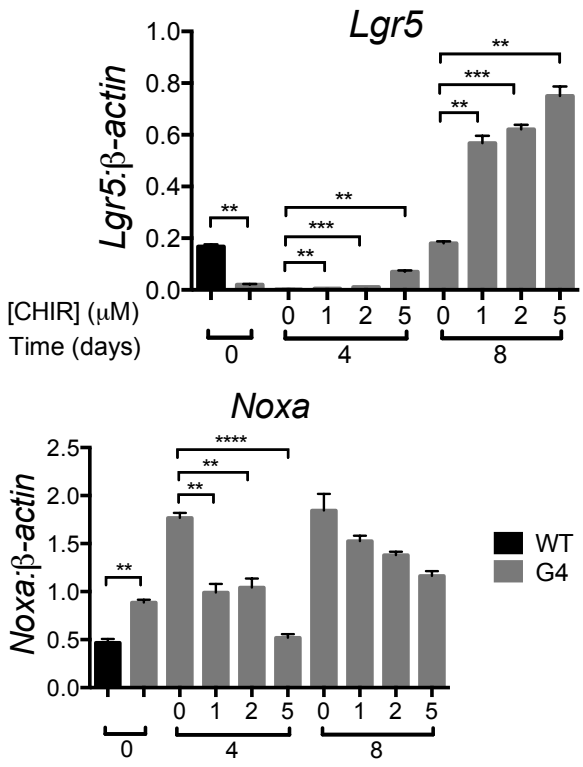

Figure 5.3. qRT-PCR analysis of *Lgr5* and *Noxa* expression in G4 *mTR*$^{-/-}$ crypts cultured with CHIR99021. qRT-PCR measurement of *Lgr5* and *Noxa* transcripts in WT and G4 *mTR*$^{-/-}$ crypts at t=0, and treated with increasing doses of CHIR99021 at days 4 or 8. ** p<0.01, **** p<0.0001.

We also see an improvement of G4 *mTR*$^{-/-}$ crypts with Wnt pathway agonists *in vivo*. Crypt apoptosis was rescued in G4 *mTR*$^{-/-}$ mice fed with chow containing lithium, a GSK-3 inhibitor and thus a Wnt pathway agonist (Figure 5.4). Since lithium has effects beyond GSK-3 inhibition, we also treated G4 *mTR*$^{-/-}$ mice with a specific Wnt/Lgr5 receptor agonist, Rspo1. Daily subcutaneous injection for eight days with Rspo1 significantly decreased crypt apoptosis and elevated *Ascl2* transcript and Sox9 protein levels (Figure 5.5). We also observed an improvement in villus blunting, although we have not quantified these changes. For both sets of treatments, comparisons among control and treated

mice were made between littermates, to avoid effects from stochastic differences in inherited telomere lengths. Rescue was not associated with improved proliferation in the crypt base as measured by Ki-67 (Figure 5.6), nor increased numbers of Paneth cells, but was associated with increased proliferation in the TA region. Therefore, reduced apoptosis of crypt epithelial cells along with increased TA cell proliferation may contribute to the rescue provided by Wnt pathway agonists.

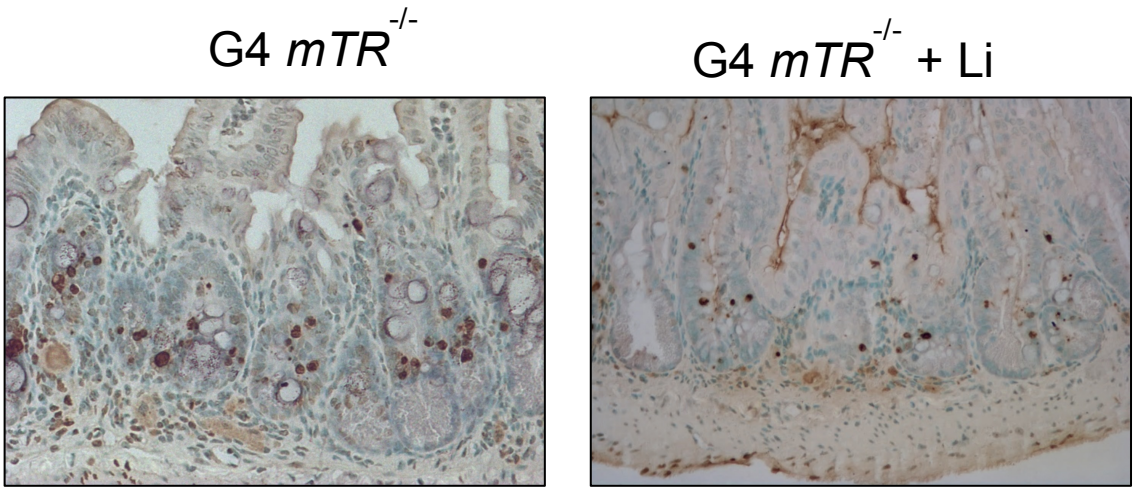

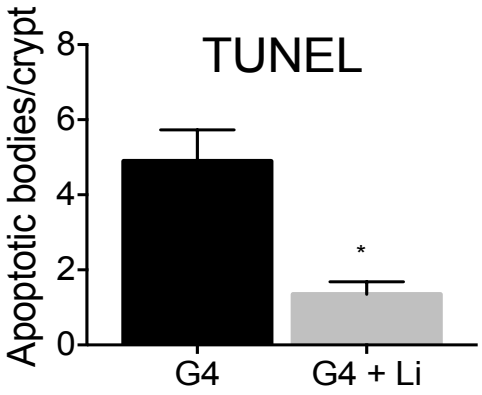

Figure 5.4. TUNEL staining of G4 *mTR*$^{-/-}$ and Li-treated G4 *mTR*$^{-/-}$ small intestinal crypts. (Top panel) G4 *mTR*$^{-/-}$ mice were treated with the GSK-3 inhibitor lithium in dietary chow (0.2% for 3 days followed by 0.4% for 7 days).

(Bottom panel) TUNEL staining was performed on the ileal crypts, and apoptotic bodies per crypt were counted. N = 3 mice per condition, * p<0.05.

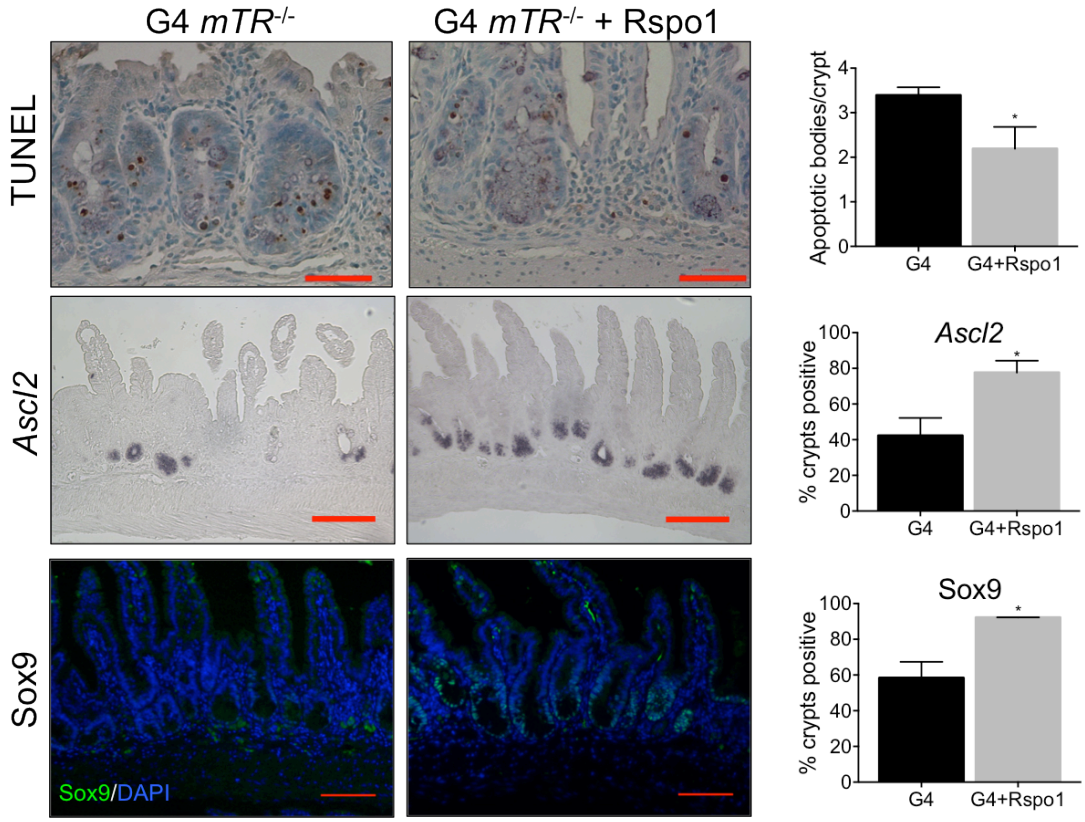

Figure 5.5. Enhanced Wnt signaling rescues G4 *mTR*$^{-/-}$ crypt apoptosis and Wnt-responsive ISC markers *in vivo*. G4 *mTR*$^{-/-}$ mice treated for eight days with subcutaneous injections of R-spondin1 (Rspo1) have reduced small intestinal apoptosis as measured by TUNEL (top panel), increased expression of *Ascl2* transcripts (middle) and Sox9 protein (bottom). N = 5 control G4 mice and 4 Rspo1-treated G4 mice for TUNEL staining; N = 3 mice per genotype for *Ascl2* staining; N = 4 control G4 mice and 3 Rspo1-treated G4 mice for Sox9 staining, * p<0.05. Scale bars: 20μm (top), 100μm (middle and bottom).

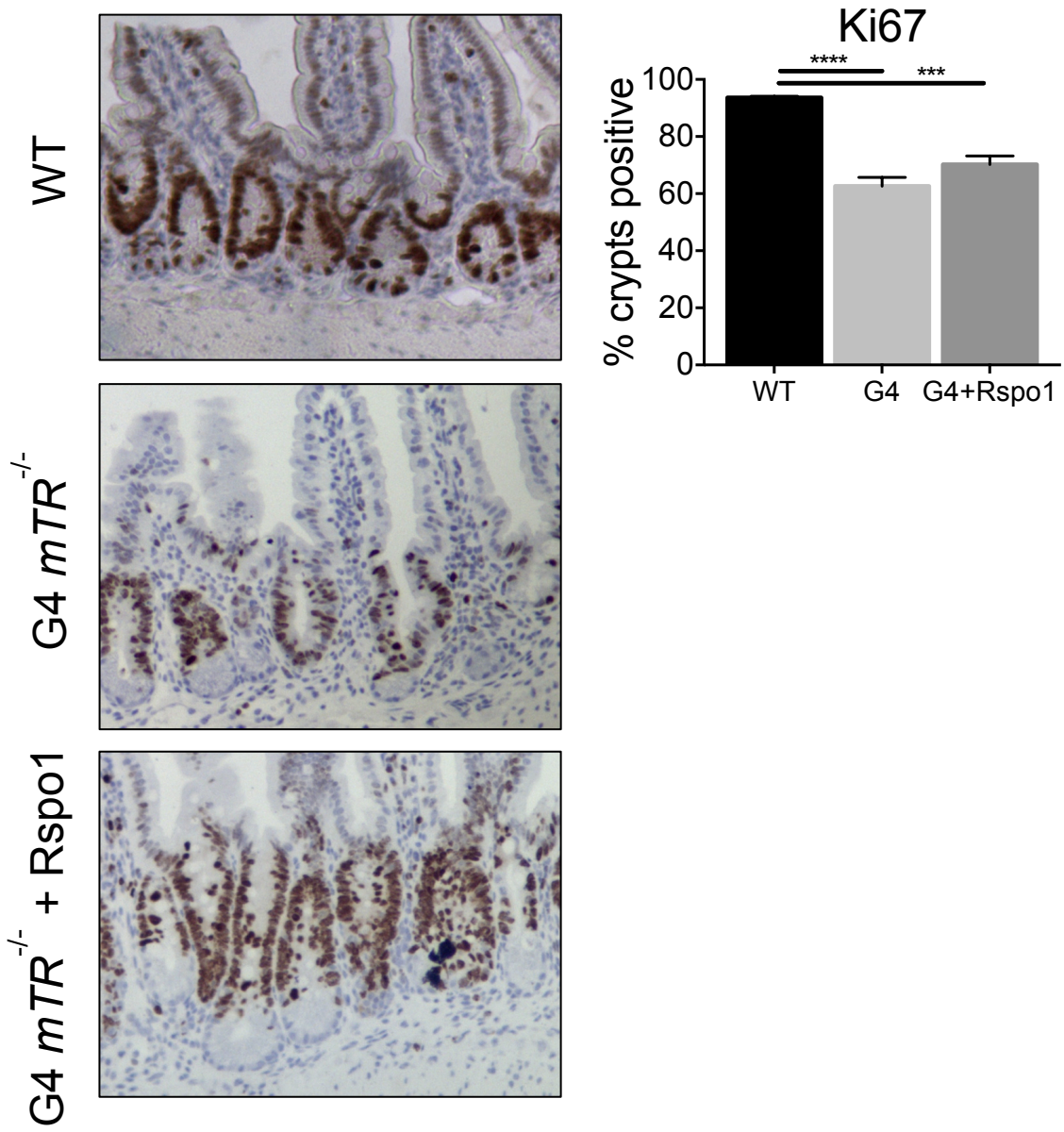

Figure 5.6. Ki67 staining in WT, G4 *mTR*$^{-/-}$, and Rspo1-treated G4 *mTR*$^{-/-}$ small intestinal crypts. (Left panel) Ki67 staining was performed on the small intestine of WT, G4 *mTR*$^{-/-}$, and Rspo1-treated G4 *mTR*$^{-/-}$ mice. (Right panel) Quantification of crypt bases positive for Ki67 staining. N = 4 WT mice, 5 control G4 mice and 5 Rspo1-treated G4 mice, *** $p<0.0005$, **** $p<0.0001$.

Wnt pathway agonists upregulate shelterin components and rescue telomere capping.

We explored the hypothesis that Wnt pathway agnoists can upregulate *Trf2* expression in the organoid culture system, and indeed, we observed dose-dependent upregulation of *Trf2* transcripts in G4 *mTR*$^{-/-}$ crypt cultures treated with CHIR99021, thus rescuing the reduced levels of *Trf2* transcripts in the mutant crypts (Figure 5.6). Other shelterin proteins are also important in the maintenance of telomere capping, and we analyzed published datasets to test for additional evidence that shelterin genes are regulated by Wnt, and found that a) *Trf2* transcripts are up and down regulated, respectively, in epithelia from APC-knockout (271) and β-catenin-knockout mice (272), b) the Wnt-responsive intestinal epithelial transcription factor TCF4 is bound at high levels within the human *TRF2*, *POT1,* and *TRF1* genes as assessed by ChIP (from the ENCODE database (273)), and c) the expression gradient of these genes within murine crypts corresponds to that of the Wnt target gene EphB2 (274) (Figure 5.7). Consistent with these observations and with Wnt pathway suppression in the mutants, we also detected significant downregulation of genes encoding other shelterin proteins, including *Pot1a*, *Pot1b*, and *Trf1*, in addition to *Trf2*, in G4 *mTR*$^{-/-}$ crypts (Figure 5.7). In addition, similar to *Trf2*, *Pot1a* transcript levels were also upregulated in response to increasing doses of CHIR99021. We confirm in MEFs that TRF2 protein levels are increased with increasing doses of LiCl (Figure 5.8).

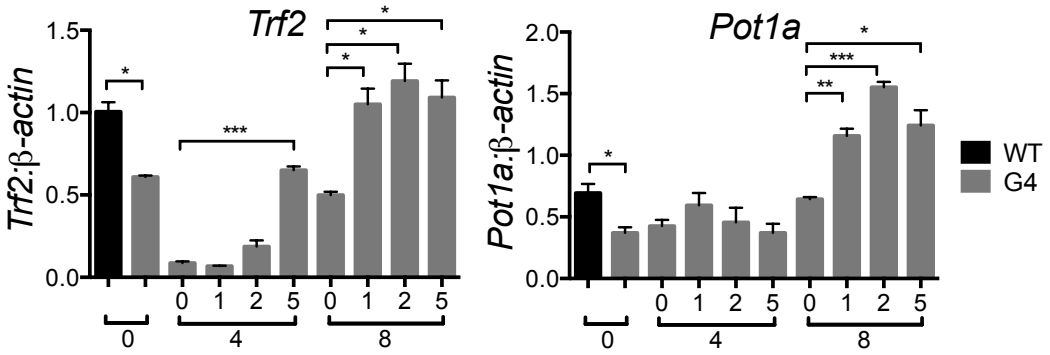

Figure 5.6. Wnt pathway agonists rescue *Trf2* and *Pot1a* expression in cultured G4 *mTR*$^{-/-}$ intestinal organoids. Dose- and time-dependent increase of *Tfr2* and *Pot1a* transcript expression as measured by qRT-PCR in WT and G4 *mTR*$^{-/-}$ crypts cultured with CHIR99021 for 4 or 8 consecutive days. * p<0.05, ** p<0.005, *** p<0.0005, **** p<0.0001.

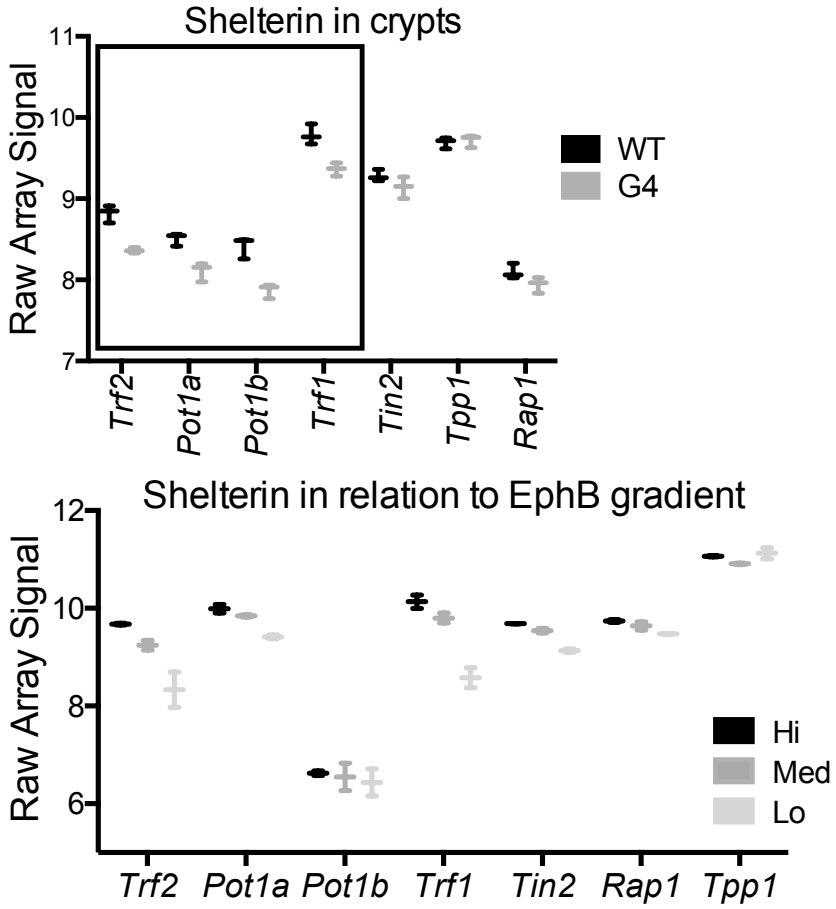

Figure 5.7. Expression of shelterin genes in WT and *mTR*$^{-/-}$ crypts, and distribution of shelterin gene expression in different EphB2-expressing crypts. (Top panel) Microarray gene profiling of shelterin genes in WT and G4 *mTerc*$^{-/-}$ crypts. (Bottom panel) Microarray gene profiling of shelterin genes in

crypt epithelial cells sorting according to surface expression levels of EphB2 (*high, medium* or *low*) (274).

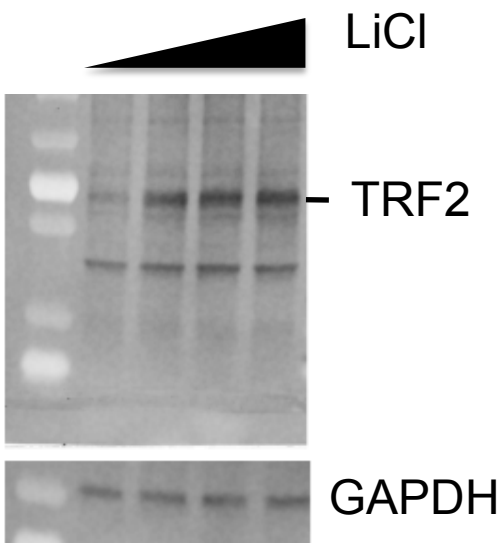

Figure 5.8. Expression of TRF2 protein in MEFs treated with LiCl. Wild-type MEFs treated with 0, 5, 10, and 20mM of LiCl were probed for TRF2 (with TRF2 antibody from Imgenex, IMG-124A) and GAPDH.

With the rescue of shelterin protein expression and tissue fitness with Wnt pathway activation, we therefore investigated whether there is an associated improvement in telomere capping. We scored telomere dysfunction-induced foci (TIFs), measured by colocalization of telomere and 53BP1 foci, and found a significant decrease in the number of TIFs in crypts of G4 *mTR*$^{-/-}$ mice treated with Rspo1 (Figure 5.9). Furthermore, Rspo1 treatment reduced anaphase bridges, a marker of break-fusion-bridge cycles caused by telomere dysfunction (Figure 5.9). Remarkably, our results therefore suggest that Wnt pathway activation is able to rescue uncapped telomeres, even in the absence of telomerase.

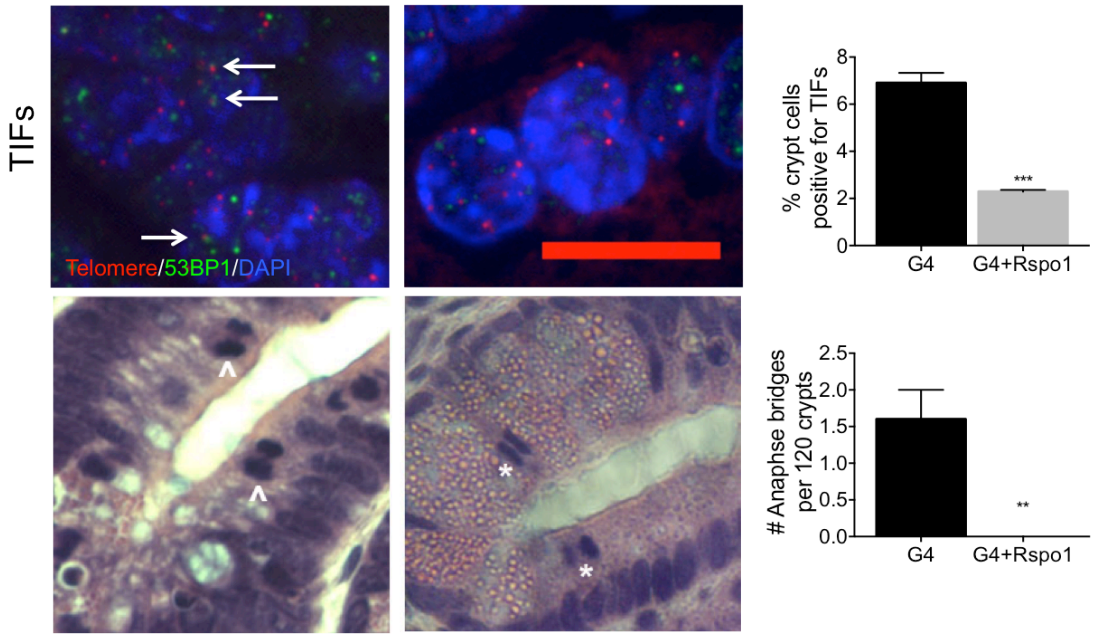

Figure 5.9. Enhanced Wnt signaling rescues telomere capping in G4 *mTR*$^{-/-}$ crypts *in vivo*. G4 *mTR*$^{-/-}$ mice treated for eight days with subcutaneous injections of R-spondin1 (Rspo1) have reduced telomere dysfunction as measured by (top panel) telomere-dysfunction induced foci (TIFs) and (bottom) anaphase bridges (arrowheads on *left* panel; asterisks mark normal anaphases in Rspo1-treated mice on *right*). 120 crypts per mouse from 5 control G4 mice and 4 Rspo1-treated G4 mice were surveyed for anaphase bridges, ** $p<0.005$, *** $p<0.0005$. Scale bars: 10μm (top panel).

Telomere capping also depends on telomere length, and Wnt signaling has recently been shown to upregulate TERT to elongate telomeres (190), but elongation by telomerase is not possible in *mTR*$^{-/-}$ mice. To rule out telomerase-independent mechanisms of telomere elongation (i.e. alternative lengthening of telomeres, ALT), we compared telomere lengths of treated and untreated G4 *mTR*$^{-/-}$ mice using quantitative telomere FISH. Telomere lengths in crypt epithelial cells of lithium or Rspo1-treated G4 *mTR*$^{-/-}$ mice were not longer than those of untreated G4 *mTR*$^{-/-}$ mice (Figure 5.10). Therefore, the rescue of uncapped telomeres is not explained by increased telomere length. Our data indicate that *Trf2* and *Pot1a* are Wnt-responsive genes, and raise the possibility that the rescue of uncapped telomeres by Wnt pathway activation may be explained by an upregulation of shelterin components to improve telomere capping.

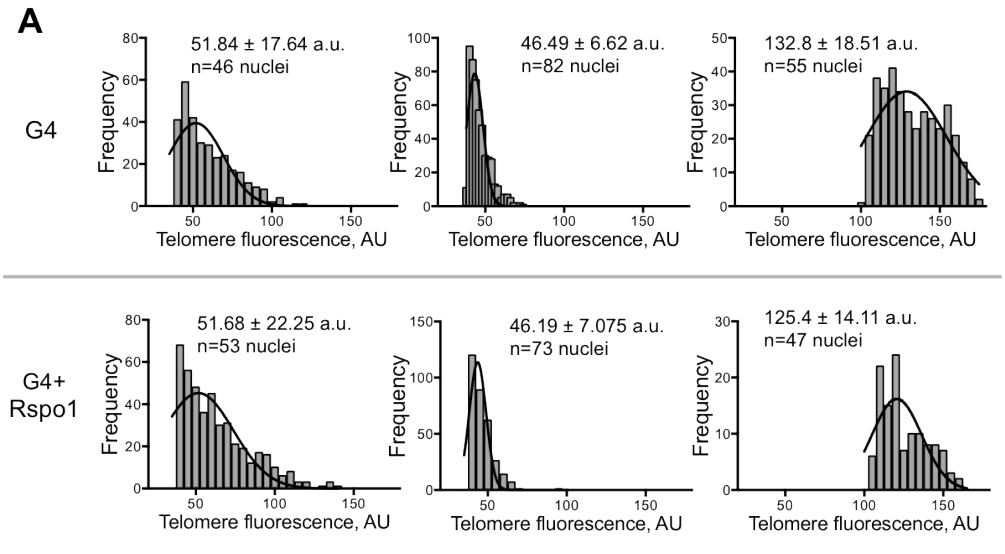

Difference between medians	+3.387 (longer in Rspo1-treated mouse)	-0.28 (shorter in Rspo1-treated mouse)	-8.251 (shorter in Rspo1-treated mouse)
Significant?	No (p=0.103)	No (p=0.269)	Yes (p=0.0002)

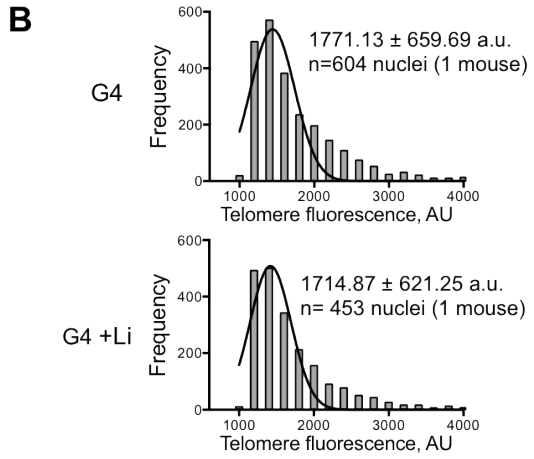

Difference between medians	-33.52 (shorter in Li-treated mouse)
Significant?	Yes (p<0.005)

Figure 5.10. Histogram of telomere fluorescence frequency by Q-FISH analysis of intestinal crypts of G4 *mTR*$^{-/-}$ mice treated with Rspo1 or lithium-chow. (A) Three pairs of untreated and Rspo1-treated G4 *mTR*$^{-/-}$ mice were stained and imaged on different days; hence comparisons were not averaged. (B) One pair of untreated and Li-treated G4 *mTR*$^{-/-}$ mice. Mean and SD of telomere fluorescence, and the number of nuclei analyzed, are indicated on each graph.

Wnt pathway suppression in human fibroblasts with telomere dysfunction is rescued by Wnt pathway agonists.

Patients with dyskeratosis congenita (DC) suffer from short telomeres secondary to telomerase deficiency, and display gastrointestinal pathology closely resembling that seen in late-generataion *mTR*$^{-/-}$ mice (275). As described in Figure 5.11, we analyzed mRNA levels in primary cultured fibroblasts from DC patients carrying mutations in the telomerase component dyskerin, and compared to primary fibroblasts from healthy controls, DC fibroblasts had reduced expression of *AXIN2*, a direct target of the Wnt pathway (Figure 5.11). Levels of *TRF2* and *POT1* transcripts were also reduced in DC fibroblasts, and upon treatment with CHIR99021, the levels of transcripts from all three genes were elevated (Figure 5.11). Similar results were obtained for primary Werner syndrome (WS) fibroblasts, which also suffer from telomere loss events, but which are caused by DNA replication defects that can be rescued by telomerase (e.g. from overexpression of *hTERT*) (120). Indeed, *hTERT* expression in WS cells led to elevated levels of *AXIN2*, *TRF2*, and *POT1*, as did CHIR99021.

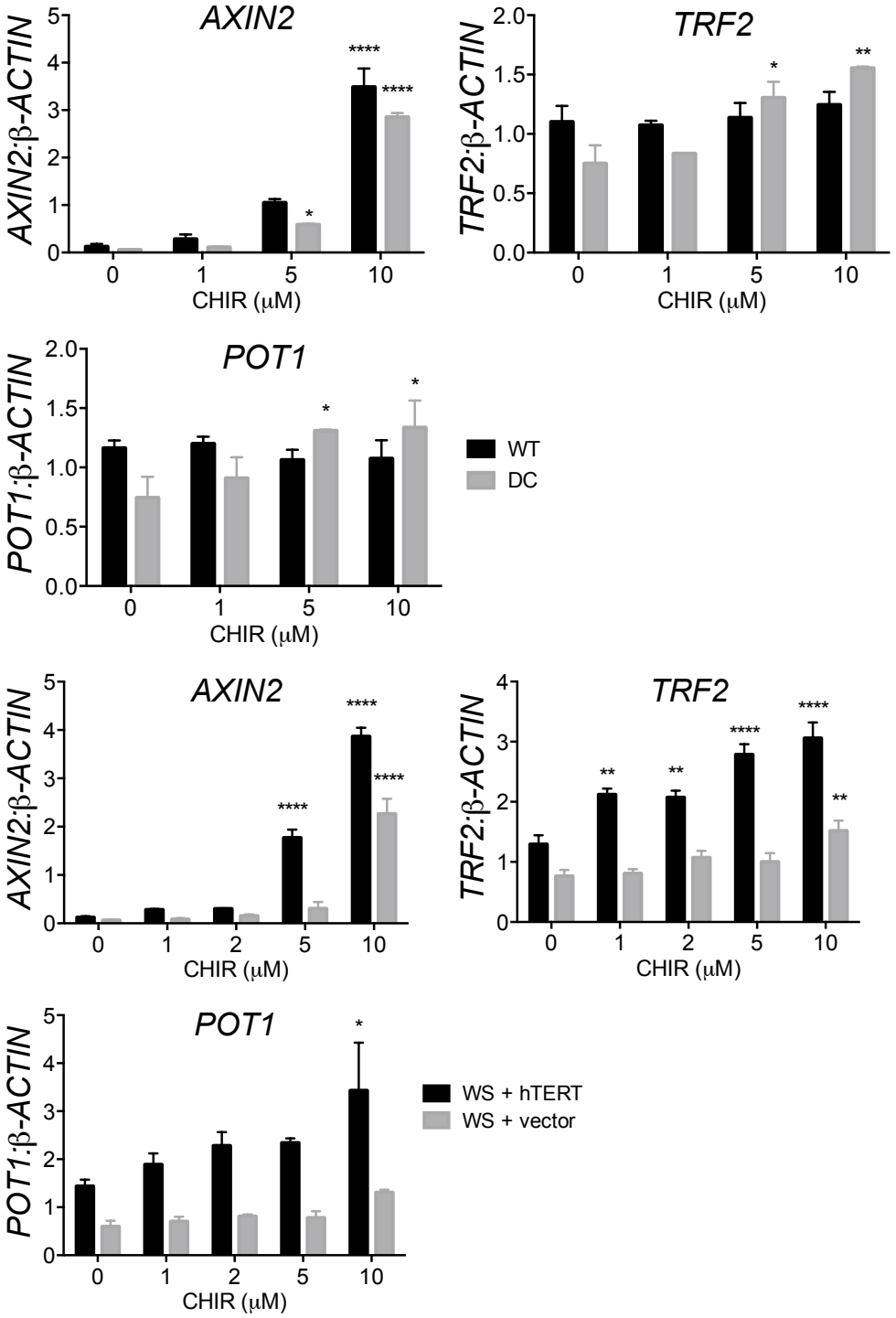

Figure 5.11. Primary human fibroblasts with telomere dysfunction display reduced expression of WNT pathway target genes include shelterins, which is rescued by CHIR99021. Expression of *AXIN2*, *TRF2*, and *POT1* mRNA levels in primary human fibroblasts from three healthy people (WT) and two people with dyskeratosis congenita (DC) treated with the indicated levels of

CHIR99021 for 48 hours (top three panels), and a person with Werner syndrome (WS) infected with retrovirus expressing hTERT or a vector control and treated with the indicated levels of CHIR99021 for four days (bottom three panels). * $p<0.05$, ** $p<0.005$, **** $p<0.0001$.

DISCUSSION

The functional importance of the Wnt pathway downregulation in the intestines of late generation *mTR*$^{-/-}$ mice is highlighted by the rescue provided by treatment of the mutant mice with Wnt pathway agonists. Treatment with lithium or Rspo1 reduces apoptosis, improves epithelial architecture and restores expression of Wnt pathway genes. Similarly, treatment of cultured mutant intestinal organoids with Rspo1 or CHIR990201 improves survival, crypt budding, and gene expression. Importantly, components of the Wnt pathway are Wnt target genes themselves (e.g. *Lgr5*, encoding the Rspo1-responsive component of the Wnt receptor complex), providing a mechanism by which the effects of Wnt pathway agonists can be amplified over time to restore the pathway. An component of the rescue was that telomere capping is reestablished, as indicated by reduced TIF levels and complete rescue of anaphase bridges. The telomere capping is not explained by telomere lengthening, but rather is associated with restoration of expression of key shelterin genes, including *Trf2* and *Pot1a*. Suboptimal levels of these factors lead to telomere dysfunction (146, 197), and *TRF2* overexpression can cap telomeres that have shortened to the point where they would otherwise be uncapped (276). We therefore suggest that restored shelterin expression plays a key role in the improved telomere capping and overall rescue.

This hypothesis will be explored in future studies, but we note that it is strongly supported by the recent demonstration that loss of telomere capping caused by diminished Wnt signaling (*via* reduced β-catenin expression) in human cancer cells can be rescued by *TRF2* overexpression (196). To see if TRF2 upregulation is sufficient to rescue uncapped telomeres and G4 crypt survival, we have begun designing experiments to express exogenous TRF2 in G4 organoids (lentiviral system) or to upregulate endogenous TRF2 in G4 organoids with statin treatment (which has been shown to stimulate TRF2 expression (277)). Regardless of the exact mechanisms by which Wnt pathway activation mediates improved telomere capping, these findings suggest that telomere capping is influenced by extracellular cues, and raise the possibility that disorders in which telomere dysfunction plays a pathogenic role (e.g. DC, and perhaps also inflammatory bowel diseases and age-related disorders (278, 279)) might be treated by Wnt pathway agonists.

CHAPTER 6: MOUSE COLONOSCOPY AS A USEFUL TOOL FOR TRACKING DISEASE IN MICE

INTRODUCTION

Mice are the most commonly used model to study diseases of the GI tract, and until most recently, there was no non-lethal way to visualize intestinal pathology – the organ in question had to be harvested and processed accordingly, which required the mouse to be killed. Owing to the small nature of the mouse and the small diameter of the murine colon, endoscopies have not been a convenient technique to perform. Instead, indirect measurements that offered hints about GI function and pathology (i.e. weight gain/loss, food and water intake/outtake, presence of blood in the stool, etc.) are used to track pathology over time in an individual mouse. However, these parameters are not sensitive or specific for minor or major changes occurring in the GI tract. Endoscopies are a useful tool to visualize the gastrointestinal tract for pathology. They are regularly used in humans as a modality for diagnostic purposes, for visualization of cancers (polyps) or sources of inflammation/bleeding, to track disease progression or improvement, among other purposes. In recent years, endoscopic technology in small mammals has improved to a point where high-resolution movies and images can be consistently obtained from the colon of a living mouse (280). More recently, advances to the technology (i.e. flexible sigmoidoscopy) allow us to visualize more proximal regions of the colon (281). Chromoendoscopy employs the use of dyes as contrast medium with endoscopy (such as methylene blue or indigo carmine) and can offer us additional information about the architecture of

the colonic crypts, and certain patterns are indicative of certain disease processes. Multiple scoring systems exist to allow us to evaluate degrees of inflammation, although there is a lack of standardization among the community (280, 281). Researchers have been slow to adopt the use of the endoscope to assess and track colonic state, since the initial equipment costs are prohibitive and there is no established protocol on scoring pathology in mouse colons.

We want to characterize and track *mTR*$^{-/-}$ mouse gastrointestinal pathology in a non-lethal and relatively non-invasive way over time, since there is a lot of variation between age-matched littermates, between generations and age of the mice. We also want to see whether the pathology we see on colonoscopy is representative of the pathology in the rest of the GI tract. In humans, different inflammatory bowel diseases have distinct regions of pathology in the GI tract. For example, Crohn's disease (CD) affects the entire length of the GI tract whereas ulcerative colitis (UC) is restricted to the colon. We do not know whether GI pathology occurs simultaneously in the *mTR*$^{-/-}$ small intestine as it does in the colon. It is also reasonable to ask whether different parts of the small intestine and colon have different degrees of pathology. Since rates of telomere shortening depend on the rates of cell division, it is reasonable to propose that the onset and degree of GI pathology depends on when telomeres become uncapped and is dependent on rates of stem cell proliferation/epithelial turnover in different parts of the GI tract.

The epithelial turnover rate generally depends in part on the length of the crypt-villus distance, and the type and function of the epithelium in question. The epithelial turnover rate of the small intestine is around 3-5 days (15 days for Paneth cells) (175). The stem cell dynamics of the ascending and descending colon are different. There are fewer proliferative stem cells and the cell cycle duration is longer in the ascending colon compared to the descending colon (282). And since the stem cells are located in the mid-crypt region in the ascending colon, there is a bi-directional movement of progeny cells whereas there is an lumenal movement of progeny cells from the base of the crypts in the descending colon. The turnover rate of the colonic epithelium is about 5 days (the ascending colon has deep crypt secretory cells that turnover every 14-21 days) (238).

It would useful to correlate the degree of pathology seen with colonoscopy to the telomere capping state (measured by TIFs) on histology. If there is good correlation between a certain degree of telomere dysfunction to the visualized pathology, we will be able to reliably use endoscopic images to assess for the progression of telomere dysfunction. We can also use endoscopy to readily see if certain factors (e.g. drugs, diets, or introducing a genetic mutation) can help prevent or even reverse the observed pathology in late generation *mTR*$^{-/-}$ mice. If we are able to track disease progression/amelioration in one mouse, there is less need for large numbers of animals per study to minimize mouse-to-mouse differences since it is internally controlled.

The intestinal pathology in *mTR*$^{-/-}$ mice has been somewhat well-characterized, but has mostly focused on the small intestine. There is certainly also disease in the colon of the *mTR*$^{-/-}$ mice, and it has been described in brief in a handful of papers, characterized to the full extent in literature by whole mount methylene blue staining of the colon (161). Otherwise, description of the pathology is vague, usually describing a loss of crypt numbers, and increased inflammation, but beyond that, there is little data. In this section, we outline our experimental plans to correlate the pathlogy seen on colonoscopy to that seen with histology, including markers of telomere dysfunction, along the length of the intestine. We provide preliminary data and give our initial impressions on the usefulness and validity of the technique. This part of the thesis was conducted in the lab of Arturo Londoño-Vallejo at Institut Curie of France.

METHODS

The following procedures were performed at Institut Curie with the collaboration and support of Drs. Arturo Londoño-Vallejo and Danijela Matic-Vignjevic. A straight-type rigid miniature Coloview mouse endoscopic system (Karl-Storz) (Figure 6.1) linked to a computer with video acquisition software was used to visualize and record videos and images of the mouse colon. The setup is as

seen in Figure 6.1.

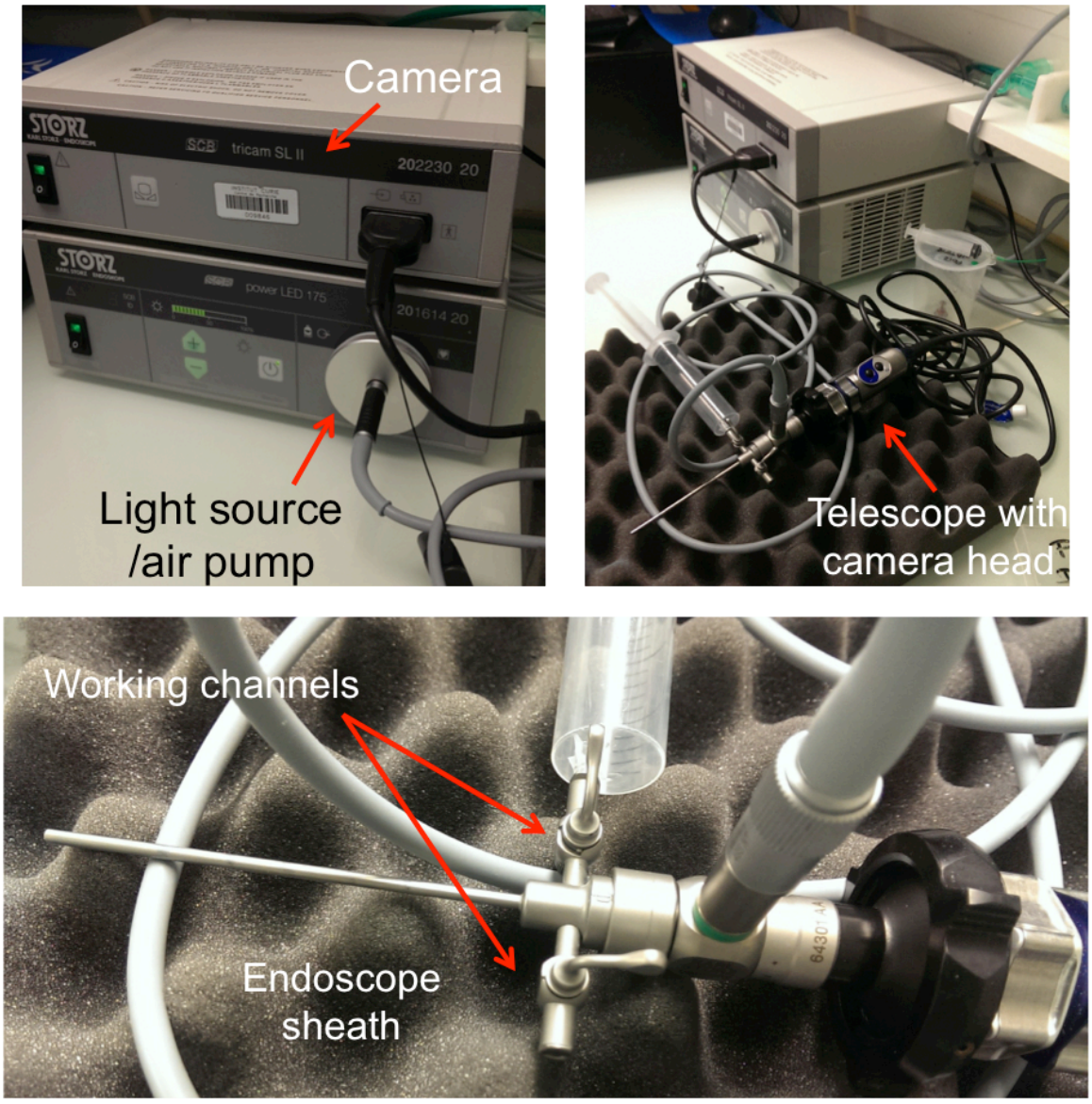

Figure 6.1. Setup of colonoscopy equipment. A straight-type rigid miniature Coloview mouse endoscopic system (Karl-Storz) was used.

After mouse anesthesia with isoflurane administered from a vaporizer connected to an enclosed chamber, the mouse anus was lubricated and the colon was flushed with a small amount of 1% methylene blue dye, and moved to a platform with isoflurane administered through a nose mask. After 3-5 minutes,

the colon was flushed with water to clean out any stool or extra methylene blue dye. The endoscope probe was introduced to the mid-descending colon, and videos and images were recorded. The images were chosen carefully to show similar viewpoints in terms of endoscopy camera orientation. Table 4 provides a summary of all of the mice we scoped, which includes their genotype, age, sex, and other measurements, such as weight and general physical appearance. We chose as many littermates as we could of various ages from different genotypes (littermates are indicated by the same age). We did not harvest intestines from all of the mice we performed colonoscopies on, but for those that we did, we waited 3-5 days after colonoscopy for the methylene dye to pass, in case the dye interfered with downstream histology analyses. We harvested the following tissues separately: duodenum, jejunum, ileum, ascending colon and descending colon.

RESULTS

We surveyed mice of different ages of different genotypes, performing one-time colonoscopies and organ harvest a few days later (Table 4). Representative images obtained from the colonoscopy will be shown in the following figures as described. In the wild-type, $mTR^{+/-}$ (F1), and G1 $mTR^{-/-}$ mice, there were no unexpected or remarkable findings in terms of age-inappropriate weight loss or pathology in outward appearance. All mice appeared healthy and normal, with no physical signs of pathology commonly seen in late generation $mTR^{-/-}$ mice (e.g. kyphosis, greying hair, rectal prolapse, diarrhea, etc.). Littermates were of

comparable age, with one G1 mouse being slightly heavier than two of its littermates.

Table 6.1. Description of mice that had undergone colonoscopies. Mice of different ages (in weeks) of each indicated genotype underwent colonoscopies and their general physical appearance were noted (including any findings during organ harvest). Their weights (in grams) were taken right before the colonoscopy and if their intestines were collected for histology, right before harvest. Lengths of small intestines from the duodenum to just before the cecum were measured if intestines were collected for histology (in centimeters).

Genotype	Age (wks)	Sex	Wt (g)	Wt at harvest	Small int length (cm)	Physical appearance
WT	6	M	16.3	19.4	33	Looks healthy
WT	47	M	30.4			Looks healthy
WT	47	M		36.6	32	Looks healthy
F1	7	M	21.1			Looks healthy
F1	7	M	21			Looks healthy
F1	7	M	19.8			Looks healthy
F1	16	M	29.6	33.7	37	Looks healthy, peritoneal 6x6mm mass (sent for histo)
F1	16	M	30.9			Looks healthy
F1	30	F	24.6	23.4	33	Looks healthy
F1	37	M	27.9			Looks healthy
G1	7	F	16.5			Looks healthy
G1	7	M	16.7			Looks healthy
G1	7	M	20.2			Looks healthy
G1	9	F	17	17.7	33	Looks healthy, ileum epithelium is bumpy/rough looking
G1	39	M	25.5	29.7	28	Looks healthy
G1	110		23.5			Looks mainly healthy, minor kyphosis
G2	7	M	20.5			Looks healthy
G2	7	M	19.4			Looks healthy
G2	7	M	14.5			Loose stool, otherwise

						healthy looking
G2	9	M	21.5			Looks healthy
G2	9	M	19.5	21.3	32	Looks healthy
G2	55	M	20.9	21.7	21	Graying hair, kyphosis
G2	55	F	25.1	24.5	29	Looks healthy
G2	57	M	20.4			Looks healthy, mild kyphosis
G2	59	F	18.9			Graying hair, kyphosis, rectal prolapse
G2	70		23			Looks healthy
G2	70		14.5			Kyphosis
G3	7	F	13			Looks healthy
G3	24	F	16.3			Looks healthy
G3	24	F	13.2			Graying hair, diarrhea
G3	32	F	21.3	22	35	Alopecia
G3	32	F	20			Alopecia, crusting around rectum
G3	45	F	18.2	17.7		Graying hair, kyphosis
G3	45	M	13.1			Looks sick and weak, graying hair, small head, kyphosis
G3	59	F	14.7			Looks sick, blood and crusting around rectum
G3	59	F	18.5	18.3	25	Skinny, kyphosis
G3	70		24.4			Looks healthy
G3	70		18.3			Looks sick, kyphosis, diarrhea
G4	7	M	15.8			Looks healthy (failed colonoscopy attempt)
G4	7	M	15.5	17.2	34	Looks healthy
G4	20		26			Looks healthy
G4	20		17			Looks healthy
G4	22	F	14.1	15.3	21	Mild kyphosis
G4	22	F	14.1	14.8	24	Looks sick, graying hair, kyphosis, bloody rectum, diarrhea

On colonoscopy (Figure 6.2, only F1 shown), the WT and F1 mice had a nice, dense honeycomb crypt pattern, with easy visualization of the underlying mucosal blood vessels. However, when comparing a 32-week and a 110-week old G1 *mTR*$^{-/-}$ mouse, there was a drastic difference in the colonoscopy exam. Like WT and F1 mice, the 32-week old G1 mouse colon also had a dense honeycomb crypt pattern with visible mucosal blood vessels, whereas the 110-week old G1 mouse colon had major crypt losses, with enlarged crypt lesions, loss of blood vessel visualization (Figure 6.3), indicative of severe inflammation (280). Given these findings, it seems that endoscopy may be more sensitive at detecting age-related pathology than other physical measurements (e.g. weight).

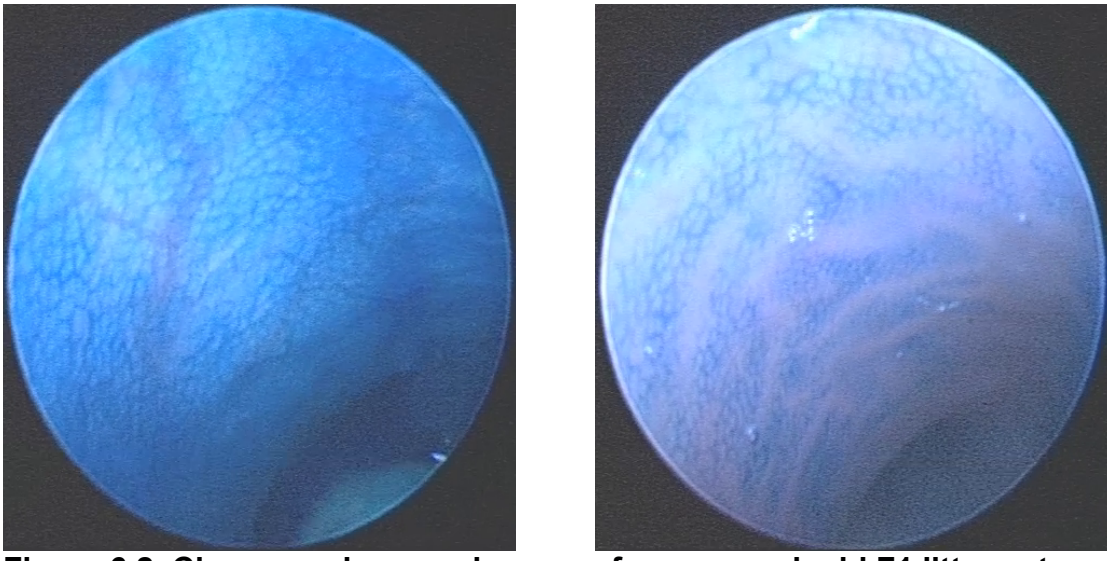

Figure 6.2. Chromoendoscopy images of seven-week old F1 littermate colons. Healthy-appearing F1 littermates weighing 21g (left panel) or 19.8g (right panel).

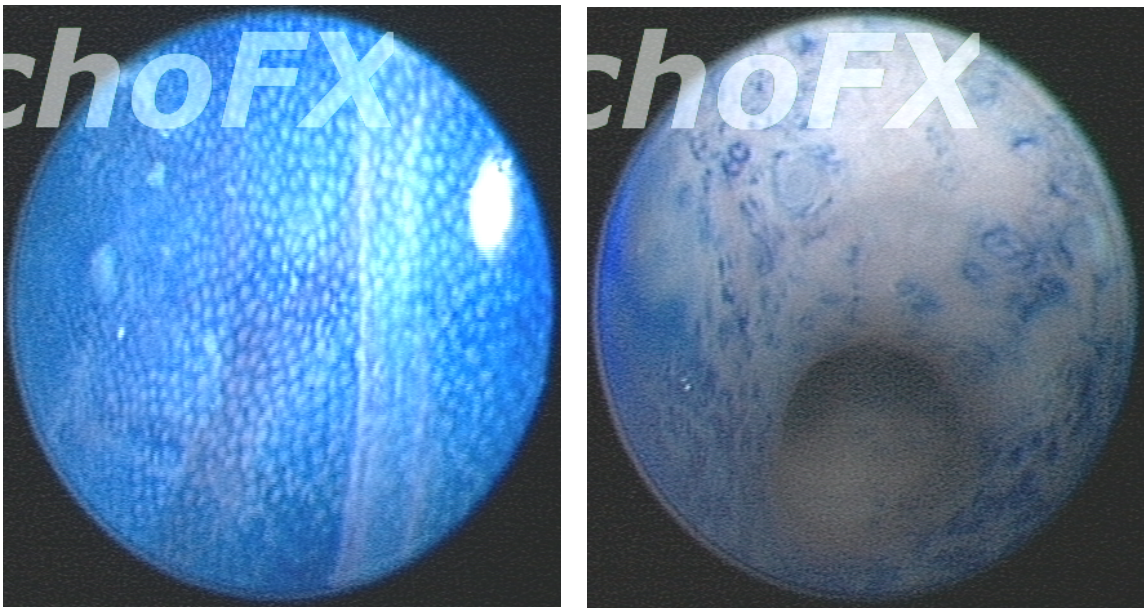

Figure 6.3. Chromoendoscopy images of G1 mouse colons. Healthy-appearing G1 mouse of 32 weeks of age weighing 33g (left panel) and a G1 mouse of 110 weeks of age weighing 23.5g with mild kyphosis (right panel)

In the G2 cohort, two out of three of the youngest littermates (seven weeks of age) had age-appropriate weights and had a healthy appearance. However, one of the littermates had markedly reduced weight and some diarrhea. On colonoscopy (Figure 6.4), both of these mice had dense honeycomb crypt structures (although perhaps not as dense or organized as the WT or young healthy F1/G1 colons) and visualization of underlying blood vessels. In this littermate matchup, there was no obvious difference in the pathology as assessed by colonoscopy. This is an instance where it would be interesting to track these littermates over time to see if weight difference is a good early predictor/parameter of: 1) degree of telomere dysfunction, 2) lifespan of the individual, and 3) degree of intestinal pathology.

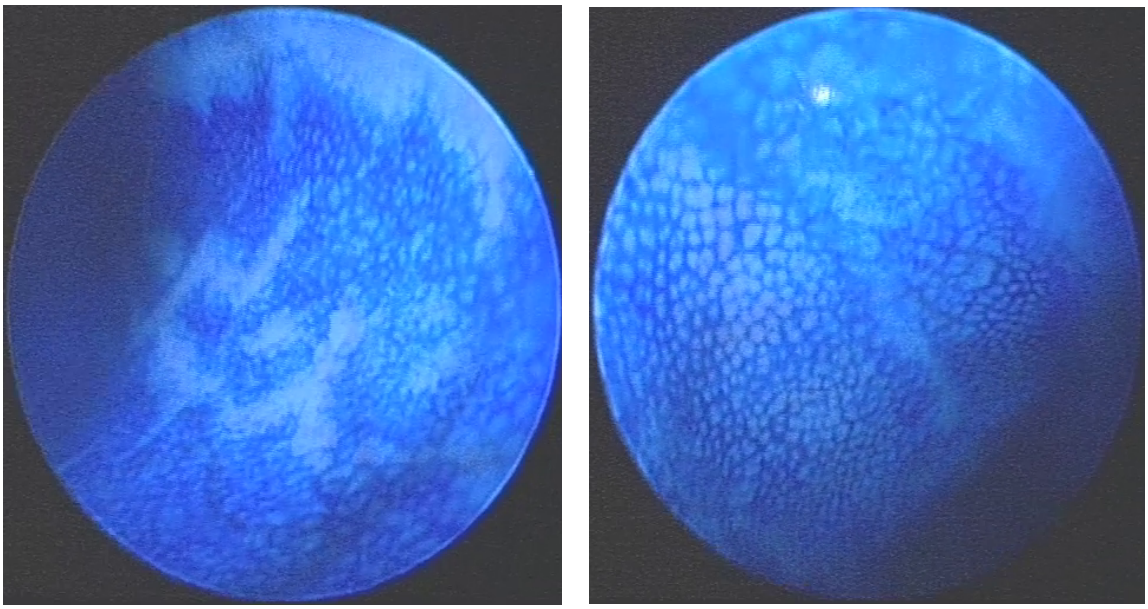

Figure 6.4. Chromoendoscopy images of seven-week old G2 littermate colons. G2 littermates weighing 20.5g (left panel) or 14.5g with loose stool (right panel).

Among the older G2 cohort (55-59 weeks of age), outward signs of pathology are more obvious, with the heaviest mouse out of the four having no obvious signs of pathology, and the other three all showing signs of kyphosis, two of which have greying hair, and the skinniest of the four also with rectal prolapse and wasting. Similarly, in the oldest G2 cohort (70-week old littermates), one sibling appears healthy while the other has kyphosis and weight loss. On colonoscopy (Figure 6.5), these 70-week old G2 littermates both have a loss of dense and organized crypt structures and loss of vessel visualization, with the smaller and sicker mouse having a more severe colonic pathology. It is interesting but perhaps not counterintuitive to see much more severe changes on the colonoscopy images than what we can detect from other physical

measurements (e.g. weight, appearance, etc). Morever, there is a trending correlation between weight, outward appearance, and colonoscopy changes.

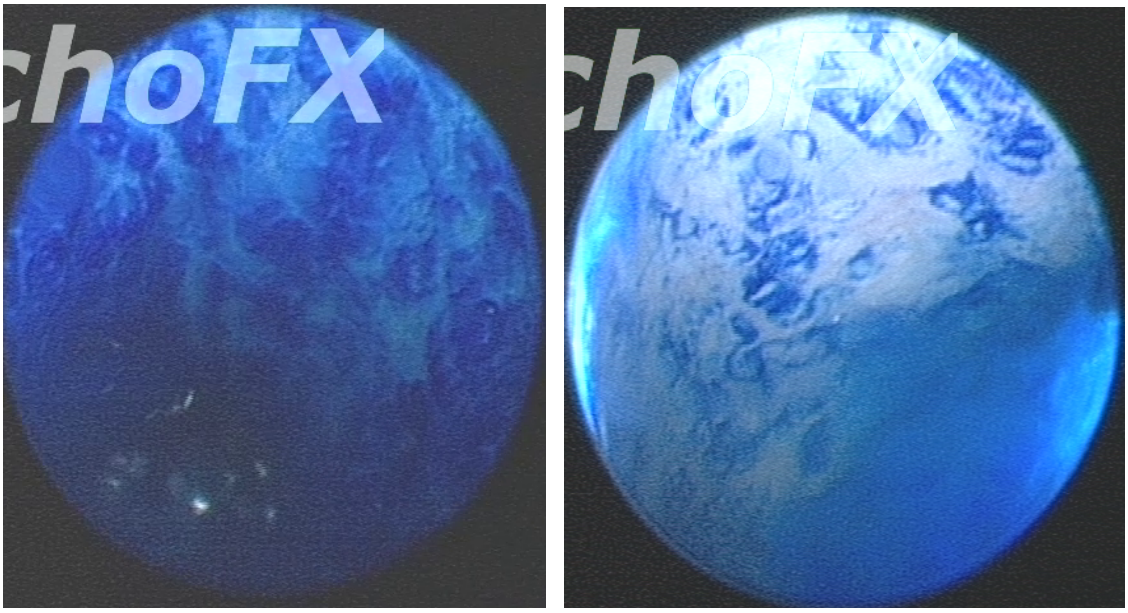

Figure 6.5. Chromoendoscopy images of 70-week old G2 littermate colons. G2 littermates weighing 23g and healthy-appearing (left panel) or 14.5g with kyphosis (right panel).

Among the G3 cohort, there are signs of disease anticipation (where pathology shows up earlier in later generations than the earlier generations due to the inheritance of shorter telomeres), as seen in the 24-week old G3 mouse with diarrhea and greying hair. Interestingly, its slightly larger littermate had no outward signs of pathology. Likewise, on colonoscopy, (Figure 6.6), the sicker littermate had signs of colonic pathology whereas the healthier littermate had very little colonic pathology.

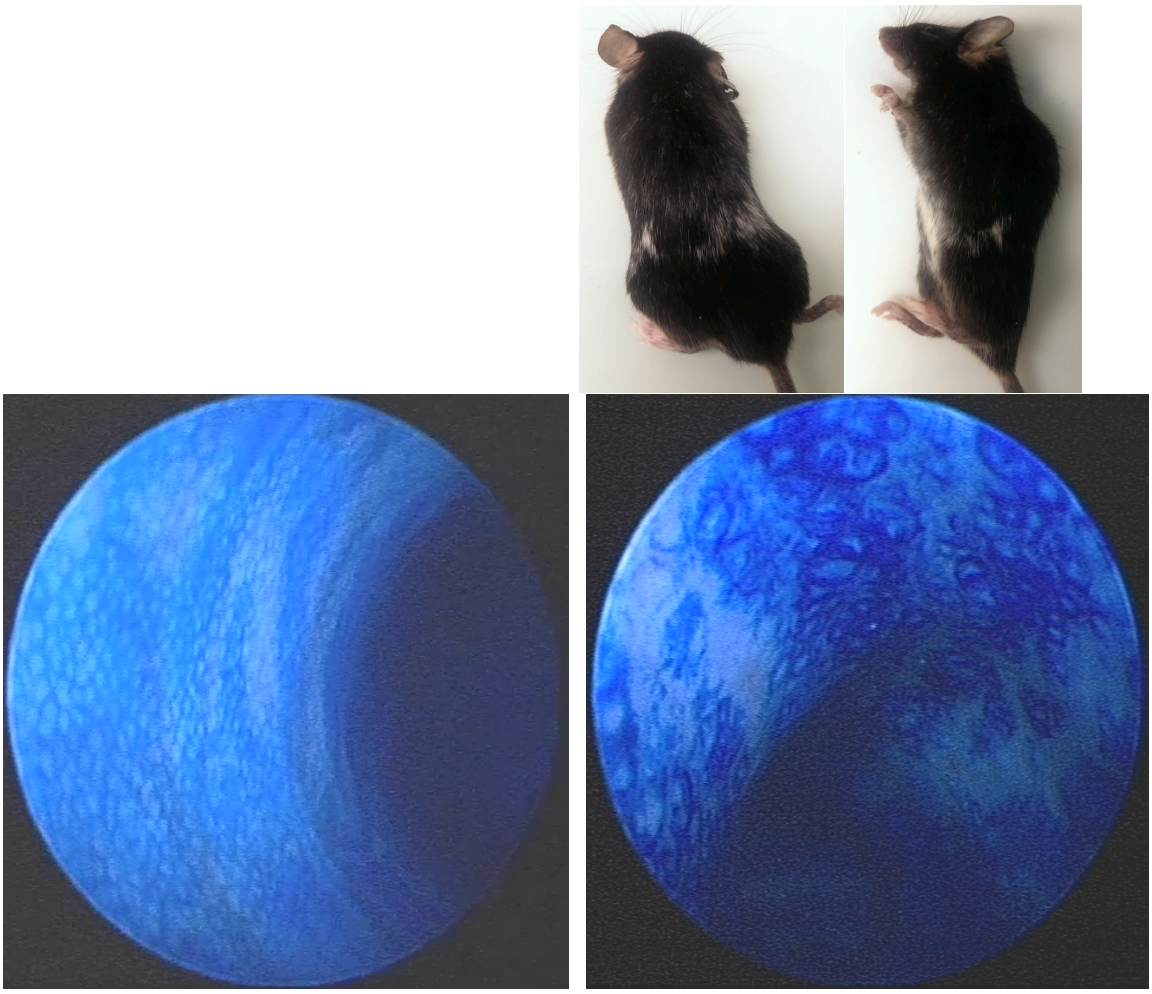

Figure 6.6. Chromoendoscopy images of 24-week old G3 littermate colons. G3 littermates weighing 16.3g and healthy-appearing (left panel) or 13.2g with kyphosis, diarrhea, and greying hair (top and right panels).

In almost all of the G3 mice older than 32 weeks of age, there were signs of wasting (age-inappropriate weight loss compared to WT, F1, and G1 mice of similar ages) and other late-generation *mTR*$^{-/-}$ related pathologies, with degenerative crypt losses seen with colonoscopy. In the pair of 70-week old littermates, one mouse looked healthy while the other had diarrhea and kyphosis. As seen in earlier examples, despite a lack of observable gross pathology in the

healthier and heavier mouse, the colonoscopy images show clear disease (Figure 6.7), and the sicker, skinner mouse had almost a complete loss of crypts.

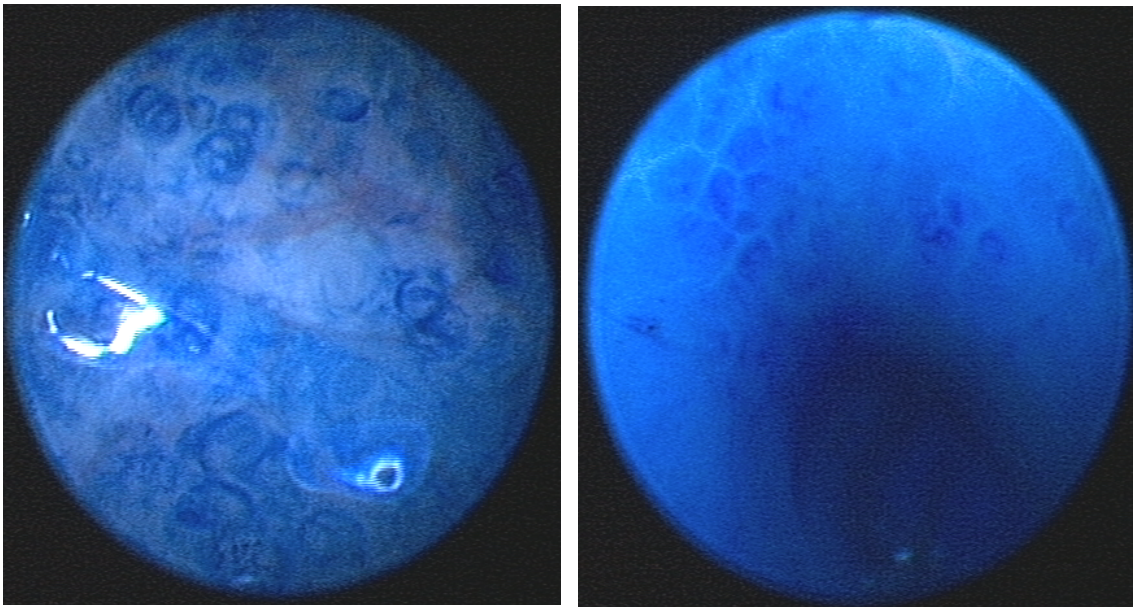

Figure 6.7. Chromoendoscopy images of 70-week old G3 littermate colons. G3 littermates weighing 24.4g and healthy-appearing (left panel) or 18.3g with kyphosis, and diarrhea (right panel).

Disease anticipation can also be seen in the G4 cohort, with both of the 22-week old littermates showing signs of wasting, kyphosis, and one of the two mice having diarrhea and rectal bleeding. On colonoscopy (Figure 6.8), both mice have comparable levels in the loss of crypts and blood vessel visibility. At 7 weeks, the two G4 littermates are comparable in weight and outward appearance, having no signs of physical pathology. One of the mice had a perforated colon during colonoscopy, and we were not able to obtain any useful images.

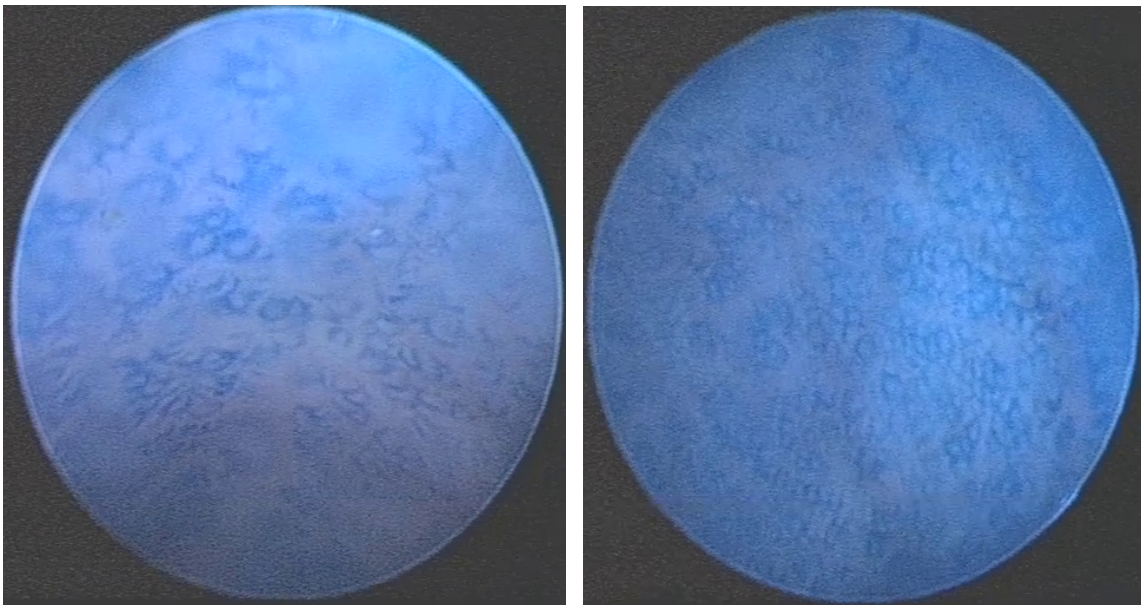

Figure 6.8. Chromoendoscopy images of 22-week old G4 littermate colons. G4 littermates weighing 14.1g and kyphosis (left panel) or 14.1g with kyphosis, diarrhea, and bloody rectum (right panel).

DISCUSSION

With our survey of cohorts of mice at different ages and genotypes, we are beginning to appreciate the huge variations that exist in physical characteristics (e.g. weight, kyphosis, diarrhea) and pathology seen with colonoscopy. What is clear is that changes in the colon (i.e. loss of vessel visualization, crypt losses and aberration) appear before any changes in weight or physical appearance occur in *mTR*$^{-/-}$ mice, which makes sense considering the higher rates of environmental insult and epithelium turnover the intestine experiences compared to other tissues. What has already been known from literature is the variation in telomere lengths between littermates and within a generation of *mTR*$^{-/-}$ mice, and we also see large variation in colon pathology within same generation *mTR*$^{-/-}$ littermates. We will have to confirm and correlate these findings with histological analyses (e.g. Q-FISH, TIFs, anaphase bridge counts, etc.). Further, our study clearly shows the disease anticipation aspect of *mTR*$^{-/-}$ pathology, with later generations displaying pathology at younger ages. We also see that if you age an early generation (110-week old G1) mouse long enough, telomeres can shorten critically within an individual to cause pathology. It is unlikely but possible that this individual G1 mouse inherited critically short telomeres at birth, and we cannot confirm it at this time since we did not perform colonoscopy on this mouse when it was younger. But with the advantages of colonoscopy (i.e. non-lethal, and we can take sample biopsies), we can longitudinally characterize the colon of an individual mouse. Histologic analyses have yet to be performed, but we plan to evaluate the H&E staining for general morphology, TUNEL staining for

apoptosis measurements, TIF staining for measurements of telomere dysfunction. In addition, we hope to be able to find a correlation between degrees of pathology seen in different parts of the small intestine to the proximal and distal colon and colonoscopy. In summary, we conclude that colonoscopies provide us with sensitive approach to evaluate *mTR*$^{-/-}$ pathology, between littermates, ages, and genotypes, or within a single mouse. It also give us a the potential to design better experiments in the future by picking mice for experiments based on degrees of pathology and not necessarily based on littermates or age-matched controls.

CONCLUSIONS AND FUTURE DIRECTIONS

This thesis has further characterized the pathology in the *mTR*$^{-/-}$ mouse model. To summarize our findings, we observe a suppression of Wnt pathway components in intestinal crypts of mice with dysfunctional telomeres (late-generation *mTR*$^{-/-}$). Multiple components of the canonical Wnt signaling pathway are downregulated in G4 crypts (i.e. ligand, receptor, and downstream effectors), which all conspire to downregulate Wnt target gene expression. Specifically, there was a dramatic loss of Wnt-responsive ISC marker expression (i.e. *Ascl2*, Sox9, and *Lgr5*, which mark CBCs) without losses in non-Wnt-responsive ISC markers (i.e. Msi1) or apparent losses of crypt cells that are intercalated between Paneth cells, which represent the CBC population. Lgr5 is a Wnt target gene but also an important Wnt receptor in CBCs, providing positive feedback on Wnt signaling, therefore, downregulation of Lgr5 in G4 crypts will further decrease Wnt signaling. We (and others) have found evidence that several components of the shelterin complex, important in the maintenance of telomere capping, are Wnt target genes. Indeed, in G4 crypts, we detect a significant downregulation in *Trf2* and *Pot1a* expression, which may add further insult to an already injured (uncapped) telomere. This positive feedback between Wnt signaling and telomere capping may be an anti-cancer mechanism that a cell with a high propensity for genomic instability and carcinogenesis (fast cycling cells with rich pro-Wnt signals) has acquired. In the case of the APC^{Min} mouse model, loss of wild-type *Apc* allele causes an unchecked activation of Wnt signaling, eventually manifesting as intestinal adenomas that initiate as microadenomas and progress

into macroadenomas, resulting in death in 100% of the animals by 4-6 months. When the *mTR*$^{-/-}$ allele is introduced into APC^{Min} mice, there is a decrease in survival in G2 and G3 *mTR*$^{-/-}$APC^{Min} compared to APC^{Min}, but there is a drastic increase in survival at G4 (all the animals survived until sacrifice at 7 months to assess tumor burden) (283). The improved survival at G4 *mTR*$^{-/-}$APC^{Min} is associated with increased microadenomas but reduced macroadenomas, which suggests that telomere dysfunction may contribute to genomic instability and cancer initiation, but ultimately, advanced telomere dysfunction can set off DNA damage responses and apoptosis to halt cancer progression. The authors did not assess for Wnt pathway defects in the G4 *mTR*$^{-/-}$APC^{Min} intestine, but it is plausible that advanced telomere dysfunction halted cancer progression in the APC^{Min} model by suppressing Wnt signaling via DNA damage responses.

The suppression of Wnt signaling appears to be dependent on DNA damage responses and p53 activation, and we hypothesize miR-34a activation by p53 to be one of the mediators of the Wnt pathway suppression. It is the most overexpressed miRNA in the G4 crypt, and it has been shown to promote senescence and tumor suppression and suppress multiple components of the Wnt pathway. Our preliminary results show a perinatal survival advantage of G4 mice lacking miR-34a and an increase in survival of G4 *miR-34a*$^{-/-}$ organoids over G4 *miR-34a*$^{+/+}$. As we have seen with the endoscopic study in this thesis, there are huge natural variations in the phenotypes of these mice, even amongst littermates (which is most likely due to the inheritance of different telomere lengths), and larger sample sizes are necessary before we can make conclusive

statements about the significance of knocking out *miR-34a* in *mTR*$^{-/-}$ mice. Moreover, since miR-34a has so many different targets, it would be difficult to determine exactly what is mediating the rescue downstream of miR-34a. The cell has evolved many mechanisms and pathways downstream of DDR to arrest cell cycle progression and the accumulation of genomic instability. In fact, a positive feedback loop also exists between p53 and miR-34a, where miR-34a inhibits Mdm4, an inhibitor of p53. Similarly, inhibition of the Wnt pathway by miR-34a is another possible anti-cancer mechanism that has evolved.

Next, we questioned the functional relevance of the Wnt suppression in G4 crypts and hypothesized that supplying exogenous Wnt signals can upregulate shelterin proteins Trf2 and Pot1a to improve telomere capping in G4 crypts. Indeed, we detect a dose-dependent upregulation of *Trf2* and *Pot1a* in organoids cultured with Wnt agonists CHIR99021, and G4 mice treated with Rspo1 had reduced TIFs and anaphase bridges in their crypt cells. The upregulation of *Trf2* and *Pot1a* and the improvement in telomere capping corresponded to an improvement in G4 organoid survival, and rescue of CBC markers (i.e. *Lgr5*, *Ascl2,* and Sox9) in the G4 crypts.

We present novel findings that demonstrate a mutually supportive feedback loop between Wnt signaling and telomere capping, which provides insight into how Wnt signaling and telomeres may interact in cancer. Recent studies show Wnt signaling to regulate TERT expression, and our study, among others, provide evidence for Wnt signaling to regulate shelterin expression. Sufficient Wnt signaling can help maintain telomeres in a capped state by

regulating shelterin and TERT expression, especially important in cells where maintenance of capped telomere is essential. However, too much Wnt activity can be detrimental, as evidenced by inactivating mutations of APC in humans, which lead to unchecked Wnt signaling and colorectal cancer. On the other hand, if telomeres become uncapped (i.e. from uncontrolled cell division in preneoplastic cells), DNA damage responses are activated to suppress Wnt signaling, which in turn suppresses shelterin and TERT expression, reinforcing the state of uncapped telomeres. This feedback loop may serve as an anti-cancer mechanism – Wnt signaling, which can be a pro-cancer signal, is suppressed. Furthermore, the reinforced uncapping of telomeres can drive preneoplastic cells towards apoptosis. In instances where preneoplastic cells with uncapped telomeres escape checkpoint responses, however, uncapped telomeres may actually contribute to genomic instability to drive cancers.

APPENDIX

Table A1. Upregulated miRNAs in G4 crypts. miRNAs upregulated in microarray with a q-value cutoff of 5%

Transcript ID	Fold-Change (G4 vs. WT)	q-value (%)	p-value (G4 vs WT)	Targets experimentally validated/Properly annotated?
miR-5097	9.65	0.00	0.00	tRNA
miR-3096b-5p	9.59	0.00	0.00	misannotation
miR-1983	8.61	0.00	0.00	dicer processed from alt tRNA seq
miR-34a	7.51	0.00	0.00	Yes
miR-3472	7.48	0.00	0.00	No
miR-712-star	6.93	0.00	0.00	712 form is potential biomarker for atherosclerosis
miR-3473b	6.25	0.00	0.00	No
miR-122	5.96	0.45	0.01	Yes
miR-2137	5.34	0.00	0.00	No
miR-3096b-3p	5.32	0.81	0.02	misannotation
miR-195-star	5.07	2.46	0.06	Yes
miR-5122	4.82	0.00	0.00	No
miR-326-star	4.80	0.00	0.00	Yes
miR-23a-star	4.79	0.45	0.01	Yes
miR-3473	4.58	0.00	0.00	Multiple forms (a-g) exist
miR-3093-3p	4.39	0.00	0.00	No, but high annotation confidence
miR-3096-3p	4.36	0.45	0.01	misannotation
miR-711	4.35	0.00	0.00	No
miR-92b-star	4.05	0.00	0.00	Yes
miR-5115	3.88	0.45	0.01	fragment of LSU rRNA
miR-1906	3.88	0.00	0.00	No
miR-762	3.87	0.00	0.00	No
miR-714	3.58	0.00	0.00	No
miR-135a-1-star	3.58	0.00	0.00	Yes
miR-16-1-star	3.58	1.28	0.03	Yes
miR-1982-star	3.51	0.00	0.00	No
miR-712	3.51	0.00	0.00	712 form is potential biomarker for atherosclerosis

miR-1894-3p	3.45	0.00	0.00	No
miR-1224	3.42	0.00	0.00	No, but confirmed by extensive cloning
miR-298	3.34	0.00	0.00	Yes
miR-1249-star	3.32	0.45	0.00	No, but high annotation confidence
miR-3096-5p	3.27	0.45	0.01	misannotation
miR-223	3.26	2.81	0.06	Yes
miR-1949	3.21	0.45	0.01	No
miR-5130	3.20	0.00	0.00	dicer processed from alt tRNA seq
miR-3104-5p	3.16	0.00	0.00	No
miR-5131	3.15	0.45	0.01	No
miR-1893	3.10	0.45	0.00	No
miR-1945	3.08	0.00	0.00	No
miR-134	3.08	0.45	0.01	Yes
miR-210	3.05	1.50	0.03	Yes
miR-3067-star	3.03	1.65	0.04	No
miR-34a-star	2.99	1.06	0.02	Yes
miR-874	2.99	0.45	0.01	Yes
miR-1946b	2.94	0.45	0.01	No
miR-1956	2.82	1.28	0.03	No
miR-5109	2.79	0.00	0.00	fragment of LSU rRNA
miR-128-2-star	2.75	3.07	0.06	Yes 128
miR-150-star	2.71	0.45	0.01	Yes, 150
miR-3100-5p	2.68	0.81	0.01	No
miR-125a-3p	2.67	2.46	0.05	Yes, mir-10 family
miR-669f-5p	2.65	1.80	0.04	No, but high annotation confidence
miR-696	2.64	1.80	0.04	No
miR-1903	2.61	0.00	0.00	No
miR-669m-5p	2.60	1.06	0.02	No, but high annotation confidence
miR-211-star	2.57	0.00	0.00	Yes
miR-328-star	2.56	0.45	0.01	Yes
miR-3077-star	2.54	0.00	0.00	No
miR-1247-star	2.49	0.45	0.01	No, but high annotation confidence
miR-3102-star	2.47	0.00	0.00	No
miR-5128	2.47	0.45	0.00	No
miR-323-5p	2.46	0.00	0.00	No, but belongs to mir-154

				family
miR-199b-star	2.45	2.46	0.05	Yes
miR-346-star	2.42	0.45	0.00	Yes
miR-760-3p	2.38	0.00	0.00	No, but high annotation confidence
miR-24-2-star	2.36	0.45	0.01	Yes
miR-504-star	2.36	4.77	0.09	Yes, -504 form negatively reg p53
miR-27a	2.36	0.00	0.00	Yes
miR-3092	2.34	0.45	0.01	No
miR-370	2.34	2.81	0.05	Yes
miR-770-3p	2.32	0.45	0.01	No, but high annotation confidence
miR-677-star	2.32	0.81	0.02	No
miR-1943	2.30	0.45	0.00	No, but high annotation confidence
miR-615-5p	2.30	2.81	0.05	Yes
miR-3090-star	2.30	0.45	0.01	No
miR-149-star	2.28	0.00	0.00	Yes, 149
miR-3113	2.28	0.81	0.02	No
miR-5120	2.26	0.00	0.00	No
miR-92a-2-star	2.26	0.45	0.01	Yes
miR-23a	2.24	0.00	0.00	Yes
miR-668	2.23	0.45	0.01	No, but high annotation confidence
miR-1940	2.22	2.46	0.04	No
miR-494	2.19	0.81	0.02	No
miR-2182	2.16	1.28	0.02	No
miR-466j	2.16	2.46	0.05	No
miR-193b-star	2.14	0.45	0.00	Yes
miR-129-5p	2.13	2.81	0.05	Yes
miR-297a	2.10	1.28	0.02	Yes
miR-212-3p	2.09	1.06	0.02	Yes
miR-214	2.08	0.45	0.01	Yes
miR-466f	2.06	0.45	0.01	No
miR-1946a	2.06	0.81	0.01	No
miR-3087-star	2.05	0.00	0.00	No
miR-22	2.05	0.45	0.01	Yes
miR-2136	2.02	4.77	0.07	No
miR-5119	2.00	1.80	0.04	No
miR-720	2.00	3.80	0.07	fragment of tRNA

miR-27a-star	1.99	2.46	0.04	Yes
miR-718	1.98	0.00	0.00	No
miR-2861	1.94	0.00	0.00	Yes, clustered with 3960
miR-5126	1.93	0.00	0.00	No
miR-466m-5p	1.92	3.07	0.06	No, but high annotation confidence
miR-204-star	1.92	1.80	0.04	Yes
miR-1199	1.92	3.07	0.05	No
miR-3960	1.90	0.00	0.00	Yes
miR-705	1.89	0.45	0.01	No
miR-1892	1.89	1.06	0.02	No
miR-3091-5p	1.88	0.00	0.00	No, but high annotation confidence
miR-497	1.88	3.07	0.06	Yes
miR-678	1.87	0.45	0.00	No
miR-29b-2-star	1.87	2.46	0.04	Yes
miR-5111	1.85	1.50	0.03	fragment of tRNA
miR-132	1.85	0.45	0.01	Yes
miR-5105	1.85	0.45	0.00	fragment of LSU rRNA
miR-1934-star	1.83	0.45	0.00	No, but high annotation confidence
miR-667	1.82	2.81	0.05	No, but high annotation confidence
miR-365-2-star	1.81	0.45	0.01	Yes
miR-290-5p	1.81	3.80	0.06	Yes
miR-199b	1.78	1.28	0.02	Yes
miR-199a-5p	1.77	3.80	0.06	Yes
miR-690	1.77	0.00	0.00	No
miR-3061-5p	1.77	3.80	0.07	No, but high annotation confidence
miR-5121	1.76	0.45	0.01	No
miR-199a-3p	1.74	1.50	0.02	Yes
miR-195	1.73	1.28	0.02	Yes
miR-5132	1.71	1.28	0.02	No, but high annotation confidence
miR-21-star	1.70	1.28	0.02	Yes
miR-505-5p	1.69	1.65	0.02	Yes
miR-3470a	1.68	1.80	0.03	No
miR-675-5p	1.66	3.07	0.05	No, but high annotation confidence
miR-99b	1.65	3.07	0.05	Yes

miR-1199-star	1.64	3.07	0.05	No
miR-1931	1.64	1.06	0.01	No
miR-126-3p	1.63	2.46	0.03	Yes
miR-432	1.62	1.28	0.02	No
miR-296-3p	1.62	0.45	0.01	Yes
miR-598-star	1.61	1.80	0.03	No, but high annotation confidence
let-7e	1.60	1.06	0.01	Yes
miR-665-star	1.59	1.28	0.02	No, but high annotation confidence
miR-5099	1.59	3.07	0.05	No
miR-3098-3p	1.56	0.45	0.00	No, but high annotation confidence
miR-292-5p	1.56	1.80	0.03	Yes
miR-5106	1.56	0.45	0.00	No
miR-203	1.55	0.45	0.01	Yes
miR-339-3p	1.53	3.07	0.05	Yes
miR-18a	1.53	2.46	0.03	Yes
miR-3081-star	1.53	3.80	0.05	No, but high annotation confidence
miR-3077	1.52	1.06	0.01	No
miR-24	1.52	0.45	0.00	Yes
miR-128-1-star	1.51	3.80	0.05	Yes 128
miR-5102	1.47	3.07	0.04	probably 28S rRNA
miR-296-5p	1.46	1.80	0.03	Yes
miR-763	1.40	1.80	0.02	No
miR-344g-3p	1.40	4.77	0.06	No
miR-1196	1.38	2.81	0.03	misannotation (Alu/B1 SINE element)
miR-212-5p	1.37	1.65	0.01	Yes
miR-1195	1.37	2.46	0.02	No
miR-3076-3p	1.36	4.77	0.05	No
miR-138	1.35	3.07	0.04	Yes
let-7b-star	1.34	1.06	0.01	Yes
miR-3065	1.33	3.07	0.03	No
miR-3102-5p.2	1.33	3.80	0.04	No
miR-1247	1.30	3.80	0.04	No, but high annotation confidence
miR-1188	1.29	1.28	0.01	No
miR-467h	1.26	3.80	0.03	No
miR-744	1.25	0.45	0.00	Yes

miR-3093-5p	1.23	2.81	0.02	No, but high annotation confidence

Table A2. Downregulated miRNAs in G4 crypts. miRNAs downregulated in microarray with a q-value cutoff of 5%

Transcript ID	Fold-Change (G4 vs. WT)	q-value (%)	p-value (G4 vs WT)	Targets experimentally validated/Properly annotated?
let-7b	-1.18	1.65	0.00	Yes
let-7f	-1.42	0.87	0.00	Yes
let-7i-star	-1.56	3.80	0.03	Yes
miR-103	-1.17	3.80	0.00	Yes
miR-106b-star	-1.41	1.28	0.00	Yes
miR-10a	-2.08	0.84	0.00	Yes, mir-10 family
miR-10a-star	-3.96	0.00	0.00	Yes, mir-10 family
miR-10b	-1.89	0.84	0.00	Yes, mir-10 family
miR-1198-5p	-1.43	1.09	0.00	No, but high annotation confidence
miR-130b	-1.70	0.84	0.00	Yes
miR-130b-star	-2.69	1.28	0.02	Yes
miR-139-5p	-2.40	1.50	0.02	Yes
miR-140-star	-1.25	2.81	0.01	Yes
miR-141	-1.84	0.84	0.00	Yes
miR-144	-1.29	1.65	0.00	Yes
miR-148a	-2.30	0.87	0.01	Yes
miR-150	-5.25	2.81	0.04	Yes
miR-151-3p	-1.41	2.46	0.01	Yes
miR-151-5p	-1.27	1.09	0.00	Yes
miR-152	-1.82	2.46	0.02	Yes
miR-15a	-1.58	0.84	0.00	Yes
miR-15b	-1.40	1.50	0.01	Yes
miR-16	-1.30	0.87	0.00	Yes
miR-17-star	-1.36	1.65	0.01	Yes
miR-181a	-4.20	0.00	0.00	Yes
miR-181b	-4.53	0.00	0.00	Yes
miR-181b-1-star	-1.18	3.80	0.01	Yes
miR-181c	-5.84	0.00	0.00	Yes
miR-181c-star	-3.30	0.84	0.00	Yes
miR-181d	-3.22	0.00	0.00	Yes

miR-1839-5p	-1.67	0.87	0.01	No, but high annotation confidence
miR-187	-2.15	1.65	0.02	Yes
miR-18b	-1.39	1.09	0.00	Yes
miR-190b-star	-1.43	4.77	0.03	No, but high annotation confidence
miR-192-star	-1.47	0.87	0.00	Yes
miR-194-2-star	-1.46	3.80	0.02	Yes
miR-196a-1-star	-3.29	2.46	0.03	Yes
miR-19b	-1.34	2.46	0.01	Yes
miR-200a	-1.94	0.00	0.00	Yes
miR-200a-star	-1.55	1.65	0.01	Yes
miR-200b	-1.53	0.84	0.00	Yes
miR-200b-star	-1.47	0.84	0.00	Yes
miR-206	-1.24	3.80	0.01	Yes
miR-20b	-1.98	0.00	0.00	Yes
miR-221	-1.31	4.77	0.02	Yes
miR-222	-1.51	2.46	0.02	Yes
miR-224	-1.80	2.81	0.02	Yes
miR-23b	-1.28	1.09	0.00	Yes
miR-25	-1.86	0.00	0.00	Yes
miR-26a	-1.36	0.00	0.00	Yes
miR-26b	-1.86	0.84	0.00	Yes
miR-27b	-1.21	3.07	0.01	Yes
miR-28-star	-1.29	2.81	0.01	Yes
miR-28c	-1.59	2.46	0.02	Yes
miR-295-star	-1.25	4.77	0.02	Yes
miR-29b	-2.08	1.09	0.01	Yes
miR-29c	-2.54	0.84	0.00	Yes
miR-3089-3p	-1.27	3.07	0.01	No
miR-30a	-1.81	0.00	0.00	Yes
miR-30a-star	-2.23	1.65	0.02	Yes
miR-30b	-1.80	0.00	0.00	Yes
miR-30b-star	-1.91	0.84	0.00	Yes
miR-30c	-1.55	0.84	0.00	Yes
miR-30c-2-star	-2.80	0.87	0.01	Yes
miR-30d	-1.78	0.00	0.00	Yes
miR-30e	-2.76	0.00	0.00	Yes
miR-30e-star	-2.22	0.84	0.00	Yes
miR-31-star	-1.68	2.46	0.02	Yes

miR-3105-3p	-2.80	0.00	0.00	No, but high annotation confidence
miR-3105-5p	-3.05	1.65	0.02	No, but high annotation confidence
miR-320	-1.75	1.28	0.01	Yes
miR-324-3p	-2.23	0.87	0.01	Yes
miR-326	-1.88	2.46	0.02	Yes
miR-340-5p	-1.52	2.81	0.02	Yes
miR-342-3p	-2.19	0.00	0.00	Yes
miR-342-5p	-2.83	1.09	0.01	Yes
miR-34b-5p	-1.43	2.46	0.01	Yes
miR-350	-1.74	0.84	0.00	No, but high annotation confidence
miR-363-3p	-6.62	0.84	0.00	Yes
miR-363-5p	-6.78	0.00	0.00	Yes
miR-374	-3.00	0.87	0.01	Yes, activates Wnt signaling
miR-375	-1.70	3.07	0.03	Yes
miR-375-star	-1.34	4.77	0.03	Yes
miR-378-star	-1.34	2.46	0.01	Yes
miR-378b	-1.50	2.81	0.02	No
miR-3962	-1.27	4.77	0.02	No
miR-411-star	-1.31	1.80	0.01	Yes
miR-433-star	-1.24	1.65	0.00	Yes
miR-450a-1-star	-1.32	0.84	0.00	Yes
miR-466p-3p	-1.49	3.80	0.03	No
miR-467a	-2.53	3.80	0.05	Yes
miR-467a-star	-1.96	1.80	0.02	Yes
miR-493-star	-1.41	1.65	0.01	Yes
miR-532-3p	-1.63	1.80	0.01	Yes
miR-532-5p	-1.23	3.80	0.01	Yes
miR-543	-1.34	4.77	0.02	No, but high annotation confidence
miR-574-3p	-2.14	0.87	0.01	Yes, activates Wnt signaling
miR-652	-1.49	0.87	0.00	Yes
miR-676	-3.29	0.84	0.00	No, but high annotation confidence
miR-700-star	-1.45	2.81	0.02	No, but high annotation confidence
miR-7a-1-star	-3.48	1.09	0.01	Yes
miR-802	-1.42	3.07	0.02	Yes

miR-871-3p	-1.36	2.46	0.01	No, but high annotation confidence
miR-872	-1.89	1.65	0.01	No, but high annotation confidence
miR-883a-3p	-1.24	3.80	0.01	No, but high annotation confidence
miR-92a	-1.66	0.84	0.00	Yes
miR-92b	-1.79	0.84	0.00	Yes
miR-93	-1.23	1.65	0.00	Yes
miR-93-star	-1.78	0.00	0.00	Yes
miR-96	-2.06	0.87	0.01	Yes
miR-99a	-2.11	0.84	0.00	Yes, mir-10 family

REFERENCES

1. Hayflick L, and Moorhead PS. The serial cultivation of human diploid cell strains. *Exp Cell Res.* 1961;25(585-621.
2. Hayflick L. THE LIMITED IN VITRO LIFETIME OF HUMAN DIPLOID CELL STRAINS. *Exp Cell Res.* 1965;37(614-36.
3. O'Sullivan RJ, and Karlseder J. Telomeres: protecting chromosomes against genome instability. *Nature reviews Molecular cell biology.* 2010;11(3):171-81.
4. Watson JD. Origin of concatemeric T7 DNA. *Nature: New biology.* 1972;239(94):197-201.
5. Olovnikov AM. A theory of marginotomy. The incomplete copying of template margin in enzymic synthesis of polynucleotides and biological significance of the phenomenon. *Journal of theoretical biology.* 1973;41(1):181-90.
6. Chow TT, Zhao Y, Mak SS, Shay JW, and Wright WE. Early and late steps in telomere overhang processing in normal human cells: the position of the final RNA primer drives telomere shortening. *Genes & development.* 2012;26(11):1167-78.
7. Wu P, van Overbeek M, Rooney S, and de Lange T. Apollo contributes to G overhang maintenance and protects leading-end telomeres. *Molecular cell.* 2010;39(4):606-17.

8. Richter T, and von Zglinicki T. A continuous correlation between oxidative stress and telomere shortening in fibroblasts. *Experimental gerontology.* 2007;42(11):1039-42.

9. von Zglinicki T, Saretzki G, Docke W, and Lotze C. Mild hyperoxia shortens telomeres and inhibits proliferation of fibroblasts: a model for senescence? *Exp Cell Res.* 1995;220(1):186-93.

10. Serra V, von Zglinicki T, Lorenz M, and Saretzki G. Extracellular superoxide dismutase is a major antioxidant in human fibroblasts and slows telomere shortening. *J Biol Chem.* 2003;278(9):6824-30.

11. Oikawa S, Tada-Oikawa S, and Kawanishi S. Site-specific DNA damage at the GGG sequence by UVA involves acceleration of telomere shortening. *Biochemistry.* 2001;40(15):4763-8.

12. Rochette PJ, and Brash DE. Human telomeres are hypersensitive to UV-induced DNA Damage and refractory to repair. *PLoS genetics.* 2010;6(4):e1000926.

13. Le PN, Maranon DG, Altina NH, Battaglia CL, and Bailey SM. TERRA, hnRNP A1, and DNA-PKcs Interactions at Human Telomeres. *Frontiers in oncology.* 2013;3(91.

14. Sfeir A, Kosiyatrakul ST, Hockemeyer D, MacRae SL, Karlseder J, Schildkraut CL, and de Lange T. Mammalian telomeres resemble fragile sites and require TRF1 for efficient replication. *Cell.* 2009;138(1):90-103.

15. Suram A, and Herbig U. The replicometer is broken: telomeres activate cellular senescence in response to genotoxic stresses. *Aging cell.* 2014.

16. Suram A, Kaplunov J, Patel PL, Ruan H, Cerutti A, Boccardi V, Fumagalli M, Di Micco R, Mirani N, Gurung RL, et al. Oncogene-induced telomere dysfunction enforces cellular senescence in human cancer precursor lesions. *EMBO J.* 2012;31(13):2839-51.

17. Blackburn EH, and Collins K. Telomerase: an RNP enzyme synthesizes DNA. *Cold Spring Harbor perspectives in biology.* 2011;3(5).

18. Palm W, and de Lange T. How shelterin protects mammalian telomeres. *Annual review of genetics.* 2008;42(301-34.

19. Kibe T, Osawa GA, Keegan CE, and de Lange T. Telomere protection by TPP1 is mediated by POT1a and POT1b. *Molecular and cellular biology.* 2010;30(4):1059-66.

20. de Lange T. How telomeres solve the end-protection problem. *Science.* 2009;326(5955):948-52.

21. Sfeir A, and de Lange T. Removal of shelterin reveals the telomere end-protection problem. *Science.* 2012;336(6081):593-7.

22. Griffith JD, Comeau L, Rosenfield S, Stansel RM, Bianchi A, Moss H, and de Lange T. Mammalian telomeres end in a large duplex loop. *Cell.* 1999;97(4):503-14.

23. Doksani Y, Wu JY, de Lange T, and Zhuang X. Super-resolution fluorescence imaging of telomeres reveals TRF2-dependent T-loop formation. *Cell.* 2013;155(2):345-56.

24. Kasbek C, Wang F, and Price CM. Human TEN1 maintains telomere integrity and functions in genome-wide replication restart. *J Biol Chem.* 2013;288(42):30139-50.

25. Wang F, Stewart JA, Kasbek C, Zhao Y, Wright WE, and Price CM. Human CST has independent functions during telomere duplex replication and C-strand fill-in. *Cell reports.* 2012;2(5):1096-103.

26. Chen LY, Redon S, and Lingner J. The human CST complex is a terminator of telomerase activity. *Nature.* 2012;488(7412):540-4.

27. Cawthon RM. Telomere measurement by quantitative PCR. *Nucleic acids research.* 2002;30(10):e47.

28. Cawthon RM. Telomere length measurement by a novel monochrome multiplex quantitative PCR method. *Nucleic acids research.* 2009;37(3):e21.

29. Kaul Z, Cesare AJ, Huschtscha LI, Neumann AA, and Reddel RR. Five dysfunctional telomeres predict onset of senescence in human cells. *EMBO reports.* 2012;13(1):52-9.

30. Hemann MT, Strong MA, Hao LY, and Greider CW. The shortest telomere, not average telomere length, is critical for cell viability and chromosome stability. *Cell.* 2001;107(1):67-77.

31. Zou Y, Sfeir A, Gryaznov SM, Shay JW, and Wright WE. Does a sentinel or a subset of short telomeres determine replicative senescence? *Molecular biology of the cell.* 2004;15(8):3709-18.

32. Xu Z, Duc KD, Holcman D, and Teixeira MT. The length of the shortest telomere as the major determinant of the onset of replicative senescence. *Genetics.* 2013;194(4):847-57.

33. Baerlocher GM, Vulto I, de Jong G, and Lansdorp PM. Flow cytometry and FISH to measure the average length of telomeres (flow FISH). *Nat Protoc.* 2006;1(5):2365-76.

34. Poon SS, and Lansdorp PM. Quantitative fluorescence in situ hybridization (Q-FISH). *Current protocols in cell biology / editorial board, Juan S Bonifacino [et al].* 2001;Chapter 18(Unit 18.4.

35. Kimura M, Stone RC, Hunt SC, Skurnick J, Lu X, Cao X, Harley CB, and Aviv A. Measurement of telomere length by the Southern blot analysis of terminal restriction fragment lengths. *Nat Protoc.* 2010;5(9):1596-607.

36. Elbers CC, Garcia ME, Kimura M, Cummings SR, Nalls MA, Newman AB, Park V, Sanders JL, Tranah GJ, Tishkoff SA, et al. Comparison between southern blots and qPCR analysis of leukocyte telomere length in the health ABC study. *The journals of gerontology Series A, Biological sciences and medical sciences.* 2014;69(5):527-31.

37. Aviv A, Hunt SC, Lin J, Cao X, Kimura M, and Blackburn E. Impartial comparative analysis of measurement of leukocyte telomere length/DNA content by Southern blots and qPCR. *Nucleic acids research.* 2011;39(20):e134.

38. Canela A, Vera E, Klatt P, and Blasco MA. High-throughput telomere length quantification by FISH and its application to human population

studies. *Proceedings of the National Academy of Sciences of the United States of America.* 2007;104(13):5300-5.

39. Vera E, and Blasco MA. Beyond average: potential for measurement of short telomeres. *Aging.* 2012;4(6):379-92.

40. Bernardes de Jesus B, Schneeberger K, Vera E, Tejera A, Harley CB, and Blasco MA. The telomerase activator TA-65 elongates short telomeres and increases health span of adult/old mice without increasing cancer incidence. *Aging cell.* 2011;10(4):604-21.

41. Weinrich SL, Pruzan R, Ma L, Ouellette M, Tesmer VM, Holt SE, Bodnar AG, Lichtsteiner S, Kim NW, Trager JB, et al. Reconstitution of human telomerase with the template RNA component hTR and the catalytic protein subunit hTRT. *Nature genetics.* 1997;17(4):498-502.

42. Bryan TM, Goodrich KJ, and Cech TR. Tetrahymena telomerase is active as a monomer. *Molecular biology of the cell.* 2003;14(12):4794-804.

43. Pfeiffer V, and Lingner J. Replication of telomeres and the regulation of telomerase. *Cold Spring Harbor perspectives in biology.* 2013;5(5):a010405.

44. Cohen SB, Graham ME, Lovrecz GO, Bache N, Robinson PJ, and Reddel RR. Protein composition of catalytically active human telomerase from immortal cells. *Science.* 2007;315(5820):1850-3.

45. Sandin S, and Rhodes D. Telomerase structure. *Current opinion in structural biology.* 2014;25(104-10.

46. Artandi SE, and DePinho RA. Telomeres and telomerase in cancer. *Carcinogenesis.* 2010;31(1):9-18.

47. Avilion AA, Piatyszek MA, Gupta J, Shay JW, Bacchetti S, and Greider CW. Human telomerase RNA and telomerase activity in immortal cell lines and tumor tissues. *Cancer research.* 1996;56(3):645-50.

48. Nakayama J, Tahara H, Tahara E, Saito M, Ito K, Nakamura H, Nakanishi T, Tahara E, Ide T, and Ishikawa F. Telomerase activation by hTRT in human normal fibroblasts and hepatocellular carcinomas. *Nature genetics.* 1998;18(1):65-8.

49. Kim NW, Piatyszek MA, Prowse KR, Harley CB, West MD, Ho PL, Coviello GM, Wright WE, Weinrich SL, and Shay JW. Specific association of human telomerase activity with immortal cells and cancer. *Science.* 1994;266(5193):2011-5.

50. Herbert BS, Hochreiter AE, Wright WE, and Shay JW. Nonradioactive detection of telomerase activity using the telomeric repeat amplification protocol. *Nat Protoc.* 2006;1(3):1583-90.

51. Wright WE, Piatyszek MA, Rainey WE, Byrd W, and Shay JW. Telomerase activity in human germline and embryonic tissues and cells. *Developmental genetics.* 1996;18(2):173-9.

52. Holt SE, Wright WE, and Shay JW. Regulation of telomerase activity in immortal cell lines. *Molecular and cellular biology.* 1996;16(6):2932-9.

53. Takubo K, Nakamura K, Izumiyama N, Mafune K, Tanaka Y, Miyashita M, Sasajima K, Kato M, and Oshimura M. Telomerase activity in esophageal carcinoma. *Journal of surgical oncology.* 1997;66(2):88-92.

54. Hiyama E, Tatsumoto N, Kodama T, Hiyama K, Shay J, and Yokoyama T. Telomerase activity in human intestine. *International journal of oncology.* 1996;9(3):453-8.

55. Yasumoto S, Kunimura C, Kikuchi K, Tahara H, Ohji H, Yamamoto H, Ide T, and Utakoji T. Telomerase activity in normal human epithelial cells. *Oncogene.* 1996;13(2):433-9.

56. Brien TP, Kallakury BV, Lowry CV, Ambros RA, Muraca PJ, Malfetano JH, and Ross JS. Telomerase activity in benign endometrium and endometrial carcinoma. *Cancer research.* 1997;57(13):2760-4.

57. Bonatz G, Klapper W, Barthe A, Heidorn K, Jonat W, Krupp G, and Parwaresch R. Analysis of telomerase expression and proliferative activity in the different layers of cyclic endometrium. *Biochemical and biophysical research communications.* 1998;253(2):214-21.

58. Broccoli D, Young JW, and de Lange T. Telomerase activity in normal and malignant hematopoietic cells. *Proceedings of the National Academy of Sciences of the United States of America.* 1995;92(20):9082-6.

59. Harle-Bachor C, and Boukamp P. Telomerase activity in the regenerative basal layer of the epidermis inhuman skin and in immortal and carcinoma-derived skin keratinocytes. *Proceedings of the National Academy of Sciences of the United States of America.* 1996;93(13):6476-81.

60. Ramirez RD, Wright WE, Shay JW, and Taylor RS. Telomerase activity concentrates in the mitotically active segments of human hair follicles. *The Journal of investigative dermatology.* 1997;108(1):113-7.

61. Belair CD, Yeager TR, Lopez PM, and Reznikoff CA. Telomerase activity: a biomarker of cell proliferation, not malignant transformation. *Proceedings of the National Academy of Sciences of the United States of America.* 1997;94(25):13677-82.

62. Hiyama K, Hirai Y, Kyoizumi S, Akiyama M, Hiyama E, Piatyszek MA, Shay JW, Ishioka S, and Yamakido M. Activation of telomerase in human lymphocytes and hematopoietic progenitor cells. *Journal of immunology.* 1995;155(8):3711-5.

63. Ulaner GA, Hu JF, Vu TH, Giudice LC, and Hoffman AR. Telomerase activity in human development is regulated by human telomerase reverse transcriptase (hTERT) transcription and by alternate splicing of hTERT transcripts. *Cancer research.* 1998;58(18):4168-72.

64. Liu K, Hodes RJ, and Weng N. Cutting edge: telomerase activation in human T lymphocytes does not require increase in telomerase reverse transcriptase (hTERT) protein but is associated with hTERT phosphorylation and nuclear translocation. *Journal of immunology.* 2001;166(8):4826-30.

65. d'Adda di Fagagna F, Reaper PM, Clay-Farrace L, Fiegler H, Carr P, Von Zglinicki T, Saretzki G, Carter NP, and Jackson SP. A DNA damage

checkpoint response in telomere-initiated senescence. *Nature.* 2003;426(6963):194-8.

66. Herbig U, Jobling WA, Chen BP, Chen DJ, and Sedivy JM. Telomere shortening triggers senescence of human cells through a pathway involving ATM, p53, and p21(CIP1), but not p16(INK4a). *Molecular cell.* 2004;14(4):501-13.

67. Takai H, Smogorzewska A, and de Lange T. DNA damage foci at dysfunctional telomeres. *Current biology : CB.* 2003;13(17):1549-56.

68. Fumagalli M, Rossiello F, Clerici M, Barozzi S, Cittaro D, Kaplunov JM, Bucci G, Dobreva M, Matti V, Beausejour CM, et al. Telomeric DNA damage is irreparable and causes persistent DNA-damage-response activation. *Nature cell biology.* 2012;14(4):355-65.

69. Hewitt G, Jurk D, Marques FD, Correia-Melo C, Hardy T, Gackowska A, Anderson R, Taschuk M, Mann J, and Passos JF. Telomeres are favoured targets of a persistent DNA damage response in ageing and stress-induced senescence. *Nature communications.* 2012;3(708.

70. Tchkonia T, Zhu Y, van Deursen J, Campisi J, and Kirkland JL. Cellular senescence and the senescent secretory phenotype: therapeutic opportunities. *J Clin Invest.* 2013;123(3):966-72.

71. Reddel RR. Senescence: an antiviral defense that is tumor suppressive? *Carcinogenesis.* 2010;31(1):19-26.

72. Munoz-Espin D, Canamero M, Maraver A, Gomez-Lopez G, Contreras J, Murillo-Cuesta S, Rodriguez-Baeza A, Varela-Nieto I, Ruberte J, Collado

M, et al. Programmed cell senescence during mammalian embryonic development. *Cell.* 2013;155(5):1104-18.

73. Campisi J. Aging, cellular senescence, and cancer. *Annu Rev Physiol.* 2013;75(685-705.

74. Michaloglou C, Vredeveld LC, Soengas MS, Denoyelle C, Kuilman T, van der Horst CM, Majoor DM, Shay JW, Mooi WJ, and Peeper DS. BRAFE600-associated senescence-like cell cycle arrest of human naevi. *Nature.* 2005;436(7051):720-4.

75. Janzen V, Forkert R, Fleming HE, Saito Y, Waring MT, Dombkowski DM, Cheng T, DePinho RA, Sharpless NE, and Scadden DT. Stem-cell ageing modified by the cyclin-dependent kinase inhibitor p16INK4a. *Nature.* 2006;443(7110):421-6.

76. Krishnamurthy J, Ramsey MR, Ligon KL, Torrice C, Koh A, Bonner-Weir S, and Sharpless NE. p16INK4a induces an age-dependent decline in islet regenerative potential. *Nature.* 2006;443(7110):453-7.

77. Molofsky AV, Slutsky SG, Joseph NM, He S, Pardal R, Krishnamurthy J, Sharpless NE, and Morrison SJ. Increasing p16INK4a expression decreases forebrain progenitors and neurogenesis during ageing. *Nature.* 2006;443(7110):448-52.

78. Franceschi C, and Campisi J. Chronic inflammation (inflammaging) and its potential contribution to age-associated diseases. *The journals of gerontology Series A, Biological sciences and medical sciences.* 2014;69 Suppl 1(S4-9.

79. Coppe JP, Patil CK, Rodier F, Sun Y, Munoz DP, Goldstein J, Nelson PS, Desprez PY, and Campisi J. Senescence-associated secretory phenotypes reveal cell-nonautonomous functions of oncogenic RAS and the p53 tumor suppressor. *PLoS biology.* 2008;6(12):2853-68.

80. Acosta JC, Banito A, Wuestefeld T, Georgilis A, Janich P, Morton JP, Athineos D, Kang TW, Lasitschka F, Andrulis M, et al. A complex secretory program orchestrated by the inflammasome controls paracrine senescence. *Nat Cell Biol.* 2013;15(8):978-90.

81. Baker DJ, Wijshake T, Tchkonia T, LeBrasseur NK, Childs BG, van de Sluis B, Kirkland JL, and van Deursen JM. Clearance of p16Ink4a-positive senescent cells delays ageing-associated disorders. *Nature.* 2011;479(7372):232-6.

82. Ye J, Renault VM, Jamet K, and Gilson E. Transcriptional outcome of telomere signalling. *Nature reviews Genetics.* 2014;15(7):491-503.

83. Shah PP, Donahue G, Otte GL, Capell BC, Nelson DM, Cao K, Aggarwala V, Cruickshanks HA, Rai TS, McBryan T, et al. Lamin B1 depletion in senescent cells triggers large-scale changes in gene expression and the chromatin landscape. *Genes & development.* 2013;27(16):1787-99.

84. Platt JM, Ryvkin P, Wanat JJ, Donahue G, Ricketts MD, Barrett SP, Waters HJ, Song S, Chavez A, Abdallah KO, et al. Rap1 relocalization contributes to the chromatin-mediated gene expression profile and pace of cell senescence. *Genes & development.* 2013;27(12):1406-20.

85. Lou Z, Wei J, Riethman H, Baur JA, Voglauer R, Shay JW, and Wright WE. Telomere length regulates ISG15 expression in human cells. *Aging.* 2009;1(7):608-21.

86. Hirashima K, Migita T, Sato S, Muramatsu Y, Ishikawa Y, and Seimiya H. Telomere length influences cancer cell differentiation in vivo. *Molecular and cellular biology.* 2013;33(15):2988-95.

87. Sahin E, and DePinho RA. Axis of ageing: telomeres, p53 and mitochondria. *Nature reviews Molecular cell biology.* 2012;13(6):397-404.

88. Passos JF, Nelson G, Wang C, Richter T, Simillion C, Proctor CJ, Miwa S, Olijslagers S, Hallinan J, Wipat A, et al. Feedback between p21 and reactive oxygen production is necessary for cell senescence. *Molecular systems biology.* 2010;6(347.

89. Guo N, Parry EM, Li LS, Kembou F, Lauder N, Hussain MA, Berggren PO, and Armanios M. Short telomeres compromise beta-cell signaling and survival. *PloS one.* 2011;6(3):e17858.

90. Sahin E, Colla S, Liesa M, Moslehi J, Muller FL, Guo M, Cooper M, Kotton D, Fabian AJ, Walkey C, et al. Telomere dysfunction induces metabolic and mitochondrial compromise. *Nature.* 2011;470(7334):359-65.

91. Neumann AA, Watson CM, Noble JR, Pickett HA, Tam PP, and Reddel RR. Alternative lengthening of telomeres in normal mammalian somatic cells. *Genes & development.* 2013;27(1):18-23.

92. Conomos D, Pickett HA, and Reddel RR. Alternative lengthening of telomeres: remodeling the telomere architecture. *Frontiers in oncology.* 2013;3(27.

93. Figueroa R, Lindenmaier H, Hergenhahn M, Nielsen KV, and Boukamp P. Telomere erosion varies during in vitro aging of normal human fibroblasts from young and adult donors. *Cancer research.* 2000;60(11):2770-4.

94. Takubo K, Aida J, Izumiyama N, Ishikawa N, Fujiwara M, Poon SS, Kondo H, Kammori M, Matsuura M, Sawabe M, et al. Chromosomal instability and telomere lengths of each chromosomal arm measured by Q-FISH in human fibroblast strains prior to replicative senescence. *Mechanisms of ageing and development.* 2010;131(10):614-24.

95. Cesare AJ, Hayashi MT, Crabbe L, and Karlseder J. The telomere deprotection response is functionally distinct from the genomic DNA damage response. *Molecular cell.* 2013;51(2):141-55.

96. Jurk D, Wang C, Miwa S, Maddick M, Korolchuk V, Tsolou A, Gonos ES, Thrasivoulou C, Saffrey MJ, Cameron K, et al. Postmitotic neurons develop a p21-dependent senescence-like phenotype driven by a DNA damage response. *Aging cell.* 2012;11(6):996-1004.

97. Bodnar AG, Ouellette M, Frolkis M, Holt SE, Chiu CP, Morin GB, Harley CB, Shay JW, Lichtsteiner S, and Wright WE. Extension of life-span by introduction of telomerase into normal human cells. *Science.* 1998;279(5349):349-52.

98. Kovalenko OA, Caron MJ, Ulema P, Medrano C, Thomas AP, Kimura M, Bonini MG, Herbig U, and Santos JH. A mutant telomerase defective in nuclear-cytoplasmic shuttling fails to immortalize cells and is associated with mitochondrial dysfunction. *Aging cell.* 2010;9(2):203-19.

99. Park JI, Venteicher AS, Hong JY, Choi J, Jun S, Shkreli M, Chang W, Meng Z, Cheung P, Ji H, et al. Telomerase modulates Wnt signalling by association with target gene chromatin. *Nature.* 2009;460(7251):66-72.

100. Flores I, Benetti R, and Blasco MA. Telomerase regulation and stem cell behaviour. *Current opinion in cell biology.* 2006;18(3):254-60.

101. Listerman I, Gazzaniga FS, and Blackburn EH. An investigation of the effects of the core protein telomerase reverse transcriptase on Wnt signaling in breast cancer cells. *Molecular and cellular biology.* 2014;34(2):280-9.

102. Rubio MA, Kim SH, and Campisi J. Reversible manipulation of telomerase expression and telomere length. Implications for the ionizing radiation response and replicative senescence of human cells. *J Biol Chem.* 2002;277(32):28609-17.

103. Baird DM, and Kipling D. The extent and significance of telomere loss with age. *Annals of the New York Academy of Sciences.* 2004;1019(265-8.

104. Ishii A, Nakamura K, Kishimoto H, Honma N, Aida J, Sawabe M, Arai T, Fujiwara M, Takeuchi F, Kato M, et al. Telomere shortening with aging in the human pancreas. *Experimental gerontology.* 2006;41(9):882-6.

105. Nakamura K, Takubo K, Izumiyama-Shimomura N, Sawabe M, Arai T, Kishimoto H, Fujiwara M, Kato M, Oshimura M, Ishii A, et al. Telomeric DNA length in cerebral gray and white matter is associated with longevity in individuals aged 70 years or older. *Experimental gerontology.* 2007;42(10):944-50.

106. Atzmon G, Cho M, Cawthon RM, Budagov T, Katz M, Yang X, Siegel G, Bergman A, Huffman DM, Schechter CB, et al. Evolution in health and medicine Sackler colloquium: Genetic variation in human telomerase is associated with telomere length in Ashkenazi centenarians. *Proceedings of the National Academy of Sciences of the United States of America.* 2010;107 Suppl 1(1710-7.

107. Youngren K, Jeanclos E, Aviv H, Kimura M, Stock J, Hanna M, Skurnick J, Bardeguez A, and Aviv A. Synchrony in telomere length of the human fetus. *Human genetics.* 1998;102(6):640-3.

108. Okuda K, Bardeguez A, Gardner JP, Rodriguez P, Ganesh V, Kimura M, Skurnick J, Awad G, and Aviv A. Telomere length in the newborn. *Pediatric research.* 2002;52(3):377-81.

109. Frenck RW, Jr., Blackburn EH, and Shannon KM. The rate of telomere sequence loss in human leukocytes varies with age. *Proceedings of the National Academy of Sciences of the United States of America.* 1998;95(10):5607-10.

110. Friedrich U, Griese E, Schwab M, Fritz P, Thon K, and Klotz U. Telomere length in different tissues of elderly patients. *Mechanisms of ageing and development.* 2000;119(3):89-99.

111. Gardner JP, Kimura M, Chai W, Durrani JF, Tchakmakjian L, Cao X, Lu X, Li G, Peppas AP, Skurnick J, et al. Telomere dynamics in macaques and humans. *The journals of gerontology Series A, Biological sciences and medical sciences.* 2007;62(4):367-74.

112. Flores I, Canela A, Vera E, Tejera A, Cotsarelis G, and Blasco MA. The longest telomeres: a general signature of adult stem cell compartments. *Genes & development.* 2008;22(5):654-67.

113. Leri A, Malhotra A, Liew CC, Kajstura J, and Anversa P. Telomerase activity in rat cardiac myocytes is age and gender dependent. *Journal of molecular and cellular cardiology.* 2000;32(3):385-90.

114. Lee JJ, Nam CE, Kook H, Maciejewski JP, Kim YK, Chung IJ, Park KS, Lee IK, Hwang TJ, and Kim HJ. Constitution and telomere dynamics of bone marrow stromal cells in patients undergoing allogeneic bone marrow transplantation. *Bone marrow transplantation.* 2003;32(9):947-52.

115. Vaziri H, Dragowska W, Allsopp RC, Thomas TE, Harley CB, and Lansdorp PM. Evidence for a mitotic clock in human hematopoietic stem cells: loss of telomeric DNA with age. *Proceedings of the National Academy of Sciences of the United States of America.* 1994;91(21):9857-60.

116. Kimura M, Cherkas LF, Kato BS, Demissie S, Hjelmborg JB, Brimacombe M, Cupples A, Hunkin JL, Gardner JP, Lu X, et al. Offspring's leukocyte telomere length, paternal age, and telomere elongation in sperm. *PLoS genetics.* 2008;4(2):e37.

117. Herbig U, Ferreira M, Condel L, Carey D, and Sedivy JM. Cellular senescence in aging primates. *Science.* 2006;311(5765):1257.

118. Mitchell JR, Wood E, and Collins K. A telomerase component is defective in the human disease dyskeratosis congenita. *Nature.* 1999;402(6761):551-5.

119. Rossi ML, Ghosh AK, and Bohr VA. Roles of Werner syndrome protein in protection of genome integrity. *DNA repair.* 2010;9(3):331-44.

120. Crabbe L, Verdun RE, Haggblom CI, and Karlseder J. Defective telomere lagging strand synthesis in cells lacking WRN helicase activity. *Science.* 2004;306(5703):1951-3.

121. Epstein CJ, Martin GM, Schultz AL, and Motulsky AG. Werner's syndrome a review of its symptomatology, natural history, pathologic features, genetics and relationship to the natural aging process. *Medicine.* 1966;45(3):177-221.

122. Castro E, Edland SD, Lee L, Ogburn CE, Deeb SS, Brown G, Panduro A, Riestra R, Tilvis R, Louhija J, et al. Polymorphisms at the Werner locus: II. 1074Leu/Phe, 1367Cys/Arg, longevity, and atherosclerosis. *American journal of medical genetics.* 2000;95(4):374-80.

123. Sebastiani P, Solovieff N, Dewan AT, Walsh KM, Puca A, Hartley SW, Melista E, Andersen S, Dworkis DA, Wilk JB, et al. Genetic signatures of exceptional longevity in humans. *PloS one.* 2012;7(1):e29848.

124. Crabbe L, Jauch A, Naeger CM, Holtgreve-Grez H, and Karlseder J. Telomere dysfunction as a cause of genomic instability in Werner syndrome. *Proceedings of the National Academy of Sciences of the United States of America.* 2007;104(7):2205-10.

125. Du X, Shen J, Kugan N, Furth EE, Lombard DB, Cheung C, Pak S, Luo G, Pignolo RJ, DePinho RA, et al. Telomere shortening exposes functions for the mouse Werner and Bloom syndrome genes. *Molecular and cellular biology.* 2004;24(19):8437-46.

126. Chang S, Multani AS, Cabrera NG, Naylor ML, Laud P, Lombard D, Pathak S, Guarente L, and DePinho RA. Essential role of limiting telomeres in the pathogenesis of Werner syndrome. *Nature genetics.* 2004;36(8):877-82.

127. Marciniak R, and Guarente L. Human genetics. Testing telomerase. *Nature.* 2001;413(6854):370-1, 3.

128. Kirkwood TB, and Austad SN. Why do we age? *Nature.* 2000;408(6809):233-8.

129. Gomes NM, Ryder OA, Houck ML, Charter SJ, Walker W, Forsyth NR, Austad SN, Venditti C, Pagel M, Shay JW, et al. Comparative biology of mammalian telomeres: hypotheses on ancestral states and the roles of telomeres in longevity determination. *Aging cell.* 2011;10(5):761-8.

130. Wright WE, and Shay JW. Telomere dynamics in cancer progression and prevention: fundamental differences in human and mouse telomere biology. *Nat Med.* 2000;6(8):849-51.

131. Hemann MT, and Greider CW. Wild-derived inbred mouse strains have short telomeres. *Nucleic acids research.* 2000;28(22):4474-8.

132. Yuan X, Ishibashi S, Hatakeyama S, Saito M, Nakayama J, Nikaido R, Haruyama T, Watanabe Y, Iwata H, Iida M, et al. Presence of telomeric G-strand tails in the telomerase catalytic subunit TERT knockout mice. *Genes to cells : devoted to molecular & cellular mechanisms.* 1999;4(10):563-72.

133. Lee HW, Blasco MA, Gottlieb GJ, Horner JW, 2nd, Greider CW, and DePinho RA. Essential role of mouse telomerase in highly proliferative organs. *Nature.* 1998;392(6676):569-74.

134. Rudolph KL, Chang S, Lee HW, Blasco M, Gottlieb GJ, Greider C, and DePinho RA. Longevity, stress response, and cancer in aging telomerase-deficient mice. *Cell.* 1999;96(5):701-12.

135. Blasco MA, Lee HW, Hande MP, Samper E, Lansdorp PM, DePinho RA, and Greider CW. Telomere shortening and tumor formation by mouse cells lacking telomerase RNA. *Cell.* 1997;91(1):25-34.

136. Prowse KR, and Greider CW. Developmental and tissue-specific regulation of mouse telomerase and telomere length. *Proceedings of the National Academy of Sciences of the United States of America.* 1995;92(11):4818-22.

137. Wang C, Maddick M, Miwa S, Jurk D, Czapiewski R, Saretzki G, Langie SA, Godschalk RW, Cameron K, and von Zglinicki T. Adult-onset, short-term dietary restriction reduces cell senescence in mice. *Aging.* 2010;2(9):555-66.

138. Tomas-Loba A, Flores I, Fernandez-Marcos PJ, Cayuela ML, Maraver A, Tejera A, Borras C, Matheu A, Klatt P, Flores JM, et al. Telomerase reverse transcriptase delays aging in cancer-resistant mice. *Cell.* 2008;135(4):609-22.

139. Liu L, Bailey SM, Okuka M, Munoz P, Li C, Zhou L, Wu C, Czerwiec E, Sandler L, Seyfang A, et al. Telomere lengthening early in development. *Nature cell biology.* 2007;9(12):1436-41.

140. Strong MA, Vidal-Cardenas SL, Karim B, Yu H, Guo N, and Greider CW. Phenotypes in mTERT(+)/(-) and mTERT(-)/(-) mice are due to short telomeres, not telomere-independent functions of telomerase reverse transcriptase. *Molecular and cellular biology.* 2011;31(12):2369-79.

141. Hathcock KS, Hemann MT, Opperman KK, Strong MA, Greider CW, and Hodes RJ. Haploinsufficiency of mTR results in defects in telomere elongation. *Proceedings of the National Academy of Sciences of the United States of America.* 2002;99(6):3591-6.

142. Herrera E, Samper E, Martin-Caballero J, Flores JM, Lee HW, and Blasco MA. Disease states associated with telomerase deficiency appear earlier in mice with short telomeres. *The EMBO journal.* 1999;18(11):2950-60.

143. Celli GB, and de Lange T. DNA processing is not required for ATM-mediated telomere damage response after TRF2 deletion. *Nature cell biology.* 2005;7(7):712-8.

144. Chiang YJ, Kim SH, Tessarollo L, Campisi J, and Hodes RJ. Telomere-associated protein TIN2 is essential for early embryonic development through a telomerase-independent pathway. *Molecular and cellular biology.* 2004;24(15):6631-4.

145. Karlseder J, Kachatrian L, Takai H, Mercer K, Hingorani S, Jacks T, and de Lange T. Targeted deletion reveals an essential function for the telomere length regulator Trf1. *Molecular and cellular biology.* 2003;23(18):6533-41.

146. Hockemeyer D, Daniels JP, Takai H, and de Lange T. Recent expansion of the telomeric complex in rodents: Two distinct POT1 proteins protect mouse telomeres. *Cell.* 2006;126(1):63-77.

147. Wu L, Multani AS, He H, Cosme-Blanco W, Deng Y, Deng JM, Bachilo O, Pathak S, Tahara H, Bailey SM, et al. Pot1 deficiency initiates DNA damage checkpoint activation and aberrant homologous recombination at telomeres. *Cell.* 2006;126(1):49-62.

148. Sfeir A, Kabir S, van Overbeek M, Celli GB, and de Lange T. Loss of Rap1 induces telomere recombination in the absence of NHEJ or a DNA damage signal. *Science.* 2010;327(5973):1657-61.

149. Leri A, Franco S, Zacheo A, Barlucchi L, Chimenti S, Limana F, Nadal-Ginard B, Kajstura J, Anversa P, and Blasco MA. Ablation of telomerase

and telomere loss leads to cardiac dilatation and heart failure associated with p53 upregulation. *The EMBO journal.* 2003;22(1):131-9.

150. Herrera E, Samper E, and Blasco MA. Telomere shortening in mTR-/- embryos is associated with failure to close the neural tube. *The EMBO journal.* 1999;18(5):1172-81.

151. Horikawa I, Fujita K, and Harris CC. p53 governs telomere regulation feedback too, via TRF2. *Aging.* 2011;3(1):26-32.

152. Martinez P, Thanasoula M, Munoz P, Liao C, Tejera A, McNees C, Flores JM, Fernandez-Capetillo O, Tarsounas M, and Blasco MA. Increased telomere fragility and fusions resulting from TRF1 deficiency lead to degenerative pathologies and increased cancer in mice. *Genes & development.* 2009;23(17):2060-75.

153. Chin L, Artandi SE, Shen Q, Tam A, Lee SL, Gottlieb GJ, Greider CW, and DePinho RA. p53 deficiency rescues the adverse effects of telomere loss and cooperates with telomere dysfunction to accelerate carcinogenesis. *Cell.* 1999;97(4):527-38.

154. Artandi SE, and DePinho RA. A critical role for telomeres in suppressing and facilitating carcinogenesis. *Current opinion in genetics & development.* 2000;10(1):39-46.

155. Flores I, and Blasco MA. A p53-dependent response limits epidermal stem cell functionality and organismal size in mice with short telomeres. *PloS one.* 2009;4(3):e4934.

156. Begus-Nahrmann Y, Lechel A, Obenauf AC, Nalapareddy K, Peit E, Hoffmann E, Schlaudraff F, Liss B, Schirmacher P, Kestler H, et al. p53 deletion impairs clearance of chromosomal-instable stem cells in aging telomere-dysfunctional mice. *Nature genetics.* 2009;41(10):1138-43.

157. Khoo CM, Carrasco DR, Bosenberg MW, Paik JH, and Depinho RA. Ink4a/Arf tumor suppressor does not modulate the degenerative conditions or tumor spectrum of the telomerase-deficient mouse. *Proceedings of the National Academy of Sciences of the United States of America.* 2007;104(10):3931-6.

158. Moser AR, Pitot HC, and Dove WF. A dominant mutation that predisposes to multiple intestinal neoplasia in the mouse. *Science.* 1990;247(4940):322-4.

159. Su LK, Kinzler KW, Vogelstein B, Preisinger AC, Moser AR, Luongo C, Gould KA, and Dove WF. Multiple intestinal neoplasia caused by a mutation in the murine homolog of the APC gene. *Science.* 1992;256(5057):668-70.

160. Schaetzlein S, Kodandaramireddy NR, Ju Z, Lechel A, Stepczynska A, Lilli DR, Clark AB, Rudolph C, Kuhnel F, Wei K, et al. Exonuclease-1 deletion impairs DNA damage signaling and prolongs lifespan of telomere-dysfunctional mice. *Cell.* 2007;130(5):863-77.

161. Sperka T, Song Z, Morita Y, Nalapareddy K, Guachalla LM, Lechel A, Begus-Nahrmann Y, Burkhalter MD, Mach M, Schlaudraff F, et al. Puma and p21 represent cooperating checkpoints limiting self-renewal and

chromosomal instability of somatic stem cells in response to telomere dysfunction. *Nature cell biology.* 2012;14(1):73-9.

162. Choudhury AR, Ju Z, Djojosubroto MW, Schienke A, Lechel A, Schaetzlein S, Jiang H, Stepczynska A, Wang C, Buer J, et al. Cdkn1a deletion improves stem cell function and lifespan of mice with dysfunctional telomeres without accelerating cancer formation. *Nature genetics.* 2007;39(1):99-105.

163. Sharma RP, and Chopra VL. Effect of the Wingless (wg1) mutation on wing and haltere development in Drosophila melanogaster. *Developmental biology.* 1976;48(2):461-5.

164. Nusse R, van Ooyen A, Cox D, Fung YK, and Varmus H. Mode of proviral activation of a putative mammary oncogene (int-1) on mouse chromosome 15. *Nature.* 1984;307(5947):131-6.

165. Nusse R, and Varmus H. Three decades of Wnts: a personal perspective on how a scientific field developed. *The EMBO journal.* 2012;31(12):2670-84.

166. van Leeuwen F, Samos CH, and Nusse R. Biological activity of soluble wingless protein in cultured Drosophila imaginal disc cells. *Nature.* 1994;368(6469):342-4.

167. de Lau W, Barker N, Low TY, Koo BK, Li VS, Teunissen H, Kujala P, Haegebarth A, Peters PJ, van de Wetering M, et al. Lgr5 homologues associate with Wnt receptors and mediate R-spondin signalling. *Nature.* 2011;476(7360):293-7.

168. Peng WC, de Lau W, Forneris F, Granneman JC, Huch M, Clevers H, and Gros P. Structure of stem cell growth factor R-spondin 1 in complex with the ectodomain of its receptor LGR5. *Cell reports.* 2013;3(6):1885-92.

169. de Lau W, Peng WC, Gros P, and Clevers H. The R-spondin/Lgr5/Rnf43 module: regulator of Wnt signal strength. *Genes & development.* 2014;28(4):305-16.

170. Niehrs C. The complex world of WNT receptor signalling. *Nature reviews Molecular cell biology.* 2012;13(12):767-79.

171. Voronkov A, and Krauss S. Wnt/beta-catenin signaling and small molecule inhibitors. *Current pharmaceutical design.* 2013;19(4):634-64.

172. Gregorieff A, and Clevers H. Wnt signaling in the intestinal epithelium: from endoderm to cancer. *Genes & development.* 2005;19(8):877-90.

173. Korinek V, Barker N, Moerer P, van Donselaar E, Huls G, Peters PJ, and Clevers H. Depletion of epithelial stem-cell compartments in the small intestine of mice lacking Tcf-4. *Nature genetics.* 1998;19(4):379-83.

174. Barker N. Adult intestinal stem cells: critical drivers of epithelial homeostasis and regeneration. *Nature reviews Molecular cell biology.* 2014;15(1):19-33.

175. Cheng H, and Leblond CP. Origin, differentiation and renewal of the four main epithelial cell types in the mouse small intestine. V. Unitarian Theory of the origin of the four epithelial cell types. *The American journal of anatomy.* 1974;141(4):537-61.

176. Barker N, and Clevers H. Tracking down the stem cells of the intestine: strategies to identify adult stem cells. *Gastroenterology.* 2007;133(6):1755-60.

177. Sato T, van Es JH, Snippert HJ, Stange DE, Vries RG, van den Born M, Barker N, Shroyer NF, van de Wetering M, and Clevers H. Paneth cells constitute the niche for Lgr5 stem cells in intestinal crypts. *Nature.* 2011;469(7330):415-8.

178. Yan KS, Chia LA, Li X, Ootani A, Su J, Lee JY, Su N, Luo Y, Heilshorn SC, Amieva MR, et al. The intestinal stem cell markers Bmi1 and Lgr5 identify two functionally distinct populations. *Proceedings of the National Academy of Sciences of the United States of America.* 2012;109(2):466-71.

179. Farin HF, Van Es JH, and Clevers H. Redundant sources of Wnt regulate intestinal stem cells and promote formation of Paneth cells. *Gastroenterology.* 2012;143(6):1518-29 e7.

180. Sato T, and Clevers H. Primary mouse small intestinal epithelial cell cultures. *Methods in molecular biology.* 2013;945(319-28.

181. Ye X, Zerlanko B, Kennedy A, Banumathy G, Zhang R, and Adams PD. Downregulation of Wnt signaling is a trigger for formation of facultative heterochromatin and onset of cell senescence in primary human cells. *Molecular cell.* 2007;27(2):183-96.

182. Liu H, Fergusson MM, Castilho RM, Liu J, Cao L, Chen J, Malide D, Rovira, II, Schimel D, Kuo CJ, et al. Augmented Wnt signaling in a mammalian model of accelerated aging. *Science.* 2007;317(5839):803-6.

183. Zhang DY, Wang HJ, and Tan YZ. Wnt/beta-catenin signaling induces the aging of mesenchymal stem cells through the DNA damage response and the p53/p21 pathway. *PloS one.* 2011;6(6):e21397.

184. Brack AS, Conboy MJ, Roy S, Lee M, Kuo CJ, Keller C, and Rando TA. Increased Wnt signaling during aging alters muscle stem cell fate and increases fibrosis. *Science.* 2007;317(5839):807-10.

185. Willert K, Brown JD, Danenberg E, Duncan AW, Weissman IL, Reya T, Yates JR, 3rd, and Nusse R. Wnt proteins are lipid-modified and can act as stem cell growth factors. *Nature.* 2003;423(6938):448-52.

186. Reya T, Duncan AW, Ailles L, Domen J, Scherer DC, Willert K, Hintz L, Nusse R, and Weissman IL. A role for Wnt signalling in self-renewal of haematopoietic stem cells. *Nature.* 2003;423(6938):409-14.

187. Kirstetter P, Anderson K, Porse BT, Jacobsen SE, and Nerlov C. Activation of the canonical Wnt pathway leads to loss of hematopoietic stem cell repopulation and multilineage differentiation block. *Nature immunology.* 2006;7(10):1048-56.

188. Scheller M, Huelsken J, Rosenbauer F, Taketo MM, Birchmeier W, Tenen DG, and Leutz A. Hematopoietic stem cell and multilineage defects generated by constitutive beta-catenin activation. *Nature immunology.* 2006;7(10):1037-47.

189. Zhang Y, Toh L, Lau P, and Wang X. Human telomerase reverse transcriptase (hTERT) is a novel target of the Wnt/beta-catenin pathway in human cancer. *The Journal of biological chemistry.* 2012;287(39):32494-511.

190. Hoffmeyer K, Raggioli A, Rudloff S, Anton R, Hierholzer A, Del Valle I, Hein K, Vogt R, and Kemler R. Wnt/beta-catenin signaling regulates telomerase in stem cells and cancer cells. *Science.* 2012;336(6088):1549-54.

191. Sarin KY, Cheung P, Gilison D, Lee E, Tennen RI, Wang E, Artandi MK, Oro AE, and Artandi SE. Conditional telomerase induction causes proliferation of hair follicle stem cells. *Nature.* 2005;436(7053):1048-52.

192. Choi J, Southworth LK, Sarin KY, Venteicher AS, Ma W, Chang W, Cheung P, Jun S, Artandi MK, Shah N, et al. TERT promotes epithelial proliferation through transcriptional control of a Myc- and Wnt-related developmental program. *PLoS genetics.* 2008;4(1):e10.

193. Vidal-Cardenas SL, and Greider CW. Comparing effects of mTR and mTERT deletion on gene expression and DNA damage response: a critical examination of telomere length maintenance-independent roles of telomerase. *Nucleic acids research.* 2010;38(1):60-71.

194. Hrdlickova R, Nehyba J, and Bose HR, Jr. Alternatively spliced telomerase reverse transcriptase variants lacking telomerase activity stimulate cell proliferation. *Molecular and cellular biology.* 2012;32(21):4283-96.

195. Nault JC, Mallet M, Pilati C, Calderaro J, Bioulac-Sage P, Laurent C, Laurent A, Cherqui D, Balabaud C, and Zucman-Rossi J. High frequency of telomerase reverse-transcriptase promoter somatic mutations in hepatocellular carcinoma and preneoplastic lesions. *Nature communications.* 2013;4(2218.

196. Diala I, Wagner N, Magdinier F, Shkreli M, Sirakov M, Bauwens S, Schluth-Bolard C, Simonet T, Renault VM, Ye J, et al. Telomere protection and TRF2 expression are enhanced by the canonical Wnt signalling pathway. *EMBO reports.* 2013;14(4):356-63.

197. van Steensel B, Smogorzewska A, and de Lange T. TRF2 protects human telomeres from end-to-end fusions. *Cell.* 1998;92(3):401-13.

198. Bartel DP. MicroRNAs: genomics, biogenesis, mechanism, and function. *Cell.* 2004;116(2):281-97.

199. Lagos-Quintana M, Rauhut R, Meyer J, Borkhardt A, and Tuschl T. New microRNAs from mouse and human. *Rna.* 2003;9(2):175-9.

200. Kim VN, Han J, and Siomi MC. Biogenesis of small RNAs in animals. *Nature reviews Molecular cell biology.* 2009;10(2):126-39.

201. Lee Y, Jeon K, Lee JT, Kim S, and Kim VN. MicroRNA maturation: stepwise processing and subcellular localization. *The EMBO journal.* 2002;21(17):4663-70.

202. Lee Y, Ahn C, Han J, Choi H, Kim J, Yim J, Lee J, Provost P, Radmark O, Kim S, et al. The nuclear RNase III Drosha initiates microRNA processing. *Nature.* 2003;425(6956):415-9.

203. Lau NC, Lim LP, Weinstein EG, and Bartel DP. An abundant class of tiny RNAs with probable regulatory roles in Caenorhabditis elegans. *Science.* 2001;294(5543):858-62.

204. Lim LP, Lau NC, Weinstein EG, Abdelhakim A, Yekta S, Rhoades MW, Burge CB, and Bartel DP. The microRNAs of Caenorhabditis elegans. *Genes & development.* 2003;17(8):991-1008.

205. Ambros V, Bartel B, Bartel DP, Burge CB, Carrington JC, Chen X, Dreyfuss G, Eddy SR, Griffiths-Jones S, Marshall M, et al. A uniform system for microRNA annotation. *Rna.* 2003;9(3):277-9.

206. Khvorova A, Reynolds A, and Jayasena SD. Functional siRNAs and miRNAs exhibit strand bias. *Cell.* 2003;115(2):209-16.

207. Schwarz DS, Hutvagner G, Du T, Xu Z, Aronin N, and Zamore PD. Asymmetry in the assembly of the RNAi enzyme complex. *Cell.* 2003;115(2):199-208.

208. Cerutti L, Mian N, and Bateman A. Domains in gene silencing and cell differentiation proteins: the novel PAZ domain and redefinition of the Piwi domain. *Trends in biochemical sciences.* 2000;25(10):481-2.

209. Hock J, and Meister G. The Argonaute protein family. *Genome biology.* 2008;9(2):210.

210. Lewis BP, Burge CB, and Bartel DP. Conserved seed pairing, often flanked by adenosines, indicates that thousands of human genes are microRNA targets. *Cell.* 2005;120(1):15-20.

211. Grimson A, Farh KK, Johnston WK, Garrett-Engele P, Lim LP, and Bartel DP. MicroRNA targeting specificity in mammals: determinants beyond seed pairing. *Molecular cell.* 2007;27(1):91-105.

212. Chi SW, Zang JB, Mele A, and Darnell RB. Argonaute HITS-CLIP decodes microRNA-mRNA interaction maps. *Nature.* 2009;460(7254):479-86.

213. Lee RC, Feinbaum RL, and Ambros V. The C. elegans heterochronic gene lin-4 encodes small RNAs with antisense complementarity to lin-14. *Cell.* 1993;75(5):843-54.

214. Reinhart BJ, Slack FJ, Basson M, Pasquinelli AE, Bettinger JC, Rougvie AE, Horvitz HR, and Ruvkun G. The 21-nucleotide let-7 RNA regulates developmental timing in Caenorhabditis elegans. *Nature.* 2000;403(6772):901-6.

215. O'Connell RM, Rao DS, and Baltimore D. microRNA regulation of inflammatory responses. *Annual review of immunology.* 2012;30(295-312.

216. Wang X, Liu P, Zhu H, Xu Y, Ma C, Dai X, Huang L, Liu Y, Zhang L, and Qin C. miR-34a, a microRNA up-regulated in a double transgenic mouse model of Alzheimer's disease, inhibits bcl2 translation. *Brain research bulletin.* 2009;80(4-5):268-73.

217. Maes OC, Sarojini H, and Wang E. Stepwise up-regulation of microRNA expression levels from replicating to reversible and irreversible growth arrest states in WI-38 human fibroblasts. *Journal of cellular physiology.* 2009;221(1):109-19.

218. Li N, Bates DJ, An J, Terry DA, and Wang E. Up-regulation of key microRNAs, and inverse down-regulation of their predicted oxidative phosphorylation target genes, during aging in mouse brain. *Neurobiology of aging.* 2011;32(5):944-55.

219. Ibanez-Ventoso C, Yang M, Guo S, Robins H, Padgett RW, and Driscoll M. Modulated microRNA expression during adult lifespan in Caenorhabditis elegans. *Aging cell.* 2006;5(3):235-46.

220. He L, He X, Lim LP, de Stanchina E, Xuan Z, Liang Y, Xue W, Zender L, Magnus J, Ridzon D, et al. A microRNA component of the p53 tumour suppressor network. *Nature.* 2007;447(7148):1130-4.

221. Zhao T, Li J, and Chen AF. MicroRNA-34a induces endothelial progenitor cell senescence and impedes its angiogenesis via suppressing silent information regulator 1. *American journal of physiology Endocrinology and metabolism.* 2010;299(1):E110-6.

222. Ito T, Yagi S, and Yamakuchi M. MicroRNA-34a regulation of endothelial senescence. *Biochemical and biophysical research communications.* 2010;398(4):735-40.

223. Christoffersen NR, Shalgi R, Frankel LB, Leucci E, Lees M, Klausen M, Pilpel Y, Nielsen FC, Oren M, and Lund AH. p53-independent upregulation of miR-34a during oncogene-induced senescence represses MYC. *Cell death and differentiation.* 2010;17(2):236-45.

224. Kumamoto K, Spillare EA, Fujita K, Horikawa I, Yamashita T, Appella E, Nagashima M, Takenoshita S, Yokota J, and Harris CC. Nutlin-3a

activates p53 to both down-regulate inhibitor of growth 2 and up-regulate mir-34a, mir-34b, and mir-34c expression, and induce senescence. *Cancer research.* 2008;68(9):3193-203.

225. Tazawa H, Tsuchiya N, Izumiya M, and Nakagama H. Tumor-suppressive miR-34a induces senescence-like growth arrest through modulation of the E2F pathway in human colon cancer cells. *Proceedings of the National Academy of Sciences of the United States of America.* 2007;104(39):15472-7.

226. Yamakuchi M, and Lowenstein CJ. MiR-34, SIRT1 and p53: the feedback loop. *Cell cycle.* 2009;8(5):712-5.

227. Yang J, Chen D, He Y, Melendez A, Feng Z, Hong Q, Bai X, Li Q, Cai G, Wang J, et al. MiR-34 modulates Caenorhabditis elegans lifespan via repressing the autophagy gene atg9. *Age.* 2013;35(1):11-22.

228. Rippo MR, Olivieri F, Monsurro V, Prattichizzo F, Albertini MC, and Procopio AD. MitomiRs in human inflamm-aging: a hypothesis involving miR-181a, miR-34a and miR-146a. *Experimental gerontology.* 2014;56(154-63.

229. Sataranatarajan K, Feliers D, Mariappan MM, Lee HJ, Lee MJ, Day RT, Yalamanchili HB, Choudhury GG, Barnes JL, Van Remmen H, et al. Molecular events in matrix protein metabolism in the aging kidney. *Aging cell.* 2012;11(6):1065-73.

230. Grillari J, Hackl M, and Grillari-Voglauer R. miR-17-92 cluster: ups and downs in cancer and aging. *Biogerontology.* 2010;11(4):501-6.

231. de Lencastre A, Pincus Z, Zhou K, Kato M, Lee SS, and Slack FJ. MicroRNAs both promote and antagonize longevity in C. elegans. *Current biology : CB.* 2010;20(24):2159-68.

232. Ciafre SA, Galardi S, Mangiola A, Ferracin M, Liu CG, Sabatino G, Negrini M, Maira G, Croce CM, and Farace MG. Extensive modulation of a set of microRNAs in primary glioblastoma. *Biochemical and biophysical research communications.* 2005;334(4):1351-8.

233. Lowery AJ, Miller N, Devaney A, McNeill RE, Davoren PA, Lemetre C, Benes V, Schmidt S, Blake J, Ball G, et al. MicroRNA signatures predict oestrogen receptor, progesterone receptor and HER2/neu receptor status in breast cancer. *Breast cancer research : BCR.* 2009;11(3):R27.

234. Xi Y, Formentini A, Chien M, Weir DB, Russo JJ, Ju J, Kornmann M, and Ju J. Prognostic Values of microRNAs in Colorectal Cancer. *Biomarker insights.* 2006;2(113-21.

235. Schaefer A, Jung M, Mollenkopf HJ, Wagner I, Stephan C, Jentzmik F, Miller K, Lein M, Kristiansen G, and Jung K. Diagnostic and prognostic implications of microRNA profiling in prostate carcinoma. *International journal of cancer Journal international du cancer.* 2010;126(5):1166-76.

236. Wei Q, Yokota C, Semenov MV, Doble B, Woodgett J, and He X. R-spondin1 is a high affinity ligand for LRP6 and induces LRP6 phosphorylation and beta-catenin signaling. *J Biol Chem.* 2007;282(21):15903-11.

237. van der Flier LG, van Gijn ME, Hatzis P, Kujala P, Haegebarth A, Stange DE, Begthel H, van den Born M, Guryev V, Oving I, et al. Transcription factor achaete scute-like 2 controls intestinal stem cell fate. *Cell.* 2009;136(5):903-12.

238. Gandara RM, Mahida YR, and Potten CS. Regional differences in stem and transit cell proliferation and apoptosis in the terminal ileum and colon of mice after 12 Gy. *International journal of radiation oncology, biology, physics.* 2012;82(3):e521-8.

239. Karim BO, and Huso DL. Mouse models for colorectal cancer. *American journal of cancer research.* 2013;3(3):240-50.

240. Potten CS. Stem cells in gastrointestinal epithelium: numbers, characteristics and death. *Philosophical transactions of the Royal Society of London Series B, Biological sciences.* 1998;353(1370):821-30.

241. Barker N, van Oudenaarden A, and Clevers H. Identifying the stem cell of the intestinal crypt: strategies and pitfalls. *Cell stem cell.* 2012;11(4):452-60.

242. Powell AE, Wang Y, Li Y, Poulin EJ, Means AL, Washington MK, Higginbotham JN, Juchheim A, Prasad N, Levy SE, et al. The pan-ErbB negative regulator Lrig1 is an intestinal stem cell marker that functions as a tumor suppressor. *Cell.* 2012;149(1):146-58.

243. Tian H, Biehs B, Warming S, Leong KG, Rangell L, Klein OD, and de Sauvage FJ. A reserve stem cell population in small intestine renders Lgr5-positive cells dispensable. *Nature.* 2011;478(7368):255-9.

244. Sangiorgi E, and Capecchi MR. Bmi1 is expressed in vivo in intestinal stem cells. *Nature genetics.* 2008;40(7):915-20.

245. Van der Flier LG, Sabates-Bellver J, Oving I, Haegebarth A, De Palo M, Anti M, Van Gijn ME, Suijkerbuijk S, Van de Wetering M, Marra G, et al. The Intestinal Wnt/TCF Signature. *Gastroenterology.* 2007;132(2):628-32.

246. Barker N, van Es JH, Kuipers J, Kujala P, van den Born M, Cozijnsen M, Haegebarth A, Korving J, Begthel H, Peters PJ, et al. Identification of stem cells in small intestine and colon by marker gene Lgr5. *Nature.* 2007;449(7165):1003-7.

247. Carmon KS, Lin Q, Gong X, Thomas A, and Liu Q. LGR5 interacts and cointernalizes with Wnt receptors to modulate Wnt/beta-catenin signaling. *Molecular and cellular biology.* 2012;32(11):2054-64.

248. Itzkovitz S, Lyubimova A, Blat IC, Maynard M, van Es J, Lees J, Jacks T, Clevers H, and van Oudenaarden A. Single-molecule transcript counting of stem-cell markers in the mouse intestine. *Nature cell biology.* 2012;14(1):106-14.

249. Munoz J, Stange DE, Schepers AG, van de Wetering M, Koo BK, Itzkovitz S, Volckmann R, Kung KS, Koster J, Radulescu S, et al. The Lgr5 intestinal stem cell signature: robust expression of proposed quiescent '+4' cell markers. *The EMBO journal.* 2012;31(14):3079-91.

250. Schepers AG, Vries R, van den Born M, van de Wetering M, and Clevers H. Lgr5 intestinal stem cells have high telomerase activity and randomly segregate their chromosomes. *The EMBO journal.* 2011;30(6):1104-9.

251. Tusher VG, Tibshirani R, and Chu G. Significance analysis of microarrays applied to the ionizing radiation response. *Proc Natl Acad Sci U S A.* 2001;98(9):5116-21.

252. Saeed AI, Sharov V, White J, Li J, Liang W, Bhagabati N, Braisted J, Klapa M, Currier T, Thiagarajan M, et al. TM4: a free, open-source system for microarray data management and analysis. *BioTechniques.* 2003;34(2):374-8.

253. Subramanian A, Tamayo P, Mootha VK, Mukherjee S, Ebert BL, Gillette MA, Paulovich A, Pomeroy SL, Golub TR, Lander ES, et al. Gene set enrichment analysis: a knowledge-based approach for interpreting genome-wide expression profiles. *Proc Natl Acad Sci U S A.* 2005;102(43):15545-50.

254. Takeda N, Jain R, LeBoeuf MR, Wang Q, Lu MM, and Epstein JA. Interconversion between intestinal stem cell populations in distinct niches. *Science.* 2011;334(6061):1420-4.

255. Maria Cambuli F, Rezza A, Nadjar J, and Plateroti M. Brief report: Musashi1-eGFP mice, a new tool for differential isolation of the intestinal stem cell populations. *Stem cells.* 2013;31(10):2273-8.

256. Martin-Rivera L, Herrera E, Albar JP, and Blasco MA. Expression of mouse telomerase catalytic subunit in embryos and adult tissues. *Proceedings of the National Academy of Sciences of the United States of America.* 1998;95(18):10471-6.

257. Liu J, Stevens J, Rote CA, Yost HJ, Hu Y, Neufeld KL, White RL, and Matsunami N. Siah-1 mediates a novel beta-catenin degradation pathway linking p53 to the adenomatous polyposis coli protein. *Molecular cell.* 2001;7(5):927-36.

258. Kim NH, Kim HS, Kim NG, Lee I, Choi HS, Li XY, Kang SE, Cha SY, Ryu JK, Na JM, et al. p53 and microRNA-34 are suppressors of canonical Wnt signaling. *Science signaling.* 2011;4(197):ra71.

259. Kaller M, Liffers ST, Oeljeklaus S, Kuhlmann K, Roh S, Hoffmann R, Warscheid B, and Hermeking H. Genome-wide characterization of miR-34a induced changes in protein and mRNA expression by a combined pulsed SILAC and microarray analysis. *Molecular & cellular proteomics : MCP.* 2011;10(8):M111 010462.

260. Cha YH, Kim NH, Park C, Lee I, Kim HS, and Yook JI. MiRNA-34 intrinsically links p53 tumor suppressor and Wnt signaling. *Cell cycle.* 2012;11(7):1273-81.

261. Kim NH, Cha YH, Kang SE, Lee Y, Lee I, Cha SY, Ryu JK, Na JM, Park C, Yoon HG, et al. p53 regulates nuclear GSK-3 levels through miR-34-mediated Axin2 suppression in colorectal cancer cells. *Cell cycle.* 2013;12(10):1578-87.

262. Boon RA, Iekushi K, Lechner S, Seeger T, Fischer A, Heydt S, Kaluza D, Treguer K, Carmona G, Bonauer A, et al. MicroRNA-34a regulates cardiac ageing and function. *Nature.* 2013;495(7439):107-10.

263. Cole KA, Attiyeh EF, Mosse YP, Laquaglia MJ, Diskin SJ, Brodeur GM, and Maris JM. A functional screen identifies miR-34a as a candidate neuroblastoma tumor suppressor gene. *Molecular cancer research : MCR.* 2008;6(5):735-42.

264. Henrich KO, Schwab M, and Westermann F. 1p36 tumor suppression--a matter of dosage? *Cancer research.* 2012;72(23):6079-88.

265. Concepcion CP, Han YC, Mu P, Bonetti C, Yao E, D'Andrea A, Vidigal JA, Maughan WP, Ogrodowski P, and Ventura A. Intact p53-dependent responses in miR-34-deficient mice. *PLoS genetics.* 2012;8(7):e1002797.

266. Krzeszinski JY, Wei W, Huynh H, Jin Z, Wang X, Chang TC, Xie XJ, He L, Mangala LS, Lopez-Berestein G, et al. miR-34a blocks osteoporosis and bone metastasis by inhibiting osteoclastogenesis and Tgif2. *Nature.* 2014;512(7515):431-5.

267. Okada N, Lin CP, Ribeiro MC, Biton A, Lai G, He X, Bu P, Vogel H, Jablons DM, Keller AC, et al. A positive feedback between p53 and miR-34 miRNAs mediates tumor suppression. *Genes & development.* 2014;28(5):438-50.

268. Yamakuchi M, Ferlito M, and Lowenstein CJ. miR-34a repression of SIRT1 regulates apoptosis. *Proceedings of the National Academy of Sciences of the United States of America.* 2008;105(36):13421-6.

269. Chhabra R, Dubey R, and Saini N. Cooperative and individualistic functions of the microRNAs in the miR-23a~27a~24-2 cluster and its implication in human diseases. *Molecular cancer.* 2010;9(232.

270. Hande MP, Samper E, Lansdorp P, and Blasco MA. Telomere length dynamics and chromosomal instability in cells derived from telomerase null mice. *The Journal of cell biology.* 1999;144(4):589-601.

271. Sansom OJ, Reed KR, Hayes AJ, Ireland H, Brinkmann H, Newton IP, Batlle E, Simon-Assmann P, Clevers H, Nathke IS, et al. Loss of Apc in vivo immediately perturbs Wnt signaling, differentiation, and migration. *Genes Dev.* 2004;18(12):1385-90.

272. Fevr T, Robine S, Louvard D, and Huelsken J. Wnt/beta-catenin is essential for intestinal homeostasis and maintenance of intestinal stem cells. *Mol Cell Biol.* 2007;27(21):7551-9.

273. Rosenbloom KR, Sloan CA, Malladi VS, Dreszer TR, Learned K, Kirkup VM, Wong MC, Maddren M, Fang R, Heitner SG, et al. ENCODE data in the UCSC Genome Browser: year 5 update. *Nucleic Acids Res.* 2013;41(Database issue):D56-63.

274. Merlos-Suarez A, Barriga FM, Jung P, Iglesias M, Cespedes MV, Rossell D, Sevillano M, Hernando-Momblona X, da Silva-Diz V, Munoz P, et al. The intestinal stem cell signature identifies colorectal cancer stem cells and predicts disease relapse. *Cell stem cell.* 2011;8(5):511-24.

275. Jonassaint NL, Guo N, Califano JA, Montgomery EA, and Armanios M. The gastrointestinal manifestations of telomere-mediated disease. *Aging cell.* 2013;12(2):319-23.

276. Karlseder J, Smogorzewska A, and de Lange T. Senescence induced by altered telomere state, not telomere loss. *Science.* 2002;295(5564):2446-9.

277. Spyridopoulos I, Haendeler J, Urbich C, Brummendorf TH, Oh H, Schneider MD, Zeiher AM, and Dimmeler S. Statins enhance migratory capacity by upregulation of the telomere repeat-binding factor TRF2 in endothelial progenitor cells. *Circulation.* 2004;110(19):3136-42.

278. O'Sullivan JN, Bronner MP, Brentnall TA, Finley JC, Shen WT, Emerson S, Emond MJ, Gollahon KA, Moskovitz AH, Crispin DA, et al. Chromosomal instability in ulcerative colitis is related to telomere shortening. *Nat Genet.* 2002;32(2):280-4.

279. Risques RA, Lai LA, Brentnall TA, Li L, Feng Z, Gallaher J, Mandelson MT, Potter JD, Bronner MP, and Rabinovitch PS. Ulcerative colitis is a disease of accelerated colon aging: evidence from telomere attrition and DNA damage. *Gastroenterology.* 2008;135(2):410-8.

280. Becker C, Fantini MC, and Neurath MF. High resolution colonoscopy in live mice. *Nature protocols.* 2006;1(6):2900-4.

281. Kodani T, Rodriguez-Palacios A, Corridoni D, Lopetuso L, Di Martino L, Marks B, Pizarro J, Pizarro T, Chak A, and Cominelli F. Flexible colonoscopy in mice to evaluate the severity of colitis and colorectal tumors using a validated endoscopic scoring system. *Journal of visualized experiments : JoVE.* 201380):e50843.

282. Chang WW, and Nadler NJ. Renewal of the epithelium in the descending colon of the mouse. IV. Cell population kinetics of vacuolated-columnar and mucous cells. *The American journal of anatomy.* 1975;144(1):39-56.

283. Rudolph KL, Millard M, Bosenberg MW, and DePinho RA. Telomere dysfunction and evolution of intestinal carcinoma in mice and humans. *Nature genetics.* 2001;28(2):155-9.